



Room 14-0551
77 Massachusetts Avenue
Cambridge, MA 02139
Ph: 617.253.5668 Fax: 617.253.1690
Email: docs@mit.edu
<http://libraries.mit.edu/docs>

DISCLAIMER OF QUALITY

Due to the condition of the original material, there are unavoidable flaws in this reproduction. We have made every effort possible to provide you with the best copy available. If you are dissatisfied with this product and find it unusable, please contact Document Services as soon as possible.

Thank you.

Some pages in the original document contain pictures, graphics, or text that is illegible.

BUBBLE GROWTH RATES AT REDUCED PRESSURE

by

Yeong-Cheng Lien

M. E. Dipl., Taipei Institute of Technology
(1962)

M. M. E. Pratt Institute
(1965)

Submitted in Partial Fulfillment

of the Requirements for the

Degree of Doctor of

Science

at the

Massachusetts Institute of

Technology

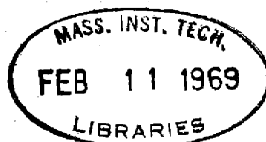
February 1969

Signature of Author . . . *Yeong-Cheng Lien* . . .
Department of Mechanical Engineering, January 13, 1969

Certified by
Thesis Supervisor

Accepted by
Chairman, Departmental Committee
on Graduate Students

Archives



BUBBLE GROWTH RATES AT REDUCED PRESSURE

by

Yeong-Cheng Lien

Submitted to the Department of Mechanical Engineering on January 13, 1969, in partial fulfillment of the requirement for the degree of Doctor of Science.

ABSTRACT

A general method is developed for calculating bubble growth in a uniform temperature field. It is verified by comparison with bubble growth data taken in water at reduced pressure. The experiments cover the following range of parameters: pressure 0.18 to 5.6 psia; Jakob number 58 to 2690. Experimental results have been correlated in the form of a normalized radius versus time curve. In these experiments bubbles were initiated by means of a spark discharge between the gap made by two wires.

It is found that the dynamic effect is of increasing importance with decreasing pressure, while the significance of heat diffusion diminishes. The interfacial mass transfer resistance does not ever appear to have appreciable influence upon the bubble growth rate.

Thesis Supervisor: Doctor Peter Griffith
Title: Professor of Mechanical Engineering

ACKNOWLEDGMENTS

It is indeed a pleasure to express my deep appreciation to Professor Peter Griffith who, as my thesis supervisor, provided expert guidance, unfailing support, and a source of inspiration throughout the course of this investigation. His original suggestions of basic problems and approaches were vital to the successful fulfillment of the objectives. I have been fortunate to be associated with him during those joyous and rewarding years at M.I.T.

I wish to thank the other members of my thesis committee, Professor J. C. Keck and Professor R. E. Stickney, for their valuable advice and constructive criticism. I am also indebted to Professor H. E. Edgerton who not only kindly granted me ready access to the facilities of the Stroboscopic Measurement Laboratory, but also introduced me to the fascinating world of high-speed photography. Further gratitude is due Professors B. B. Mikic, W. M. Rohsenow, and W. J. Bornhorst for giving generously their time to discuss various aspects of the program.

To Messrs. C. W. Deane, J. Horowitz, S. Hynek, C. Graham, and J. M. Gonzalez, and Drs. T. S. Yih and B. S. Shiralkar goes my sincere appreciation for their helpful discussions and their fellowship. Thanks are due to Mr. F. Johnson and Mr. N. MacRoberts who assisted in the construction of the apparatus.

I am very grateful to Miss Lucille Blake for all her assistances and many favors these past few years, and especially I should like to thank her for the masterful typing of this manuscript.

This work was supported partially by the National Aeronautics and Space Administration under contract NAS 8-20013. The experimental work was performed in part at the Heat Transfer Laboratory and the Stroboscopic Measurement Laboratory. Numerical computations were carried out at the Computer Facility of the Department of Mechanical Engineering.

Finally, I should like to thank my parents for their continual support and encouragement. To them, this thesis is dedicated.

TABLE OF CONTENTS

	Page
TITLE PAGE	1
ABSTRACT	2
ACKNOWLEDGMENTS	3
TABLE OF CONTENTS	5
LIST OF ILLUSTRATIONS	7
LIST OF TABLES	8
NOMENCLATURE	9
CHAPTER I - INTRODUCTION	12
I.1 Previous Work	13
I.2 The Problem	14
I.3 Purpose of This Work	15
CHAPTER II - REVIEW OF BUBBLE GROWTH THEORY	16
II.1 Overall Remarks	16
II.2 General Assumptions	17
II.3 Growth Controlled by Liquid Inertia	18
II.4 Growth Limited by Heat Diffusion	20
II.5 Growth Limited by Evaporation Rate	23
II.6 Comparison of Bubble Growth Equations	26
CHAPTER III - APPARATUS AND PROCEDURES OF EXPERIMENT	29
III.1 Experimental Methods	29
III.1.1 Attainment of Uniform Water Temperature	30
III.1.2 Method of Bubble Generation	31
III.2 Description of Apparatus	37
III.3 Experimental Procedures	41
CHAPTER IV - EXPERIMENTAL RESULTS AND DATA REDUCTION	43
IV.1 Experimental Results	43
IV.2 Data Reduction	44
IV.2.1 Assumptions and Equations for Data Reduction	44

	Page
CHAPTER V - DISCUSSION	53
V.1 Concerning the Applicability of Existing Bubble Growth Equations	53
V.1.1 Relative Importances of Heat Diffusion and Dynamic Effects	53
V.1.2 The Upper Bound of Bubble Growth Curves	57
V.1.3 Generalized Bubble Growth Curve	58
V.1.4 Recommendations for Bubble Growth Rates Calculation	61
V.1.5 Application to Bubble Growth Problem of Liquid Metals	61
V.2 Concerning the Interfacial Nonequilibrium Effect and the Evaporation Coefficient	63
CHAPTER VI - CONCLUSIONS	66
BIBLIOGRAPHY	67
APPENDICES A. ILLUSTRATIONS	72
B. EXPERIMENTAL DATA	101
C. REDUCED DATA	109
D. JUSTIFICATION FOR THE NEGLECT OF THE AIR CONTENT OF BUBBLE	117
E. EMPIRICAL EQUATIONS	119
F. ERROR ANALYSIS	120
BIOGRAPHICAL NOTE	125

LIST OF ILLUSTRATIONS

Figure No.	Captions	Page
1	Low Pressure Data of Cole and Shulman	72
2	Spherical Bubble Model	73
3	Sketch of Bubble Triggering Device	74
4	Photographic History of Bubble B6	75
5	Comparison of Atmospheric Bubble Growth Data	76
6	Schematic of Apparatus	77
7	Photograph of Experimental Setup	78
8	Close-up Picture of Test Section	79
9	Wiring Diagram of Instrumentation	80
10	Flow Diagram of Data Reduction	81
11 - 18	Radius vs Time and Temperature vs Radius Curves of Bubbles B1 - B8	82 - 89
19	Coordinate System for Temperature Distribution Function	90
20	System Pressure Curves for Bubble D7	91
21	Comparison of Theory with Experiment at One Atmosphere	92
22	System Pressure Curves for Bubble B1	93
23 - 28	Log-Log Plots of Radius vs Time, Bubbles B1, B2, B4-B7	94 - 99
29	Generalized Bubble Growth Curve	100

LIST OF TABLES

Table No.	Title	Page
II-1	Comparison of the Coefficient ϕ	23
II-2	Experimental Values of the Evaporation or Condensation Coefficient of Water	27
II-3	Comparison of Theoretical Bubble Growth Rates	28
IV-1	Operating Conditions of B Bubbles	43
IV-2	Values of c_1 and c_2	52
V-1	Values of \bar{R}	60
V-2	Representative Results of Sodium Bubble Calculations	62
V-3	Representative Values of the Ratios $\Delta T_1/\Delta T_s$ and $\Delta T_i/\Delta T_h$	64
B-1 to B-8	Experimental Data for Bubbles B1 to B8	101 - 108
C-1 to C-8	Reduced Data for Bubbles B1 to B8	109 - 116
F-1	Results of Representative Uncertainty Calculations	123

NOMENCLATURE

a	minor diameter of a spheroidal bubble
b	major diameter of a spheroidal bubble
C	capacitance
c_1	constant, defined in Equation (IV-6)
c_2	constant, defined in Equation (IV-7)
c_e	heat capacity of the electrode
c_l	specific heat of liquid
D_b	bubble diameter
D_e	diameter of the electrode
d, d_1	apparent and actual sizes of reference object
E	voltage
h_{fg}	latent heat of vaporization
I	frame number
Ja	Jakob number
k_l	thermal conductivity of liquid
n	number of gram-moles of gases
P	pressure
P_∞	system pressure
P_g, P_{O_2}, P_{H_2}	partial pressures of the inert gas, oxygen, and hydrogen
P_i	saturation pressure at T_i
$P_{sat}(T_\infty)$	saturation pressure at T_∞
P_v	vapor pressure
Q	electric charge
r	radius

R	bubble radius
\dot{R}	bubble growth rate
\ddot{R}	d^2R/dt^2
R^*	radius, defined in Equation (V-3)
\bar{R}	dimensionless radius, defined in Equation (V-5)
R_c	critical radius of a vapor bubble
R_g	gas constant
\dot{R}_m	maximum bubble growth rate, defined in Equation (V-1)
R_r	reference radius, equal to 0.1 inch
R_u	universal gas constant
T	temperature
T_∞	uniform liquid temperature
T_i	interface temperature
$T_{sat}(P_\infty)$	saturation temperature at P_∞
T_v	vapor temperature
ΔT_d	temperature difference, $T_v - T_{sat}(P_\infty)$
ΔT_h	temperature difference $T_\infty - T_v$
ΔT_i	interfacial temperature drop, $T_v - T_i$
ΔT_s	liquid superheat, $T_\infty - T_{sat}(P_\infty)$
t	time
t^*	time, defined in Equation (V-4)
U	uncertainty
u	radial liquid velocity
v_l	specific volume of liquid
v_v	specific volume of vapor

V	bubble volume
w	mass flow rate per unit area in unit time
x	radial distance measured from bubble wall

Greek Letters

α_l	thermal diffusivity of liquid
Γ	defined in Equation (II-20)
δ	thermal boundary layer thickness
θ	temperature difference $T - T_i$
θ_o	temperature difference, $T_\infty - T_i$
ρ_e	density of the electrode material
ρ_l	liquid density
ρ_v	vapor density
σ_c	condensation coefficient
σ_e	evaporation coefficient
σ	surface tension
ϕ	constant, defined in Equation (II-16)

CHAPTER I - INTRODUCTION

One of the important safety problems related to liquid-metal-cooled fast reactor is the vapor voidage of a subchannel in a loss-of-flow accident. During the normal operations, ebullition is avoided by maintaining the coolant temperature well below the saturation value. When the accident occurs, the temperature increases rapidly since the reactor power density is extremely high. It has been shown that the liquid may become superheated in about half a second (1). Because liquid metals have the peculiar behavior of being able to sustain superheat up to several hundred degrees Fahrenheit prior to the incipience of boiling (2), the subsequent growth of a bubble may be explosive in nature. If the growth rate is sufficiently high, the expanding bubble displaces a large amount of coolant from the subchannel, causing reactivity changes and, possibly, melt-down of the fuel cladding material. Once the latter happens, the dispersed fuel gives ever bigger changes in reactivity. Moreover, the excessive pressure force associated with the collapse of the vapor bubble in regimes where the coolant is still subcooled could seriously damage the whole core assembly.

For these reasons knowledge of bubble growth rates is essential to the fast reactor safety analysis. There emerges the question of whether the existing bubble growth theory can be directly applied to the liquid metals. This leads to the broader problem concerning the applicability of the well-documented bubble growth equations under general conditions. It is to this general problem that the present work is addressed.

I.1 Previous Work

Bubble growth rates were first studied in a uniform temperature field by Rayleigh (3), Plesset and Zwick (4,5,6), Forster and Zuber (7), Scriven (8), Bankoff et al (9), Dergarabedian (10,11), and others. Later, other investigators such as Griffith (12), Savic (13), Han and Griffith (14), Bankoff and Mikesell (15), Zuber (16), Cole (17), and Mikic and Rohsenow (18) investigated the bubble growth problem involving nonuniform temperature field.

The most successful analytical result appears to be the simple solution of Plesset and Zwick. This solution was derived from consideration of asymptotic growth of a spherical vapor bubble in a uniformly superheated liquid. The asymptotic bubble growth is characterized by negligible surface tension and dynamic effects so that the growth rate of the bubble is limited by the heat diffusion process in the liquid to the bubble wall. The Plesset and Zwick solution, which has been modified by other investigators (16,17,19,20) for the general case of nonuniform temperature field, is in satisfactory agreement with experimental growth rate data of water vapor bubbles at pressure levels ranging from 1/2 atm. up to 100 atm. (2,10,11,12,14,21,22,23).

However, recent experiments on water by Cole and Shulman (24) show that bubble growth rates at reduced pressure are almost an order of magnitude lower than might be predicted by the heat diffusion limited theory. The discrepancy increases with decreasing pressure, as can be seen from Figure 1. These experiments were run in such a way that the thermal initial conditions were not known. Consequently, the cause of this large discrepancy cannot be properly assessed.

I.2 The Problem

Why does the heat diffusion limited theory, which seems so reliable at high pressure levels, fail to predict bubble growth rates at reduced pressure?

It is suspected that the dynamic effect, which is considered as negligible in the heat diffusion limited theory, may be significant under reduced pressure conditions. Scriven's analysis (8) indicated that the asymptotic solution is a good approximation only for values of Jakob number, * Ja, much greater than unity. On the other hand, Griffith (12) stated that: "For very large values of the parameter Ja, the assumption that the dynamic effects are unimportant is not valid." The maximum Jakob number in those experiments that showed agreement with the asymptotic solution is 119, whereas it is as high as 792 in Cole and Shulman's experiment. The dynamic effect could be important in those runs with high values of Ja.

It was suspected that the reason for the discrepancy is a large mass transfer resistance at the liquid-vapor interface, also known as

* Jakob number, Ja, is defined as

$$Ja = \frac{\Delta T_s \rho_l c_l}{h_{fg} \rho_v} \quad (I-1)$$

In this equation ΔT_s is the liquid superheat, c_l is the specific heat of liquid, h_{fg} is the latent heat of vaporization, ρ_l and ρ_v , respectively, are the liquid and vapor densities. The Jakob number is a measure of the energy excess per unit volume of the liquid relative to the energy required for the formation of the unit volume of vapor.

the nonequilibrium effect.* The theoretical analysis of Bornhorst (25) shows that discontinuities of chemical potential and temperature profiles at the interface during a nonequilibrium phase change process become appreciable at low pressures. The discontinuities can be interpreted as additional resistances to interphase mass and heat transfer. Neglecting this nonequilibrium effect at low pressures could also contribute to the discrepancy.

Therefore, in the light of the above discussion, the objective of the present investigation is to examine under closely controlled conditions these two effects--namely, the dynamic effect and the nonequilibrium effect--upon bubble growth rates, at reduced pressures.

I.3 Purpose of This Work

The purpose of this work is to obtain water vapor bubble growth rates at reduced pressure under known thermal conditions so that the relative importances of the heat diffusion, dynamic, and nonequilibrium effects can be determined. The results may then be used to examine the applicability of existing bubble growth theory under general conditions.

In addition, it was hoped that numerical values of the evaporation coefficient for water might be inferred from the boundary conditions for a clean liquid-vapor interface.

*The nonequilibrium effect is dependent essentially on an empirical quantity called evaporation coefficient. In evaporation, this coefficient is defined as the ratio of the number of molecules per unit surface per unit time that actually escape from the liquid-vapor interface to the maximum evaporation rate predicted by the kinetic theory. Thus its value lies between zero and unity. Exact value of this coefficient has not yet been established (26).

CHAPTER II - REVIEW OF BUBBLE GROWTH THEORY

II.1 Overall Remarks

A bubble starts growing from a critical size nucleus, or nucleation site, in a superheated liquid pool as a result of a thermal fluctuation that upsets the otherwise metastable equilibrium condition. In the process toward a new equilibrium state of the liquid-vapor system, evaporation of the liquid at the bubble boundary maintains the bubble growth; but the bubble is not entirely free to expand, as its expansion is subject to retarding effects of surface tension, liquid inertia, and nonequilibrium interfacial resistance to mass transfer. In addition, the rate of evaporation depends on the rate of heat diffusion into the liquid. The observed bubble growth rate is a result of both of these phenomena acting.

During the earlier phases of bubble growth, the growth rate is small, but it is greatly enhanced with small increases in bubble size since the effects of surface tension rapidly become negligible. With increased growth rate, the latent heat of vaporization causes cooling of the liquid that surrounds the bubble. This cooling decreases the bubble growth rate; therefore, the bubble growth rate reaches a maximum value and then decreases. Eventually, the growth depends solely on the rate at which energy is being supplied from the liquid to the liquid-vapor interface. This heat-diffusion-limited phase of bubble growth is termed the "asymptotic stage."

A theoretical analysis of the bubble growth problem, which has just been described qualitatively, is by no means easy. Mathematical

formulation of this problem involves all three of the conservation equations applied to both the liquid and the vapor phases. It is further complicated by the nonequilibrium interfacial boundary condition. As is to be expected, it is not possible, nor practical or worthwhile, to solve the complete problem exactly. With several major simplifying assumptions, a few limiting cases of bubble growth have been studied and documented in the literature. Three special cases, i.e., growth limited separately by liquid inertia, heat diffusion, and evaporation rate, relevant to the present investigation are briefly reviewed in this chapter.

II.2 General Assumptions

It is appropriate to begin with statements of the various basic assumptions that are common to all the limiting cases to be considered in the following sections. The assumptions have been justified by many investigators (4,7,8,9). The justification statements will not be reproduced here. It suffices to say that solutions thus obtained are applicable only to situations that conform reasonably well to the stated assumptions, or requirements.

In essence, the system consists of a spherical vapor bubble growing in a initially quiescent, uniformly superheated liquid of infinite extent. The analysis will consider only incompressible, inviscid Newtonian liquids. The bubble growth is assumed to be strictly spherically symmetric, and the liquid motion purely radial and laminar. Other assumptions include constant thermophysical properties and liquid density and negligible vapor inertia. Asymmetric external body forces are excluded from consideration. Finally, temperature and pressure gradients within the bubble are neglected.

II.3 Growth Controlled by Liquid Inertia

Lord Rayleigh (3) was first to solve the bubble growth problems from the dynamic point of view. Assuming the growth process to be isothermal, he considered the motion of the liquid as a spherically symmetric, incompressible flow caused by the differences in pressures of the vapor and the liquid phases. Thus bubble growth rate is controlled by the liquid inertia only. His conclusion is that the bubble grows at a constant speed, except during the earliest stage when the bubble radius is small and the surface tension effect is dominant.

Based on the general assumptions, the continuity equation may be written as follows in terms of the bubble radius, R , for constant vapor density and for when it is negligibly small compared to the liquid density.

$$ur^2 = \dot{R}R^2 \quad (\text{II-1})$$

where u denotes the radial velocity of a liquid element at distance r from the center of the bubble. \dot{R} is the bubble growth rate. The coordinate system is shown in Figure 2.

The momentum equation for the liquid phase is

$$\frac{\partial u}{\partial t} + u \frac{\partial u}{\partial r} = - \frac{1}{\rho_l} \frac{dp}{dr} \quad (\text{II-2})$$

where t is time, and p is pressure. The expression for u given by (II-1) can be substituted into (II-2), and the resulting equation can be integrated from the bubble wall out to infinity to obtain the familiar

Rayleigh Equation:

$$\rho_l (\ddot{R}R + \frac{3}{2} \dot{R}^2) = p_v(T_\infty) + p_g - p_\infty - \frac{2\sigma}{R} \quad (\text{II-3})$$

In this equation \ddot{R} is the second derivative of R with respect to time t , $p_v(T_\infty)$ is the vapor pressure at system temperature T_∞ , p_g is the partial pressure of inert gases within the bubble, and σ is the surface tension. The Rayleigh Equation is the foundation of bubble dynamics. This equation relates the dynamic pressure, which is the term on the left-hand side of the equation, to the total pressure within the bubble, the system pressure, p_∞ , and the pressure drop across the bubble wall. Assumption is made for the following considerations that $p_g = 0$; that is, the bubble contains no inert gases. It can be shown that, for equilibrium, $p_v(T_\infty)$ and p_∞ are related to the critical radius R_c by the expression

$$R_c = \frac{2\sigma}{p_v(T_\infty) - p_\infty} \quad (\text{II-4})$$

In terms of R_c , Equation (II-3) can be recast in the following form:

$$\frac{1}{2R^2} \frac{d}{dt} (R^3 \dot{R}^2) = \frac{1}{\rho_l} \left(\frac{2\sigma}{R_c} \right) \left(1 - \frac{R_c}{R} \right) \quad (\text{II-5})$$

With the initial conditions $\dot{R} = 0$ and $R = R_c$ at $t = 0$, Equation (II-5) can be integrated to obtain

$$\dot{R}^2 = \frac{4\sigma}{3\rho_l R_c} \left(1 - \frac{R_c^3}{R^3} \right) - \frac{2\sigma}{\rho_l R} \left(1 - \frac{R_c^2}{R^2} \right) \quad (\text{II-6})$$

For $R \gg R_c$,

$$\dot{R}^2 = \frac{4\sigma}{3R_c \rho_l} = \frac{2}{3} \frac{p_v(T_\infty) - p_\infty}{\rho_l} \quad (\text{II-7})$$

This is the liquid inertia controlled bubble growth equation. It will also be referred to as the Rayleigh solution. The significance

of this result is that the bubble grows at constant speed; hence the bubble radius is directly proportional to the growth time.

In the derivation of Equation (II-7), the driving force $\Delta \bar{p} = p_v(T_\infty) - p_\infty$ was assumed to be constant. But in reality, the actual driving force is less than $\Delta \bar{p}$ due to the cooling effect of evaporation; hence the Rayleigh solution gives an estimate of the upper limit of bubble growth rate under any circumstances.

II.4 Growth Limited by Heat Diffusion

Plesset and Zwick (4, 5, 6) as well as Forster and Zuber (7) and others (8, 9) studied the asymptotic growth of a spherical bubble in uniformly superheated liquid and found that the bubble growth rate is inversely proportional to the square root of growth time. In this case, the nonequilibrium effect is ignored by assuming thermodynamic equilibrium at the bubble wall. The solution of Plesset and Zwick is presented below.

The problem is formulated as a heat transfer problem coupled with a dynamic problem. Hence in addition to the equations of continuity and momentum conservation, the energy equation is introduced into the analysis. The energy equation appropriate for the liquid phase is

$$\frac{\partial T}{\partial t} + u \frac{\partial T}{\partial r} = \alpha_l \left(\frac{\partial^2 T}{\partial r^2} + \frac{2}{r} \frac{\partial T}{\partial r} \right) \quad (\text{II-8})$$

where T denotes the liquid temperature $T(r)$, and α_l is the thermal diffusivity of liquid. Equations (II-1), (II-2), and (II-8) together with the following initial and boundary conditions completely specify the problem of asymptotic bubble growth.

The initial conditions are:

$$T = T_{\infty} \text{ for all } r, t = 0, \quad (\text{II-9})$$

$$\dot{R} = 0, t = 0 \quad (\text{II-10})$$

$$R = R_c, t = 0, \quad (\text{II-11})$$

and the boundary conditions,

$$T = T_{\infty}, \quad r \rightarrow \infty \quad (\text{II-12})$$

$$k_l \left(\frac{\partial T}{\partial r} \right)_{r=R} = \rho_v h_{fg} \dot{R} \quad (\text{II-13})$$

where k_l is the thermal conductivity of liquid, and h_{fg} is the latent heat of vaporization. Equation (II-13) is a simplified form of the complete boundary condition at the bubble wall, obtained by applying the first law to a control volume consisting of the vapor bubble.

Simplification was made by neglecting smaller terms due to desuperheating of vapor molecules and pdv work of expansion. Justification of this simplifying measure is given in Reference (51).

In order to solve the heat transfer part of the problem, Plesset and Zwick made a "thin thermal boundary layer" assumption. They assumed that "the drop in temperature from T_{∞} to the value T at the bubble wall takes place in a layer of liquid surrounding the bubble which has small thickness compared with $R(t)$." It is justified physically in the cases where the thermal diffusivity of liquid is small. Employing a successive approximation technique, Plesset and Zwick obtained a solution for the temperature at the bubble wall, for which the zeroth-order approximate expression is

$$T = T_{\infty} - \left(\frac{\alpha_l}{\pi}\right)^{1/2} \int_0^t \frac{R^2(x) \left(\frac{\partial T}{\partial r}\right)_{r=R(x)}}{\left[\int_x^t R^4(y) dy\right]^{1/2}} dx . \quad (\text{II-14})$$

The value of T thus calculated was estimated to be accurate within 10 percent. With the expression for T given by (II-14), Plesset and Zwick then solved the dynamic part of the problem. The solution for the asymptotic stage of bubble growth was in the form of an infinite series, of which the leading term can be reduced to

$$R = \left(\frac{12}{\pi}\right)^{1/2} Ja(\alpha_l t)^{1/2} . \quad (\text{II-15})$$

Although Plesset and Zwick attempted to account for the effect of temperature variation at the bubble wall, the above equation does not include any effect of this nature. It can be seen that the driving force $\Delta T_s = T_{\infty} - T_{sat}(p_{\infty})$ contained in the Jakob number, Ja, is a fixed value. Thus Equation (II-15) is expected to be applicable only to the isobaric bubble growth problems. In other words, the pressure field, within and without the bubble, is uniform and is equal to p_{∞} .

Other investigators have obtained similar solutions for the same problem, with only slight differences in the value of the coefficient ϕ , which is defined in the following equation:

$$R = \phi Ja(\alpha_l t)^{1/2} . \quad (\text{II-16})$$

Table II-1 lists the values of ϕ obtained by different investigators.

TABLE II-1

Comparison of the Coefficient ϕ

<u>Investigator(s)</u>	<u>Value of ϕ</u>	<u>Reference</u>
Plesset and Zwick	$\sqrt{12/\pi}$	(4)
Scriven	$\sqrt{12/\pi}$	(8)
Forster and Zuber	$\sqrt{\pi}$	(7)
Fritz and Ende	$2/\sqrt{\pi}$	(21)
Birkhoff, et al	$\sqrt{12/\pi}$	(9)

It has been mentioned in Chapter I that the asymptotic solution, Equation (II-16) with $\phi = (12/\pi)^{1/2}$, or Equation (II-15), compares well with experimental data obtained at high pressures. Forster and Zuber's solution underestimates the bubble growth rates by 9 percent, at high pressures.

II.5 Growth Limited by Evaporation Rate

Kinetic theory predicts a finite rate of evaporation. As a consequence, there is a possibility that the growth rate of a bubble might be limited by the evaporation rate. Recently a bubble growth equation based on this concept has been developed (27, 28). This equation is derived in the following paragraphs.

First of all, consider a liquid-vapor system which is in equilibrium at interfacial temperature T_1 . For equilibrium, the number of molecules entering and leaving the phase boundary must be equal, as must the molecular velocities since no net energy is being transferred. According to the kinetic theory, the mass flux of vapor molecules striking a surface is

$$w' = \frac{p_i}{(2\pi R_g T_i)^{1/2}} \quad (\text{II-17})$$

where w' = mass flow rate of molecules striking unit surface area in unit time.

p_i = saturation vapor pressure at T_i

R_g = gas constant per unit mass of gas.

If a fraction σ_c of the w' unit of mass condenses on the liquid-vapor interface, then in order to maintain equilibrium conditions, it is necessary to have w units of mass evaporate from the interface per unit area per unit time, with

$$w = \frac{\sigma_c p_i}{(2\pi R_g T_i)^{1/2}} \quad (\text{II-18})$$

The fraction σ_c is referred to as "condensation coefficient" or "mass accommodation coefficient." In the similar fashion, an "evaporation coefficient" σ_e is defined.

Schrage (30) investigated the mass transfer problem in a slightly nonequilibrium liquid-vapor system. In the case of evaporation, the interfacial mass transfer rate was found as

$$w = \left(\frac{1}{2\pi R_g}\right)^{1/2} \left(\frac{\sigma_e p_i}{T_i^{1/2}} - \frac{\sigma_c \Gamma p_v}{T_v^{1/2}}\right) \quad (\text{II-19})$$

in which p_i and p_v are the saturation pressure corresponding to the interface temperature T_i and the vapor temperature T_v , respectively.

Γ is a correction factor that takes into account the effect of vapor velocity. For small mass transfer rates, the factor Γ is given by the following approximate expression (30):

$$\Gamma = 1 - \frac{w}{p_v} \cdot \left(\frac{\pi R T_i}{2} \right)^{1/2} \quad (\text{II-20})$$

At equilibrium when there is no net evaporation, $w = 0$. Then $\Gamma = 1$, $p_i = p_v$, and $T_i = T_v$. Thus $\sigma_e = \sigma_c$. For small mass transfer rates, if it is assumed that $\sigma_e = \sigma_c$, then the expression for w becomes

$$w = \sigma_e \left(\frac{1}{2\pi R_g} \right)^{1/2} \left(\frac{p_i}{T_i^{1/2}} - \frac{\Gamma p_v}{T_v^{1/2}} \right) \quad (\text{II-21})$$

Equation (II-21) implies discontinuity of the temperature distribution at the interface. The vapor pressure and temperature are assumed uniform up to the interface; thus the vapor molecules striking the interface are characterized by the temperature T_v . On the other hand, the molecules escaping the interface are identified by the interface temperature T_i . The interfacial temperature drop is

$$\Delta T_i = T_i - T_v \quad (\text{II-22})$$

With the help of the perfect gas law, the Clausius-Clapeyron equation, and assuming $T_v^{1/2} = T_i^{1/2}$ in the denominator of the brackets of Equation (II-21), the latter can be combined with (II-20) and (II-22) to give (29)

$$w = \frac{2\sigma_e}{2 - \sigma_e} \left(\frac{1}{2\pi R_g T_v} \right)^{1/2} \frac{h_{fg} \rho_v \Delta T_i}{T_v} \quad (\text{II-23})$$

In the bubble growth problem, the quantity w is simply

$$w = \rho_v \dot{R} \quad (\text{II-24})$$

The bubble growth rate \dot{R} is therefore

$$\dot{R} = \frac{2\sigma_e}{2 - \sigma_e} \left(\frac{1}{2\pi R_g T_v} \right)^{1/2} \frac{h_{fg} \Delta T_i}{T_v}$$

The growth rate R can be evaluated by means of (II-25) provided the value of σ_e is known. The evaporation coefficient must be determined experimentally. Unfortunately at the present time, we are not certain of the value of this empirical coefficient due to lack of precision in temperature-measuring techniques. For many years the evaporation coefficient of clean water has been accepted as 0.04. But more refined experiments in recent investigations (31,32,33,34) have raised the value to approach the theoretical upper limit, unity. A collection of experimental values of the evaporation or condensation coefficient of water is tabulated in Table II-2. It is evident from Equation (II-25) that if σ_e turns out to be of order 0.01, the evaporation rate will govern the bubble growth. If σ_e is close to unity, then it will have negligible effect.

In Equation (II-25) the driving force is ΔT_i , or the temperature drop at the interface. Since in this special case the evaporation rate is the only controlling factor of bubble growth, the driving force has been assumed by Shai (27) and Labuntsov et al (28) as equal to ΔT_s , or the superheat of the system. In this way, it is questionable whether the calculated growth rate has any practical significance.

As far as the prediction of limiting bubble growth rate is concerned, Equation (II-25) has no value at all in view of the fact that the exact value of σ_e has not been determined and that ΔT_i cannot be estimated.

II.6 Comparison of Bubble Growth Equations

The liquid inertia controlled and the heat diffusion limited bubble growth equations are quite different in nature. It is interesting to compare the growth rates predicted by these equations for identical sets

TABLE II-2

Experimental Values of the Evaporation or
Condensation Coefficient of Water

(References 32, 33, 34, 35)

<u>Coefficient σ_e</u>	<u>Temperature, $^{\circ}\text{C}$</u>	<u>Investigator</u>
.006 - .016	18 - 60	Alty (1931)
.01 - .02	18 - 60	Alty (1931)
.04	-8 - +4	Alty (1933)
.036	15	Alty (1935)
.02	100	Pruger (1940)
.045	20	Hammeche (1953)
.04	30	Boudart (1962)
.0415	0	Delaney (1963)
.0265	43	Delaney (1963)
.42	0	Hickman (1954)
.35 - 1*	7 - 50	Nabavian (1963)
.35*	0 - 70	Jamieson (1964)
Close to 1*		Berman (1963)
Close to 1*		Mills (1967)

*This is the condensation coefficient. It can be shown that at thermal equilibrium, the condensation and the evaporation coefficients are equal.

of conditions under which a bubble grows. Table II-3 shows the comparison for six different arbitrary conditions. In the heat diffusion limited case, growth rates were evaluated at $R = 2$ cm.

Since the liquid inertia controlled growth equation yields maximum rates of bubble growth, it is observed from Table II-3 that the asymptotic solution overestimates growth rates for liquid metals and water at reduced pressure. With water, at atmospheric pressure, the growth is definitely heat diffusion limited. But at the same pressure, the growth rates calculated by means of both equations are about the same in the case of liquid metals. This comparison shows that dynamic effect can be significant, but the observations are by no means conclusive. From the data of two water-vapor bubbles, an apparent switchover from the heat diffusion limited growth at high pressure to the liquid inertia controlled growth at low pressure can be noticed. Quantitative analysis of this phenomena in the subsequent chapters leads to the establishment of a criteria with the aid of which one can choose with ease the appropriate bubble growth equation when calculating bubble growth rates under general conditions.

TABLE II-3

Comparison of Theoretical Bubble Growth Rates

<u>Fluid</u>	P_{∞}	ΔT_s	<u>Growth Rate, m/sec</u>	
			<u>Liquid Inertia</u>	<u>Heat Diffusion</u>
Mercury*	1.0 bar	50 °C	2.7	3
Mercury*	.02 bar	50 °C	0.7	6×10^3
Sodium*	1.0 bar	50 °C	8	10
Sodium*	.02 bar	50 °C	1.5	2×10^4
Water	14.7 psia	5.6 °F	2.86	1.38×10^{-3}
Water	.176 psia	23.9 °F	1.04	78

* The liquid metal data were taken from Reference (28).

CHAPTER III - APPARATUS AND PROCEDURES OF EXPERIMENT

III.1 Experimental Methods

An apparatus has been designed to generate bubble-growth-rate data at reduced pressure. The purpose of the experiment is to take high-speed movie pictures of single bubbles growing in a uniformly superheated pool of water. Growth-rate data are then obtained from the bubble history recorded in the film.

The major design problem of this experiment is the necessity to meet the requirements that:

1. test water must be heated evenly to a predetermined temperature without any disturbance prior to the regulated nucleation of a single bubble in the bulk of water; and
2. bubble formation must be activated only upon command both in time and place in order to synchronize the high-speed movie camera operation with the bubble event and to permit proper focusing of the photographic equipment.

The method of Dergarabedian as described in Reference (10) was adopted in this experiment. Dergarabedian demonstrated the feasibility of attaining fairly uniform temperature in a pool of superheated water by radiation heating. However, he had no control over the formation of bubbles at all. In his experiments bubbles formed randomly both in time and in space within the beaker. Hence the probability of recording sharp and clear images of a bubble on a strip of film 50 feet long which runs through the camera in about 1/2 sec. is very small. The addition of a bubble-triggering device would certainly be a positive improvement

over Dergarabedian's original method. Such a device has been developed and used in this work. A description of this device is given in Section III.1.2.

Experimental methods that approximately meet the two requirements are discussed in the following sections.

III.1.1 Attainment of Uniform Water Temperature

Two 250-watt infrared lamps were used to heat the distilled, degassed water, which was held in a pyrex glass container located between the lamps. Using this arrangement, water can be heated slowly, and more or less uniformly, but without excessive temperature gradient in the vicinity of the container wall. With special care of the cleanliness and smoothness of the inner wall, very high superheat condition is obtainable. Depending on the system pressure, superheat as high as 30 °F has been attained without incipience of nucleate boiling.

The reason for the success of this method has been given by Dergarabedian. Briefly, the infrared lamp emits radiation energy at the tungsten-filament temperature, which is approximately 2500 °K for a line voltage of 115 volts. The wavelength corresponding to the maximum energy output is about 1.16 μ ($\mu = 10^{-4}$ cm). The construction material of the water container, pyrex glass, has the special property that it is transparent to radiation emitted at wavelengths between 0.3 μ to 3 μ , but it absorbs essentially all the radiant energy beyond 3 μ . Thus the container walls transmit roughly 80 percent of the energy supplied from the source. Water itself is an excellent absorber of infrared radiation (36). The overall result is that the temperature of the container wall, due to its

high heat capacity, is not much higher than that of the main body of water. Heat conduction in the water flatten out the nonuniform temperature distribution.

Dergarabedian measured the water temperature with a mercury-in-glass thermometer and found the temperature was raised in a uniform fashion. Preliminary test runs of this work detected, however, a slight stratification of water temperature distribution. The deviations were only a few degrees Fahrenheit though. During the course of these runs, it was observed that water evaporated continuously from the free surface. Thus the temperature in the neighborhood of the free surface is expected to be closer to the saturation value than the presumed constant superheat temperature of the bulk. The evaporation problem was eliminated by covering the water with silicon oil. According to Drummond (37), oil film of considerable thickness is necessary to effectively curb the evaporation of water. In the formal runs, the test water was covered with a layer of oil about 1/8 inch in thickness.

Under vacuum conditions, measurements made with a copper-constantan thermocouple showed no appreciable variation in temperature levelwise, and a maximum difference of 0.5 °F over a height of 1 inch in the central part of water body where a bubble was expected to grow. This nonuniformity in water temperature is considered tolerable.

III.1.2 Method of Bubble Generation

Boiling in the bulk of superheated liquid is not a spontaneous process. Bubbles form only at points of discontinuity, or nucleation sites, within the liquid. These sites could be inert gas or vapor bubbles of critical size, or solid particles suspended in the liquid.

In order to make a bubble growing at a desired spot in the liquid, it is therefore necessary to provide a nucleation site right there. In this experiment the need to assume positive control over the timing and the location of bubble formation calls for the development of a technique capable of generating artificial nucleation site at command. The idea is to cause a small localized disturbance in the superheated liquid.

The feasibility of employing the ultrasound focusing method (38) used in neurosurgery was first investigated. This method enables one to focus precisely controlled bursts of high intensity ultrasound at specific points in the brain in such a manner that there are minimal or zero effects in the surrounding regions. The principle involved is as follows: Radio-frequency power developed by a tuned-plate triode oscillator is applied to a quartz crystal transducer. By the piezoelectric effect of the crystal, pressure waves are generated which then pass through a focusing lens located adjacent to the transducer and concentrate at the desired spot. Unfortunately, this method was found unsuitable for operating conditions involving high temperatures, besides other experimental difficulties.

A mechanical version of the acoustic focusing method was then examined. A beaker made of a section of pyrex glass tubing with a plexiglas focusing lens attached at the bottom was constructed. The lens was placed in contact with the end of an inverted conical wave guide, the apex of which was to be subjected to an impulsive force. This force generates pressure waves which, after passing through the wave guide and the lens, are concentrated at the focusing point, which

is within the liquid, of the lens. In principle if the applied force is large enough, this concentration of energy should disturb the unstable liquid phase sufficiently to trigger bubble formation. The apparatus was tested and found to be unsuccessful. In all the test runs a great number of bubbles emerged at spots other than the expected one when the external impulses were suddenly applied. It appears that the high density of nucleation sites on the container walls more than compensated for the less severe pressure disturbances occurring away from the point at which the sound was focused.

After the attempts to apply these ideal techniques, which have the advantage of not disturbing the system where necessary, turned out to no avail, it was thought that a device similar to an automobile spark plug might serve the purpose. In the bubble experiment, a seed bubble could be created by electrolytic gases generated by passing electric current through a narrow gap between two wire electrodes submerged in water. The presence of these electrodes in the system is certainly not desirable. But its effects on bubble growth can be minimized by using the smallest possible size of wires. Based on these underlying principles, a bubble-triggering device has been successfully developed.

A sketch of this device is shown in Figure 3. The major element is simply two chromel wire electrodes facing each other with their tips slightly apart. The electrodes are supported by a frame that has provision for alignment and fine adjustment of the gap between the electrode tips and are connected to a D.C. power source in parallel with a capacitor. Electric current is introduced into the trigger system by discharging the capacitor.

Chromel is used as electrode material primarily because the electrodes must be placed in water for a prolonged period of time. The smooth surface of drawn metal wire makes it difficult for bubbles to form randomly on the wire. The wire diameter should be as small as possible. Taking into consideration the required stiffness of these electrodes, wires 0.005 inch in diameter (36 gauge) were used.

Appropriate values of the capacitance of the capacitor, C, and the voltage, E, for successful operation of this device were determined by experimental means. It was found that a combination of $C = 10^{-4}$ μfd and $E = 250$ volts gave satisfactory results for slightly superheated water at 1 atm. The energy introduced into the system was 3×10^{-9} Btu. This is a very small amount indeed as compared to the latent heat requirement for the formation of a vapor bubble 1/8 inch in diameter, which is equal to $h_{fg} \rho_v V$, or 2.14×10^{-5} Btu. In another set of preliminary runs under the condition of 70 °F and 15 mm Hg. abs., it was necessary to increase the energy input by an order of magnitude. Still, this increased input is within the acceptable level without seriously disturbing the thermal condition of the system.

Numerous test runs proved the reliable performance of this device. A single bubble forms promptly upon the discharge of the capacitor, provided a proper gap is maintained between the electrodes. Experience shows that proper spacing between the electrode tips is vital to the success of this device. Optimum spacing was found by trial and error to be about one thousandth of an inch when the line voltage was 300 volts.

Some interesting observations were made during the early stages of the development of the bubble-triggering device. More than once, pictures of a pair of twin bubbles were obtained. On these occasions, the electrode tips were far apart, and the voltage high. It is thought that, with proper modification, the device could be used to study the coalescence phenomena of two bubbles. With the wires touching each other, a pulse of electric current that would otherwise produce a bubble failed to trigger one. Instead, the electrodes fused together.

As can be seen from Figure 4, a bubble triggered by this device envelopes the electrodes. Question arises as to whether the presence of the electrode has significant influence on the bubble growth.

To consider the worst case, let's assume that the electrode temperature is equal to the liquid temperature T_{∞} ; the vapor temperature within the bubble is T_v . The energy excess contained in that part of the electrode which is enveloped by the bubble is equal to

$$\left(\frac{4}{\pi} D_e^2\right) \cdot D_b \rho_e c_e (T_{\infty} - T_v) .$$

In this D_e and D_b denote the diameters of the electrode and the bubble, and ρ_e and c_e the density and the specific heat of the electrode, respectively. The latent heat required to form a vapor bubble whose diameter is equal to D_b is, roughly,

$$\frac{\pi}{6} D_b^3 \rho_v h_{fg} .$$

The ratio of the above two expressions gives an indication of the maximum magnitude of heat interaction between the electrode and the bubble.

The ratio is, after simplification,

$$\frac{3}{2} \left(\frac{D_e}{D_b} \right)^2 \cdot \frac{\rho_e c_e (T_\infty - T_v)}{\rho_v h_{fg}} = \text{Ratio} .$$

If the value of this ratio is small, then the effect of the electrode on the bubble growth is expected to be negligible. Calculations have been made, and the magnitude of this ratio is shown in the following tabulation for bubbles representing the extreme cases presented in the next chapter. It can be seen that this effect can be appreciable at small bubble radii; however, the effect decreases in proportion to the inverse square of the bubble diameter.

	<u>Bubble B1</u>		<u>Bubble B8</u>	
Radius, cm	.1076	.4663	.1529	.3990
Ratio	.674	.0528	.128	.0201

The electrodes have some effect on the bubble shape, as one can notice slight changes in bubble curvature in the vicinity of the electrodes (Figure 4). However, this minute effect is no cause for concern because the bubble is not perfectly spherical anyway, and the error caused by the electrode effect is far less than the error resulting from using the greatly simplified method to estimate the equivalent radius of nonspherical bubble (24). At most, the bubble is affected appreciably by the electrodes only when the bubble size is quite small.

It is believed that the effect of the electrodes on bubble growth is negligible during most of the bubble life. This is borne out by the result of attempts to reproduce atmospheric bubble growth data of

Dergarabedian (10), using the bubble-triggering device. Satisfactory agreement between the two sets of data is evident, as can be seen in Figure 5.

III.2 Description of Apparatus

The apparatus consists of a test section, a vacuum system, two heating lamps, photographic equipment, instrumentation, and auxiliary equipment. Schematic of the apparatus as well as a photograph of the actual experimental setup are shown in Figures 6 and 7. Major pieces of equipment are described below.

Test Section

Figure 8 shows a close-up picture of the test section, which includes a water container, the bubble trigger, a thermocouple well, and appropriate supports. The water container was made of two segments of a pyrex glass tubing 2-1/2 inches in diameter and 4 inches long, two pieces of 1-1/2-inch by 4-inch pyrex glass plates, and a bottom plate of the same material. The flat plates were built in for photographic purposes, and the curved segments made it easier to clean the container, especially at the four corners. These pieces were fused together to form a container, the inside walls of which were annealed carefully to obtain smooth surfaces free from scratches and pits. Before each experiment the container was cleaned with a glass cleansing detergent and rinsed with distilled water. These special precautions are necessary in order to eliminate nucleation sites on the container wall.

The two electrodes of the bubble trigger were of such a size as to be accommodated in the water container. The relative position of

the electrodes and the container can be seen from Figure 8. Also shown in the figure is a 3mm glass tube which is sealed at the bottom end. This tube contains a copper-constantan thermocouple for water temperature measurement. The test section is placed inside the vacuum system, with a pair of glass dishes, served as an insulating seal, separating the container from the steel base plate of the vacuum system. The whole assembly is located between two infrared heating lamps.

Vacuum System

A bell jar, a steel base plate, together with a vacuum pump and necessary piping were used to provide the required vacuum environment. The jar is made of heavy molded pyrex glass, with a 7/8-inch opening in the top. The inside height of the straight section of the jar is 15 inches, and the inside diameter is 8-3/4 inches. Two flat glass windows approximately 2 inches in diameter were installed on the bell jar for optical reasons. The base plate, 10-3/4 inches in diameter, was provided with an O-ring groove to accommodate an O-ring seal between the plate and the jar, and with outlet connection to a CENCO HYVAC 2 two-stage vacuum pump. The base plate and the vacuum pump were connected with rubber tubings, with provisions for connection to a manometer for pressure measurements, a metering valve for adjusting the pressure in the system and for a liquid nitrogen trap where moisture and oil vapors were condensed before reaching the pump. Despite some leakage, the system was capable of maintaining a minimum pressure of 5 mm Hg abs.

Photographic Equipment

A General Radio streak camera plus a General Radio type 1538-A stroboscope, a condensing lens, and Eastman High-Speed 35 mm Type 5305

Safety Film were used for photography purposes. The camera was fitted with a fl.5 Wollensak 2-inch lens.

Instrumentation

In order to facilitate recording of the bubble history, the camera along with a number of other instruments were integrated electrically with the bubble trigger. The wiring diagram shown in Figure 9 gives the details. Synchronization of the camera with the bubble growth event is achieved by the following arrangements:

1. Both the camera and the delay timer are put into operation at the same time when the whole control system is connected to the external AC power source by pushing on the main switch. The delay timer makes it possible for the film speed to reach a constant value before a bubble is triggered. The strobe flashes at a predetermined speed, independent of this control system.
2. Once the preset delay time is up, the delay timer energizes the mercury wetted contact relay, which in turn discharges the capacitor, causing the formation of a bubble. In this way, pictures of the bubble can be taken while it is growing.
3. After the camera runs out of film, which is 50 feet in length, the operation is completed by turning off the main switch manually.

The operating condition of each experimental run is specified by only two variables, namely, the system pressure p_{∞} and the water temperature T_{∞} . A copper-constantan thermocouple, made of 30-gauge wires by a thermocouple welder, was used to measure water temperature. It was placed in the thermocouple well, which has been described under Test Section. The tip of this thermocouple was approximately levelled with

the electrode tips of the bubble trigger. The well was filled with silicon oil in order to obtain better measurements of the bulk water temperature. Since the absorptivity of the thermocouple material is different from those of oil, water, and glass, the temperature measured by the thermocouple is higher than the water temperature when the heating lamp is on. Thus the procedure of experiment is to cut off the heating source for a few minutes before taking the temperature reading and triggering the bubble. This ensures thermal equilibrium between the thermocouple and water. The thermocouple output was read from a Leeds and Northrup potentiometer. With the temperature measuring equipment properly connected, the thermocouple was calibrated at the boiling point and the ice point of water. It was also calibrated at room temperature with a Will Scientific precision grade fractional degree mercury-in-glass thermometer. A calibration curve was constructed from these three calibration points. The curve appears to be linear. But there is some doubt about the linearity of this curve. The slight nonuniformity of the bulk water temperature also contributes to the measurement errors. The overall uncertainty in temperature measurement due to calibration and temperature uniformity is estimated to be ± 0.5 °F.

The system pressures were measured with a Manostat Absolute Manometer. The working fluid was mercury. With the system connected to this manometer, the resulting mercury level in the manometer tube was read by a vernier on the plastic scale. The uncertainty in pressure measurement is estimated to be ± 0.2 mmHg.

Auxiliary Equipment

An oil applicator, placed through the top hole of the bell jar, was used to apply silicon oil film on the water surface under vacuum conditions.

The applicator is a pyrex funnel with a built-in pinch valve. The bottom end of it is attached to a piece of bented plastic tubing, the opening of which is located 1/2 inch above the water. With this arrangement, oil can be applied slowly to cover the water without being entrained in the interior of it. The superstructure, shown in Figure 7, above the bell jar contains a crank that facilitates rapid removal and replacement of the jar.

III.3 Experimental Procedures

The preparatory work for each run includes degassing the water, cleaning the water container, loading the film, and checking the instruments. Deaeration of water is very important in that the dissolved air in water could act as nucleation sites when the water is superheated. For the subsequent analysis of experimental data, it is desirable to estimate the amount of air contained in the testing water. Thus water degassing is carried out in two stages. The first stage is done with the water being exposed to the atmosphere. Approximately 1000 ml of distilled water, contained in a narrow-neck beaker, is heated by a Bunsen burner. After two hours of heating, the volume of water decreases to about 500 ml. At this stage the air content of water has been reduced, but the exact amount of air is not known. The beaker opening is then sealed with a rubber stopper to prevent the partially degassed water from being exposed to the environment and is then cooled down to room temperature. The second stage of degassing is performed at reduced pressure without heating. The treated water is introduced into the system, and the system pressure is reduced to a value at which pool boiling of water take place. This process has the effect of extracting

more air out of water, and gradually the water ceases to boil. The system pressure is then reduced, step by step, to about 10 mm Hg abs. This degassing pressure is maintained for about thirty minutes before the silicon oil is applied to cover the water.

After this elaborate treatment, it is fair to assume that the test water contains a saturated amount of dissolved air corresponding to the degassing pressure. The amount of air can be estimated by Henry's Law (41).

With the water properly treated and the apparatus in order, it is a simple matter to obtain a bubble growth film. The desired operating condition can be attained quickly by radiation heating and by pumping. The strobe is then put into action. After shutting off the heating lamps for a few minutes to allow the thermocouple and the water to reach thermal equilibrium, the main switch is turned on, and a new baby bubble is born. Pressure and temperature readings were taken immediately before this moment.

The success rate of this experiment is better than 70 percent. A few cases of failure were due to improper spacing between the electrodes of the bubble trigger and due to inadequate cleaning of the water container. The data produced by this method are highly reproducible, as can be seen by comparing the two bubble growth curves, Figures 17 and 18. These two curves were obtained under almost identical conditions.

CHAPTER IV - EXPERIMENTAL RESULTS AND DATA REDUCTION

IV.1 Experimental Results

Experimental data of eight(8) bubbles have been analyzed and are reported in this thesis. The bubbles are identified as "B" bubbles in order to avoid any confusion when comparing data of other investigators. The operating conditions under which these eight bubbles were obtained are tabulated below:

TABLE IV-1

Operating Conditions of B Bubbles

<u>Bubble Number</u>	<u>System Pressure, P_{∞}</u>	<u>Superheat, ΔT_s</u>	<u>Jakob Number, Ja</u>
B1	0.1759 psia	23.95 °F	2370.0
B2	0.1831	28.34	2690.0
B3	0.5922	3.09	95.6
B4	0.5962	16.56	509.1
B5	1.8259	19.21	201.1
B6	1.9345	13.21	130.8
B7	5.6072	16.21	57.5
B8	5.6324	16.42	58.0

In this table, the pressure P_{∞} includes correction for hydrostatic pressure which was determined from the height of water and oil column above the electrode tips. A set of pictures of a typical bubble is shown in Figure 4. These pictures were obtained with a film speed

of two thousand frames per second. Thus the time interval between two frames is 0.0005 sec. The glass tube containing a thermocouple also appears in the picture. This tube was used as a reference object with the aid of which the actual bubble sizes were deduced. The films on which the bubbles were recorded have been analyzed frame by frame with a Nikon Measurescope. Under this scope, the pictures were magnified, and measurements were made of the major and the minor diameters of each bubble and of the outside diameter of the glass tube. These data, together with the known size of the glass tube, were used to calculate the equivalent radii of the bubbles. The definition of the equivalent bubble radius and the way the bubble growth time is determined are discussed in the next section. Tabulations of the bubble radius, growth time, and other pertinent data are given in Appendix B. The resulting radius-time curves are shown in the upper halves of Figures 11 through 18, and the results are discussed in Chapter V.

IV.2 Data Reduction

The procedures used in reducing the experimental data are shown in the Flow Diagram of Data Reduction, Figure 10. Most of the numerical calculations were done by an IBM 1130 computer. The end results are presented in Appendix C. The following is a detailed discussion on various assumptions and equations used in the data reduction program.

IV.2.1 Assumptions and Equations for Data Reduction

Equivalent Bubble Radius, R

The bubbles are not perfectly spherical, thus it is necessary to find an equivalent radius for each bubble. Since the shape of the bubbles resemble that of a spheroid characterized by its major and minor diameters

b and a, the equivalent bubble radius R is defined arbitrarily as the radius of a sphere having the same volume as a spheroid of diameters b and a. The bubble radius can therefore be calculated according to the following equation (24)

$$R = \frac{d}{2d_1} (ab^2)^{1/3} \quad (\text{IV-1})$$

where d = apparent O.D. of the glass tube measured from the film

d_1 = actual O.D. of the tube.

Figure 4 shows that the bubbles in general are nearly spherical; hence no gross error results from using Equation (IV-1) to calculate the equivalent radius.

Bubble Growth Time, t

Since the time interval between successive frames of the picture is constant, a plot of radius versus frame number is equivalent to a radius-time curve. The zero time is determined by extrapolating the curve to $R = 0$; this is justified because the critical radius is very small. The time $t(1)$ corresponding to the first visible bubble recorded in film is then determined graphically. If a frame number I, $I = 1, 2, 3 \dots$, is assigned to each frame starting from the first one in which the bubble appears, then the growth time $t(I)$ corresponding to frame No. I is

$$t(I) = t(1) + 0.0005 (I - 1) \text{ in seconds.} \quad (\text{IV-2})$$

Evaluation of \dot{R} and \ddot{R}

Values of \dot{R} and \ddot{R} at time t are obtained by successive differentiation of the function $R = R(t)$ with respect to time. For each set of data, this function is obtained by fitting all the data points by the least

square method. Comments on curve fitting are presented in Appendix E. Naturally, errors inherent in the equation $R = R(t)$ are compounded upon each differentiation operation. In general the fitted curve deviates from experimental data points most for small bubble radius, due to surface tension effect; differences between the calculated and the real values of \dot{R} and \ddot{R} are expected to be considerable when the bubble radius is less than 0.1 cm.

Determination of Thermophysical Properties

Properties of water used in the calculations are: (1) thermal conductivity of liquid, k_ℓ ; (2) surface tension at the liquid-vapor interface σ ; (3) specific heat of liquid, c_ℓ ; (4) latent heat of vaporization, h_{fg} ; (5) specific volume of liquid, v_ℓ ; and (6) specific volume of vapor, v_v . The following table shows the thermodynamic state at which each of these properties was evaluated.

<u>Property</u>	<u>State</u>
k_ℓ	Saturated liquid at T_∞
σ	Saturated liquid at T_∞
c_ℓ	Saturated liquid at T_∞
h_{fg}	Saturated state at P_∞
v_ℓ	Saturated liquid at T_∞
v_v (variable)	Saturated vapor at P_v

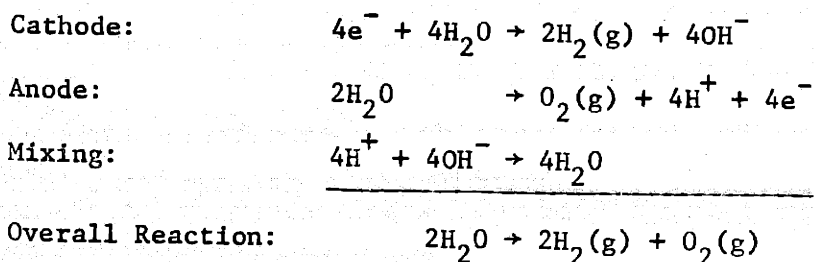
Values of the thermal conductivity k_ℓ are taken from the ASME Steam Tables (42) and those of the surface tension σ from Reference (43). The rest of the properties are based on Keenan and Keyes' Steam Tables (44). For each bubble, all properties except the specific volume of vapor are

assumed as constants. At reduced pressure the value of v_v changes drastically even with small variations of pressure; hence it is evaluated corresponding to the vapor pressure inside the bubble, P_v , which varies with time. To calculate Jakob number, the saturation value of v_v corresponding to the system pressure P_∞ is used.

Amount of Foreign Gases in the Bubble

The bubble contains a certain amount of inert gases which comes from two sources: (1) electrolysis of the water and (2) dissolved air in the liquid. It is shown in Appendix D that the contribution of partial pressure of air to the total bubble pressure is negligible. Electrolysis of water produces oxygen and hydrogen gases the amount of which can be estimated in accordance with Faraday's Law.

Faraday's Law of Electrolysis states that the mass of substance produced at an electrode is proportional to the amount of electricity transferred through the electrode and to the gram-equivalent mass of the substance (40). For water, the reactions are:



The above set of equations can be interpreted as: Four faradays of electricity produces two gram-moles of H_2 and one gram-mole of O_2 . The number of faradays introduced into the system of the present experiment can be deduced from the capacitance C and the voltage E , which have been measured. For example, in the cases of bubbles B1, B2, and B4

through B8, $C = 0.001 \mu\text{fd}$ and $E = 300 \text{ volts}$; hence $Q = CE/96500 = 3.1088 \times 10^{-12}$ faradays. This amount of electricity produces 1.5544×10^{-12} gm-mole of H_2 and 0.7772×10^{-2} gm-mole of O_2 . The numbers of gm-moles of O_2 and H_2 present in Bubble B3 can be calculated likewise.

The amounts of O_2 and H_2 , or n_{O_2} and n_{H_2} , are only approximate values. It is assumed that the electrochemical process happens instantaneously, as the actual reaction time is much smaller than the bubble growth time ($\sim 10^{-3}$ sec). No line losses of electric energy have been taken into account, and the process is assumed isothermal. Subsequent calculations showed that the presence of O_2 and H_2 gases has only slightly noticeable effect on the vapor pressure of the first visible bubble in each set of film. The effect dies out rapidly in proportion to $1/R^3$. Physically this means that the presence of foreign gases in a bubble is important to bubble nucleation, but its effect upon the subsequent growth of the bubble is nil.

Vapor Pressure in the Bubble

The vapor pressure within a bubble at any instant t is calculated in accordance with the Rayleigh Equation

$$P_v = P_\infty + \frac{2\sigma}{R} + \rho_l (R\ddot{R} + \frac{3}{2} \dot{R}^2) - P_g \quad (\text{IV-3})$$

where $P_g = P_{\text{O}_2} + P_{\text{H}_2}$

$$= \frac{3}{4\pi} \frac{(n_{\text{O}_2} + n_{\text{H}_2}) R_u T_\infty}{R^3}$$

or $P_g = \frac{9}{4\pi} \frac{n_{\text{O}_2} R_u T_\infty}{R^3} \quad (n_{\text{H}_2} = 2n_{\text{O}_2}) \quad (\text{IV-4})$

With the use of Rayleigh Equation, the assumptions associated with the derivation of this equation, discussed in Chapter II, are automatically carried over.

P - T, P - v Relationships

To minimize efforts in interpolating the tabulated values of the Steam Tables, the approximate functional relationship between pressure and specific volume of vapor, for each bubble, has been established by fitting five points from the tables to a fourth-order polynomial. The points are chosen in such a way as to cover only the calculated vapor pressure range. In a similar fashion, the relationship between vapor pressure and vapor temperature has also been expressed by a fourth-order polynomial.

Temperature Drop Across Bubble Wall

The temperature drop, ΔT_i , across the liquid vapor interface is defined as

$$\Delta T_i = T_i - T_v . \quad (IV-5)$$

The value of T_v is assumed to be equal to the saturation temperature at the vapor pressure P_v . This assumption implies thermal equilibrium of the vapor phase, up to the bubble wall. The determination of T_i , or the temperature of the interface on the liquid side, presents major difficulty. The expression for the bubble wall temperature, Equation (II-14) which was obtained by Plesset and Zwick with the assumption of thermal equilibrium at the bubble wall, or $\Delta T_i = 0$, apparently does not apply here. In order to estimate T_i , an integral method (45) has been used in the present investigation.

The application of the integral method involves many arbitrary assumptions. First of all, a "thin" thermal boundary layer surrounding the bubble wall is assumed. It is also necessary to assume a self-similar temperature profile in the thermal boundary layer; this assumption means that once the shape of the profile is chosen, it remains unchanged. The temperature T_i can then be back-calculated by extrapolating, to the bubble wall, the assumed temperature distribution from a point which lies at the other end of the thermal boundary layer where the local temperature gradient is approximately equal to zero.

Using the integral technique, one applies the heat conduction equation to the thermal layer and obtains

$$\rho_v h_{fg} \dot{R} = k_l \frac{c_1 (T_\infty - T_i)}{\delta} \quad (IV-6)$$

An energy balance gives

$$\frac{4}{3} \pi R^3 \rho_v h_{fg} = c_2 \delta (4\pi R^2) \rho_l c_l (T_\infty - T_i) \quad (IV-7)$$

In Equations (IV-6) and (IV-7), c_1 and c_2 are constants the values of which depend only on the shape of the assumed temperature profile. δ , the thermal boundary layer thickness, can be eliminated by combining the two equations. The resulting expression for T_i is

$$T_i = T_\infty - \frac{\rho_v h_{fg}}{\rho_l c_l} \left(\frac{\dot{R} R}{3c_1 c_2 \alpha_l} \right)^{1/2} \quad (IV-8)$$

where α_l is the thermal diffusivity of liquid.

With the exception of constants c_1 and c_2 , all other variables that appear on the right-hand side of this equation are known from experimental data. The values of c_1 and c_2 are determined as follows:

If one uses the coordinate system as shown in Figure 19, it can be shown easily that a second-order temperature distribution function of the form (45)

$$\frac{\theta}{\theta_o} \equiv \frac{T - T_i}{T_\infty - T_i} = 2\left(\frac{x}{\delta}\right) - \left(\frac{x}{\delta}\right)^2 \quad (\text{IV-9})$$

satisfies the necessary boundary conditions

$$T = T_i, \quad x = 0 \quad (\text{IV-10})$$

$$T = T_\infty, \quad x = \delta, \text{ and} \quad (\text{IV-11})$$

$$\frac{dT}{dx} = 0, \quad x = \delta. \quad (\text{IV-12})$$

Differentiate (IV-9) with respect to x , and set $x = 0$, then

$$\left[\frac{d\theta}{dx}\right]_{x=0} = 2 \frac{\theta_o}{\delta}. \quad (\text{IV-13})$$

But, according to the integral method,

$$\left[\frac{d\theta}{dx}\right]_{x=0} = c_1 \frac{\theta_o}{\delta}. \quad (\text{IV-14})$$

By comparison between Equations (IV-13) and (IV-14), $c_1 = 2$ if the temperature profile is a second-order one. To find c_2 , one writes

$$\rho_l c_l (T_\infty - T_i) \cdot c_2 \cdot \frac{4\pi}{3} [(R + \delta)^3 - R^3] = 4\pi R^2 \rho_l c_l \int_0^\delta (T_\infty - T) dx. \quad (\text{IV-15})$$

Since δ is assumed to be very small for a "thin" thermal layer and since

$$\frac{T_\infty - T}{T_\infty - T_i} = 1 - \frac{\theta}{\theta_o}, \quad (\text{IV-16})$$

Equation (IV-15) can be simplified to

$$c_2 \delta = \int_0^\delta \left[1 - \frac{2x}{\delta} - \left(\frac{x}{\delta}\right)^2\right] dx. \quad (\text{IV-17})$$

Whence $c_2 = 0.334$. The values of c_1 and c_2 appropriate for other types of distribution functions have also been determined; the results are tabulated below.

TABLE IV-2

Values of c_1 and c_2

<u>Function, θ/θ_0</u>	<u>c_1</u>	<u>c_2</u>	<u>$\sqrt{c_1 c_2}$</u>
$\frac{x}{\delta}$	1.0	0.500	0.707
$2\left(\frac{x}{\delta}\right) - \left(\frac{x}{\delta}\right)^2$	2.0	0.334	0.817
$\frac{3}{2}\left(\frac{x}{\delta}\right) - \frac{1}{2}\left(\frac{x}{\delta}\right)^3$	1.5	0.375	0.750
$2\left(\frac{x}{\delta}\right) - 2\left(\frac{x}{\delta}\right)^3 + \left(\frac{x}{\delta}\right)^4$	2.0	0.300	0.774
$\frac{5}{3}\left(\frac{x}{\delta}\right) - \frac{5}{3}\left(\frac{x}{\delta}\right)^4 + \left(\frac{x}{\delta}\right)^5$	1.67	0.334	0.747
$\sin\left(\frac{\pi x}{2\delta}\right)$	1.57	0.363	0.755
$\operatorname{erf}\left(\frac{x}{\delta}\right)$	4.07	0.157	0.798

It is seen that the assumption regarding the shape of temperature profile is not critical.

Evaporation Coefficient σ_e

The evaporation coefficient σ_e is calculated, for each value of R , according to Equation (II-25) developed in Chapter II.

CHAPTER V - DISCUSSION

V.1 Concerning the Applicability of Existing Bubble Growth Equations

The range of experimental conditions of this investigation varies from those for which the heat-diffusion limited theory is applicable to those under which the liquid inertia appears to be the controlling factor. Between these two extremes, the transition region in which both the heat diffusion and the liquid inertia effects have approximately equal importance has also been covered. The interfacial nonequilibrium effect does not seem to have any significant influence over the bubble growth rates for all the cases investigated in this work. This last statement will be justified in Section V.2.

Analysis of the experimental data leads to the establishment of a simple criteria concerning the regions of applicability of the two existing bubble growth equations, namely, the Rayleigh solution and the Plesset and Zwick's asymptotic solution. A single normalized bubble growth curve has also been constructed from the low-pressure bubble growth data of this work. This curve is believed applicable to the transition region where both the Rayleigh solution and the asymptotic solution overestimate the bubble growth rates. Before introducing these interesting results, we begin with discussions on the relative importances of the liquid inertia and the heat diffusion effects under given conditions.

V.1.1 Relative Importances of Heat Diffusion and Dynamic Effects

The radius versus time curves for all eight bubbles are plotted in the upper halves of Figures 11 through 18. Superimposed on these plots are the growth curves predicted by the Rayleigh solution and the Plesset and Zwick solution, which are reproduced here for convenience.

$$\text{Rayleigh} \quad R = \dot{R}_m t; \quad \dot{R}_m = \left(\frac{2}{3} \frac{P_{\text{sat}}(T_{\infty}) - P_{\infty}}{\rho_l} \right)^{1/2} \quad (\text{V-1})$$

$$\text{Plesset and Zwick} \quad R = \left(\frac{12}{\pi} \right)^{1/2} \text{Ja}(\alpha_l t)^{1/2} \quad (\text{V-2})$$

It is observed from these diagrams that:

1. With pressures about 5.6 psia and the Jakob numbers approximately equal to 60, the experimental curves coincide with those of Plesset and Zwick (Bubbles B7 and B8).
2. With lower pressures and higher Jakob numbers, the theoretical curves lie above the experimental ones.
3. With pressures being reduced to 0.18 psia and Jakob number increased to high values around 2500, the data points approach the Rayleigh curves (Bubbles B1 and B2).

These observations clearly indicate the effects of pressure and Jakob number on the bubble behavior. The physical explanation for this phenomena can best be obtained by studying the accompanying temperature-radius plots of the radius-time diagrams, presented in the lower halves of the same figures. Three different temperatures are shown in each plot: These are T_{∞} , the liquid temperature; T_v , the vapor temperature within the bubble; and $T_{\text{sat}}(p_{\infty})$, the saturation temperature corresponding to system pressure p_{∞} . The temperature difference $\Delta T_s = T_{\infty} - T_{\text{sat}}(p_{\infty})$ is the potential driving force that would have caused the bubble to grow, and the difference $\Delta T_h = T_{\infty} - T_v$ is the actual driving force that causes the bubble growing. ΔT_h accounts for the temperature drop across the thermal boundary layer in the liquid adjacent to bubble wall and across the liquid-vapor interface. On the other hand, the difference $\Delta T_d = T_v - T_{\text{sat}}(p_{\infty})$

shows the effects of liquid inertia and surface tension; this can be seen by inspection of the Rayleigh Equation (Equation II-7). The vapor pressure p_v , and hence vapor temperature T_v , includes the contributions due to surface tension and dynamic effects.

As a bubble gets bigger, surface tension effects die out, and ΔT_d can be attributed to the dynamic effect only. It will be shown in Section V.2 that the temperature drop in the liquid contributes to more than half of the total ΔT_h ; hence ΔT_h is an approximate indication of the heat diffusion effect. Consequently, a comparison of ΔT_h and ΔT_d shows roughly the relative importance of heat diffusion and liquid inertia in their influence over bubble growth.

With this in mind, let's examine the group of temperature versus bubble radius curves carefully. In the case of bubbles B1 and B2, liquid inertia is definitely the dominant factor, as is shown by the large temperature difference ΔT_d in comparison with ΔT_h . Although the magnitude of ΔT_h is small comparing with ΔT_d , it is still sufficiently large to prevent the bubble growth rate from approaching the value predicted by the Rayleigh solution. The discrepancy, for both bubbles, is about 14 percent. The liquid inertia controlled-growth curve is characterized by its linearity; on the other hand, the shape of a heat diffusion limited-growth curve is a parabola, because of the $R \sim t^{1/2}$ relationship.

The curves for the bubbles B7 and B8 show that the temperature difference ΔT_d is practically nil for $R > 0.15$ cm; thus the growth of these bubbles is limited by heat diffusion, and the data in agreement with Plesset and Zwick solution. The slight difference in the case of B8 is

apparently due to improper location of the time origin during the data-reducing process.

The transition region of bubble growth is typified by the behavior of the remaining four bubbles. Temperature-radius curves of this group show the approximately equal effects of liquid inertia and heat diffusion. It can be seen that the dynamic effect diminishes rapidly in the case of B6, with higher pressure and lower Jakob number; but it remains approximately constant in the case of B4, with lower pressure and higher Jakob number. In the latter case, where the dynamic effect is slightly more pronounced than the heat diffusion effect, the R-t curve is linear, and it is closer to the Rayleigh curve than the Plesset and Zwick curve. B3 is obviously not a good bubble. There are two plausible explanations. First, the liquid superheat, ΔT_s , may not be properly determined. Error analysis showed that the uncertainty level in ΔT_s is 0.55 °F, which amounts to a large error of 17.5 percent in the reported value of 3.09 °F. Second, an excess amount of energy was introduced into the system in order to trigger this particular bubble. It is shown in the Appendix B that approximately ten times as much electricity was used for this bubble as compared to the other seven.

A detailed error analysis is given in Appendix F. It is found that the errors contained in the values of ΔT_s , ΔT_d , and ΔT_h are not large enough to alter the above discussions concerning the relative importances of the various effects.

It was mentioned in Chapter II that the asymptotic solution is only applicable to isobaric bubble growth process. That this statement is

valid can be made clear by studying Figure 20, which is a pressure-versus-time plot based on the data (10) of Dergarabedian's bubble No. 7, identified here as D7. Figure 20 shows that the vapor pressure within the bubble is essentially the system pressure p_{∞} . Hence the process is isobaric. If the Plesset and Zwick solution, Equation (V-2), is used, it can be shown that the dynamic pressure term $\rho_l(R\ddot{R} + \frac{3}{2}\dot{R}^2)$ in the Rayleigh equation is equal to $(\phi^2 J_a^2 \alpha_l \rho_l)8t$. This pressure is negligibly small compared to the system pressure which is 1 atm. Figure 21 shows the agreement between the asymptotic theory and data of this bubble.

For comparison, a pressure-time diagram has been drawn on the basis of experimental data of B1. It is shown in Figure 22. In this case, the bubble growth process is hardly isobaric. Consequently, the asymptotic solution is not expected to be applicable for this low pressure case. Based on the above considerations, it becomes obvious that the large discrepancy reported by Cole and Shulman (24), which was mentioned in Chapter I, between the heat diffusion limited theory and the experimental data is due primarily to complete neglect of the dynamic effects.

V.1.2 The Upper Bound of Bubble Growth Curves

Figures 11 through 18 show that bubble growth curves are bounded by the two theoretical curves at all times and under any conditions. A better way to make this point more clear is to plot the same set of curves in the log-log scale. This has been done and the resulting curves are presented in Figures 23 through 28. Excluded from this set of figures are the growth curves of bubbles B3 and B8, the latter being almost identical to that of B7. In each diagram, the intersection point of the two theoretical curves is of greatest interest. It can be seen that to the

left of the point, the growth data are closer to the Rayleigh curve than the Plesset and Zwick curve; and to the right of this point, it is the other way around. On the right side of the intersection point, the growth curve approaches the Plesset and Zwick limit quickly; while on the left side of this point, the experimental curve approaches the Rayleigh limit only asymptotically.

The upper bound of bubble growth curve therefore consists of the Rayleigh curve, to the left of the intersection point, and of the Plesset and Zwick curve, to the right of the same point. Maximum deviation of experimental data from this upper bound occurs at the time the two theoretical curves cross over each other.

V.1.3 Generalized Bubble Growth Curve

The coordinates of the intersection point, defined as R^* and t^* for radius and time, are obtained by solving Equations (V-1) and (V-2) simultaneously as

$$R^* = \frac{\phi^2 Ja^2 \alpha_l}{R_m} ; R_m = \left[\frac{2}{3} \frac{P_{sat}(T_\infty) - P_\infty}{\rho_l} \right]^{1/2}, \phi^2 = \frac{12}{\pi} \quad (V-3)$$

and

$$t^* = \frac{R^*}{R_m} \quad (V-4)$$

It is found that all the bubble radius-time curves, with the exception of that of bubble B3, can be correlated to form a single curve in a dimensionless plot provided nondimensionalizations of R and t are made in the following fashion:

$$\frac{R}{R^*} = \frac{R_m R}{\phi^2 Ja^2 \alpha_l} \quad (V-5)$$

and

$$\frac{t}{t^*} = \frac{R_m^2 t}{\phi^2 Ja^2 \alpha_l} \quad (V-6)$$

The resultant bubble growth curve is shown in Figure 29 along with the two theoretical ones. Considering the wide range of experimental conditions covered in this investigation, it is believed that this is the generalized curve for the transition region of bubble growth. This, in effect, bridges the gap between the liquid-inertia controlled region and the heat-diffusion limited region.

The region boundaries will now be defined through the consideration of a dimensionless group. Since the radius R^* expressed by Equation (V-3) contains all the pertinent variables, such as Jakob number and system pressure p_∞ , related to bubble growth, it can be used to form a useful dimensionless radius, \bar{R} , by the following definition:

$$\bar{R} = \frac{R_r}{R^*} \quad (V-7)$$

In this equation, R_r is a reference radius the magnitude of which has yet to be determined. In most engineering applications, a bubble grows from the critical radius to a certain size which is limited by the arrangement of the equipment and by the operating conditions. Usually this size is not very large. The critical radius cannot be used as a reference radius because surface tension plays an important role during the growth of a bubble of this size. It should be borne in mind that both the Rayleigh solution and the Plesset and Zwick solution were obtained by neglecting the surface tension effect. Obviously the

reference radius should not be too big. As a compromise, it is decided to use 0.1 inch as the reference. This decision is quite arbitrary; any other radii of similar order of magnitude would have served the purpose as well. Thus the dimensionless radius is defined as

$$\bar{R} = \frac{0.1}{R^*} \quad (V-8)$$

where R^* is in inches.

Table V-1 summarizes the values of \bar{R} for the group of B bubbles:

TABLE V-1

Values of \bar{R}

<u>Bubble No.</u>	<u>\bar{R}</u>
B1	8.45×10^{-4}
B2	7.44×10^{-4}
B4	2.30×10^{-2}
B5	2.48×10^{-1}
B6	4.77×10^{-1}
B7	4.14×10^0

This table has been studied together with Figure 29, and the conclusion has been drawn that the three different regions of bubble growth can be specified as follows:

1. $\bar{R} < 10^{-4}$, Liquid-inertia-controlled region
 2. $10^{-4} < \bar{R} < 1$, Transition region
 3. $\bar{R} > 1$, Heat-diffusion-limited region.
- (V-9)

It is seen from Figure 29 that the region boundaries cannot be clearly defined. But as a rough approximation, the above definitions serve the purpose well as a guide line based on which one could pick with ease appropriate equations for bubble growth rate calculations.

Although the specification of bubble growth regions is made on the basis of low-pressure data of water, it is nevertheless general in nature and is expected to be applicable to other fluids and other operating conditions. In a study of bubble growth problem of water, at one atmosphere, Abdelmessih (20) found that the heat-diffusion limited equation no longer applies for ΔT_s greater than 15 °F. The value of \bar{R} in this case is 2.44. It is indeed consistent with the prediction implied in Equation (V-9). For the bubble D7 mentioned in Section V.1.1, $\bar{R} = 130$, hence well within the heat-diffusion limited region.

V.1.4 Recommendations for Bubble Growth Rates Calculation

Based on the above discussions, it is apparent that one cannot always calculate bubble growth rates by means of the asymptotic bubble growth equation without resulting in a large error. The recommended procedure is then to check the bubble growth region first. This can be done easily by using Equations (V-3), (V-8), and (V-9). If the growth is found to be liquid-inertia controlled, then Equation (V-1) can be used; if it is heat diffusion limited, Equation (V-2). If the growth falls into the transition region, one can use the generalized bubble growth curve given in Figure 29.

V.1.5 Application to Bubble Growth Problem of Liquid Metals

Many investigators (2,46,47) have expressed doubts about the applicability of the asymptotic solution to the bubble growth problem

of liquid metals, due to the very high thermal conductivity of the same. In this respect, the criteria developed in the Section V.1.3 of this chapter can be helpful.

For a typical set of assumed operating conditions (p_{∞} , ΔT_s), one can calculate the nondimensionalized radius \bar{R} . These calculations have been performed for sodium bubbles, and representative results are shown in Table V-2.

TABLE V-2

Representative Results of Sodium Bubble Calculations

<u>Bubble No.</u>	<u>p_{∞}, psia</u>	<u>ΔT_s, °F</u>	<u>Ja</u>	<u>\bar{R}</u>
S1	24.99	9.0	2.80	14.1
S2	24.99	18.0	5.59	4.95
S3	24.99	36.0	11.18	1.78
S4	24.99	90.0	27.85	0.48
S5	24.99	180.0	55.56	0.19
S6	24.99	360.0	108.14	0.086
S7	24.99	720.0	222.87	0.042
S8	14.70	90.0	45.12	0.14
S9	0.29	90.0	1770.44	0.24×10^{-4}

In these calculations the sodium property data were taken from Reference (48). by comparing the values of \bar{R} listed in the above table with the conditional statements given in Equation (V-9), it is concluded that for bubbles at 24.99 psia, or 1.7 atm, the asymptotic solution is applicable provided the superheat ΔT_s is less than 36 °F. At

higher superheats, the bubble growths are in the transition region where the dynamic effect cannot be neglected. According to Deane (49), stable boiling of liquid sodium usually occurs with the steady-state values of ΔT_s less than 30 °F under atmospheric conditions; hence, the bubble growth rates can be, in this case, estimated by means of the asymptotic solution. On the contrary, under certain circumstances, the liquid sodium has been found able to sustain superheat up to several hundred degrees Fahrenheit prior to the incipience of boiling (50). Such being the case, the asymptotic solution is no longer adequate for bubble-growth rate calculations.

The two bubbles S8 and S9 that appear in Table V-2 are the same ones which have been considered in Section II-6. Based on the present bubble growth criterion, the growth of bubble S8 is in the transition region; i.e., the dynamic and the heat diffusion effects are both of considerable importance; whereas the growth of bubble S9 is primarily liquid-inertia controlled. These observations are in accord with those made in Chapter II.

V.2 Concerning the Interfacial Nonequilibrium Effect and the Evaporation Coefficient

In order to estimate the influence of the nonequilibrium effect on bubble growth, one can examine the ratio of the interfacial temperature drop ΔT_i to the superheat of the system, ΔT_s . The ratio $\Delta T_i/\Delta T_s$ is that fraction of the potential driving force which is not available for bubble expansion, due to the nonequilibrium effect. As part of the results of data reduction program, the values of ΔT_i have been obtained. For these calculations a second-order temperature distribution function,

Equation (IV-9), was assumed. Table V-3 summarizes the representative values of $\Delta T_i / \Delta T_s$ for the B bubbles.

TABLE V-3

Representative Values of the Ratios $\Delta T_i / \Delta T_s$ and $\Delta T_i / \Delta T_h$

<u>Bubble Number</u>	<u>$\Delta T_i / \Delta T_s$</u>	<u>$\Delta T_i / \Delta T_h$</u>	<u>P_∞, psia</u>
B1	0.075	0.431	0.1759
B2	0.070	0.415	0.1831
B3	- 0.097	- 0.201	0.5922
B4	0.145	0.356	0.5962
B5	0.042	0.053	1.8259
B6	0.032	0.034	1.9345
B7	0.013	0.012	5.6072
B8	0.018	0.018	5.6324

It is evident according to the above tabulation that the interfacial nonequilibrium effect is not important as far as bubble growth is concerned. Because on the average, more than 90 percent of ΔT_s is accounted for by the heat diffusion and the dynamic effects.

Also shown in the same table are the ratios $\Delta T_i / \Delta T_h$. The quantity ΔT_h is the sum of ΔT_i and the temperature drop across the thermal boundary layer. Thus a small value of $\Delta T_i / \Delta T_h$ implies that the majority of the temperature difference ΔT_h occurs in the thermal layer. Table V-3 shows that this is the case.

Similar results have been obtained by assuming an error-function temperature profile in the thermal boundary layer. This is expected,

in view of the discussions in Section IV.2.1. Any one of the seven arbitrary function listed in Table IV-2 can be used, but the calculated value of ΔT_i is maximum if the second-order profile is assumed. It can be seen by studying Equations (IV-5) and (IV-8) and Table IV-2.

Only "representative" values are used in Table V-3. There is quite a little scatter in the original data of ΔT_i , given in Appendix C. Being a small quantity, ΔT_i is very sensitive to the measurement errors and to the gross simplifying assumptions imposed on the data reduction program. Error analysis (Appendix F) shows that the uncertainty in ΔT_i is of the same magnitude as the value of ΔT_i itself. In this respect, it is fortunate that most of the ΔT_i data are positive quantities.

Even though the uncertainty in ΔT_i is enormous, its effect on the ratio $\Delta T_i/\Delta T_s$ is not significant enough to alter the conclusion that the interfacial nonequilibrium effect on bubble growth is not important.

Unfortunately, the evaporation coefficient is a strong function of ΔT_i ; hence we are not in a position to ascertain the value of the evaporation coefficient. Numerical values of this coefficient inferred from the experimental data are given in Appendix C. These values appear to be erratic, as a consequence of the propagation of errors involving almost all of the primitive and the derived variables of this investigation.

CHAPTER VI - CONCLUSIONS

1. Bubble growth rates are limited primarily by the liquid inertia and by the heat diffusion rates at all pressures. The interfacial nonequilibrium effect on bubble growth is insignificant.
2. The relative importances of the two governing effects depend on a dimensionless parameter \bar{R} , defined as

$$\bar{R} = \frac{0.1\pi}{12} \frac{\dot{R}_m}{Ja^2 \alpha_\ell} ;$$

$$\text{with } \dot{R}_m = \left[\frac{2}{3} \frac{P_{\text{sat}}(T_\infty) - P_\infty}{\rho_\ell} \right]^{1/2} .$$

The dynamic effect is of increasing importance with decreasing values of \bar{R} ; the reverse is true for the heat diffusion effect.

3. The asymptotic solution of Plesset and Zwick is found applicable only for the cases with $\bar{R} > 1$. On the other hand, the Rayleigh solution predicts bubble growth rates satisfactorily when $\bar{R} < 10^{-4}$.
4. For the transition region, $10^{-4} < \bar{R} < 1$, the generalized bubble growth curve (Figure 29) may be used to estimate bubble growth rates.

BIBLIOGRAPHY

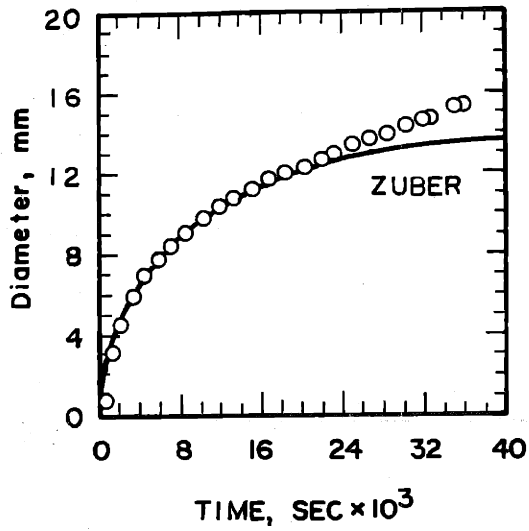
1. Judd, A. M., "Sodium Boiling and Fast Reactor Safety Analysis," AEEW-R 561 (1967).
2. Kosky, P. G., "Some Aspects of Boiling and Vapour Voidage Growth Problems in a Liquid-Metal Cooled Reactor," Presented at the Int. Conf. on the Safety of Fast Reactors, Aix-en-Provence, France (1967).
3. Rayleigh, Lord, "Pressure Due to Collapse of Bubbles," *Phil. Mag.* 34, 94 (1917).
4. Plesset, M. S. and Zwick, S. A., "The Growth of Vapor Bubbles in Superheated Liquids," *J. Appl. Phys.* 25, 493 (1954).
5. Plesset, M. S. and Zwick, S. A., "A Nonsteady Heat Diffusion Problem with Spherical Symmetry," *J. Appl. Phys.* 23, 95 (1952).
6. Zwick, S. A. and Plesset, M. S., "On the Dynamics of Small Vapor Bubbles in Liquids," *J. Math. and Phys.* 33, 308 (1955).
7. Forster, H. K. and Zuber, N., "Growth of a Vapor Bubble in a Superheated Liquid," *J. Appl. Phys.* 25, 474 (1954).
8. Scriven, L. E., "On the Dynamics of Phase Growth," *Chem. Eng. Sci.*, 10, 1 (1959).
9. Birkhoff, G., Margulies, R. S. and Horning, W. A., "Spherical Bubble Growth," *Phys. of Fluids*, 1, 201 (1958).
10. Dergarabedian, P., "The Rate of Growth of Vapor Bubbles in Superheated Water," *J. Appl. Mech.* 20, 537 (1953).
11. Dergarabedian, P., "Observations on Bubble Growths in Various Superheated Liquids," *J. Fluid Mech.* 9, 39 (1960).
12. Griffith, P., "Bubble Growth Rates in Boiling," *Trans. ASME* 80, 721 (1958).

13. Savlc, P., "Discussion on Bubble Growth Rates in Boiling," Trans. ASME 80, 762 (1958).
14. Han, C. Y. and Griffith, P., "The Mechanism of Heat Transfer in Nucleate Pool Boiling, Part I and II," Int. J. Heat Mass Transfer, 8, 887 (1965).
15. Bankoff, S. G. and Mikesell, R. D., "Growth of Bubbles in a Liquid of Initially Non-uniform Temperature," ASME Paper 58-A-105 (1958).
16. Zuber, N., "The Dynamics of Vapor Bubbles in Nonuniform Temperature Fields," Int. J. Heat Mass Transfer, 2, 83 (1961).
17. Cole, R., "Bubble Dynamics in Boiling," Ph.D. Thesis, Clarkson College of Technology (1965).
18. Mikic, B. B. and Rohsenow, W. M., "Bubble Growth Rates in Nonuniform Temperature Field," to be published in Int. J. Heat Mass Transfer (1968).
19. Van Stralen, J. D., "The Mechanism of Nucleate Boiling in Pure Liquids and in Binary Mixture Part I and II," Int. J. Heat Mass Transfer, 9, 995 (1966).
20. Abdelmessih, A. H., "The Flashing of Superheated Liquids," Ph.D. Thesis, Univ. of Toronto (1966).
21. Fritz, V. W. and Ende, W., "Uber den Verdampfungsvorgang nach kinematographischen Aufnahmen an Dampfblasen," Phys. Z. 37, 391 (1936).
22. Staniszewski, B. M., "Nucleate Boiling Bubble Growth and Departure," Tech. Rep. 16, Div. Sponsored Res., M.I.T., (1959).
23. Labuntsov, D. A., et al., "Study of the Growth of Bubbles During Boiling of Saturated Water Within a Wide Range of Pressures by means of High-Speed Moving Pictures," High Temperature, 2, 404 (1964).

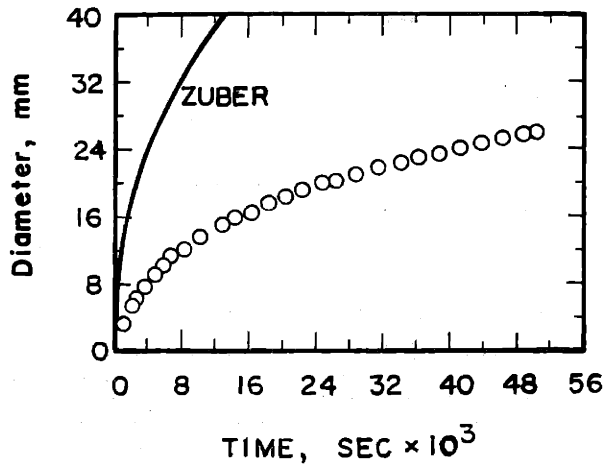
24. Cole, R. and Shulman, H. L., "Bubble Growth Rates at High Jakob Numbers," *Int. J. Heat Mass Transfer* 9, 1377 (1966).
25. Bornhorst, W. J., "Irreversible Thermodynamics of a Phase Change," Ph.D. Thesis, M.I.T. (1966).
26. Paul, B., "Compilation of Evaporation Coefficients," *ARS J.* 32, 1321 (1962).
27. Shai, I., "The Mechanism of Nucleate Pool Boiling Heat Transfer to Sodium and the Criterion for Stable Boiling," Report No. DSR 76303-45, M.I.T. (1967).
28. Labuntsov, D. A., Shevchuk, E. N., and Pazyuk, P. A., "On the Limiting Levels of Heat Transfer During the Boiling of Liquid Metals," *High Temperature*, 3, 246 (1965).
29. Griffith, P., "Condensation Heat Transfer," 14th Annual Heat Transfer Conference, Oklahoma State Univ. March 14-15, (1968).
30. Schrage, R. W., "A Theoretical Study of Interphase Mass Transfer," Columbia Univ. Press, New York (1953).
31. Hickman, K.C.D., "Maximum Evaporation Coefficient of Water," *Ind. Eng. Chem.* 46, 1442 (1954).
32. Nabavian, K. and Bromley, L. A., "Condensation Coefficient of Water," *Chem. Eng. Sci.* 18, 651 (1963).
33. Jamieson, D. T., "The Condensation Coefficient of Water," Third Symposium on Thermophysical Properties, ASME, p. 230 (1965).
34. Mills, A. F. and Seban, R. A., "The Condensation Coefficient of Water," *Int. J. Heat Mass Transfer* 10, 1815 (1967).
35. Berman, L. D., "Soprotivlenie na granitse Razdela faz pri plenochnoi kondensatzii para nizkogo Dableniya," *Tr. Vses. n-i i Konstrukt in-t, Khim Mashinost.* 36, 66 (1961).

36. Dorsey, N. E., "Properties of Ordinary Water Substances," Reinhold Publishing Corp., New York, p. 326 (1940).
37. Drummond, T. G., "The Effect of Surface Films on Evaporation," M. S. Thesis, Mech. Eng. Dept., M.I.T. (1964).
38. Cosman, B. J. and Hueter, T. F., "Instrumentation for Ultrasonic Neurosurgery," Electronics, p. 53, Issue of May 15 (1959).
39. Rohsenow, W. M., "Heat Transfer with Boiling," Developments in Heat Transfer, M.I.T. Press, Cambridge, Mass. (1964).
40. Rusk, R. D., "Introduction to College Physics," Appleton-Century-Crofts, Inc. (1960).
41. "Handbook of Chemistry and Physics," 34th Edition, Chemical Rubber Publishing Co., Cleveland, Ohio (1952).
42. "ASME Steam Tables," Table 11. Thermal Conductivity of Steam and Water, (1967).
43. Volyak, L. D., Doklady Akademii Nauk, USSR, vol. LXXIV, No. 2, p. 307 (1950).
44. Keenan, J. H. and Keyes, F. G., "Thermodynamic Properties of Steam," First Edition (1967).
45. Rohsenow, W. M. and Choi, H. Y., "Heat, Mass and Momentum Transfer," Prentice Hall, Inc., New Jersey (1961).
46. Wichner, R. P. and Hoffman, H. W., "Vapor Bubble Growth Rates in Superheated Liquid Metals," ORNL-TM-1413 (1966).
47. Judd, A. M., "Sodium Boiling and Fast Reactor Safety Analysis," AEEW-R561 (1967).
48. Golden, G. H., Tokar, J. V., and Miller, D., "Thermophysical Properties of Sodium-Recommended Values," Reactor and Fuel-Processing Tech. 11, 27 (1967).

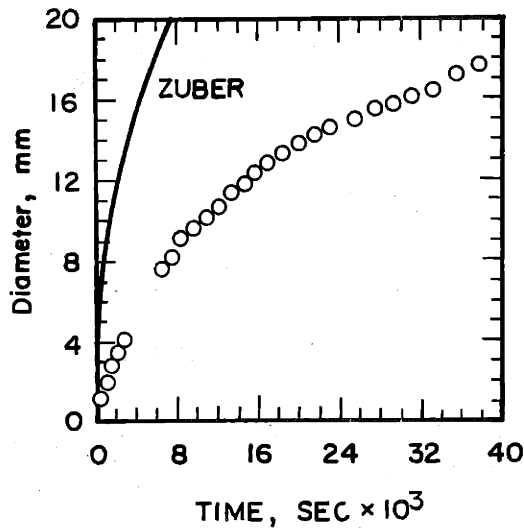
49. Deane, C., Personal Communication (1968).
50. Spiller, K. H., Grass, G., and Perschke, D., "Superheating and Single Bubble Ejection in the Vaporization of Stagnating Liquid Metals," AERE-Trans. 1078 (1967).
51. Murdock, J. W. and Brown, G. A., "An Investigation of High Velocity Flashing Flow in a Straight Tube," M.I.T. Report 27530-46 (1967).
52. Kline, S. J. and McClintock, F. A., "Describing Uncertainties in Single-Sample Experiments," Mechanical Engineering, p. 3, Issue of January (1953).



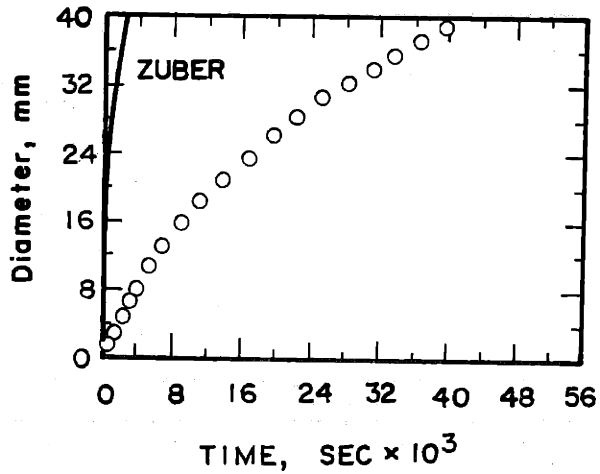
(a)



(c)



(b)



(d)

Figure 1 Bubble Growth Data for Water are compared with the Asymptotic Solution of Zuber, Eq. (II-16) with $\phi = \sqrt{\pi}$. Conditions of Experiments are Tabulated below:

Diagram	Pressure, mm Hg	$T_{wall} - T_{sat}, ^\circ F$	Ja
(a)	360	27	87.7
(b)	195	33	191
(c)	98	27	301
(d)	50	37	792

From Cole and Shulman (24).

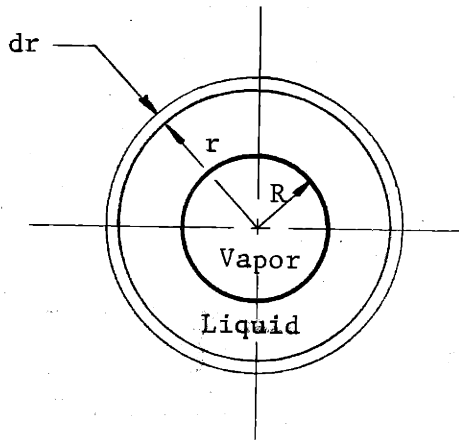


Figure 2 Spherical Bubble Model

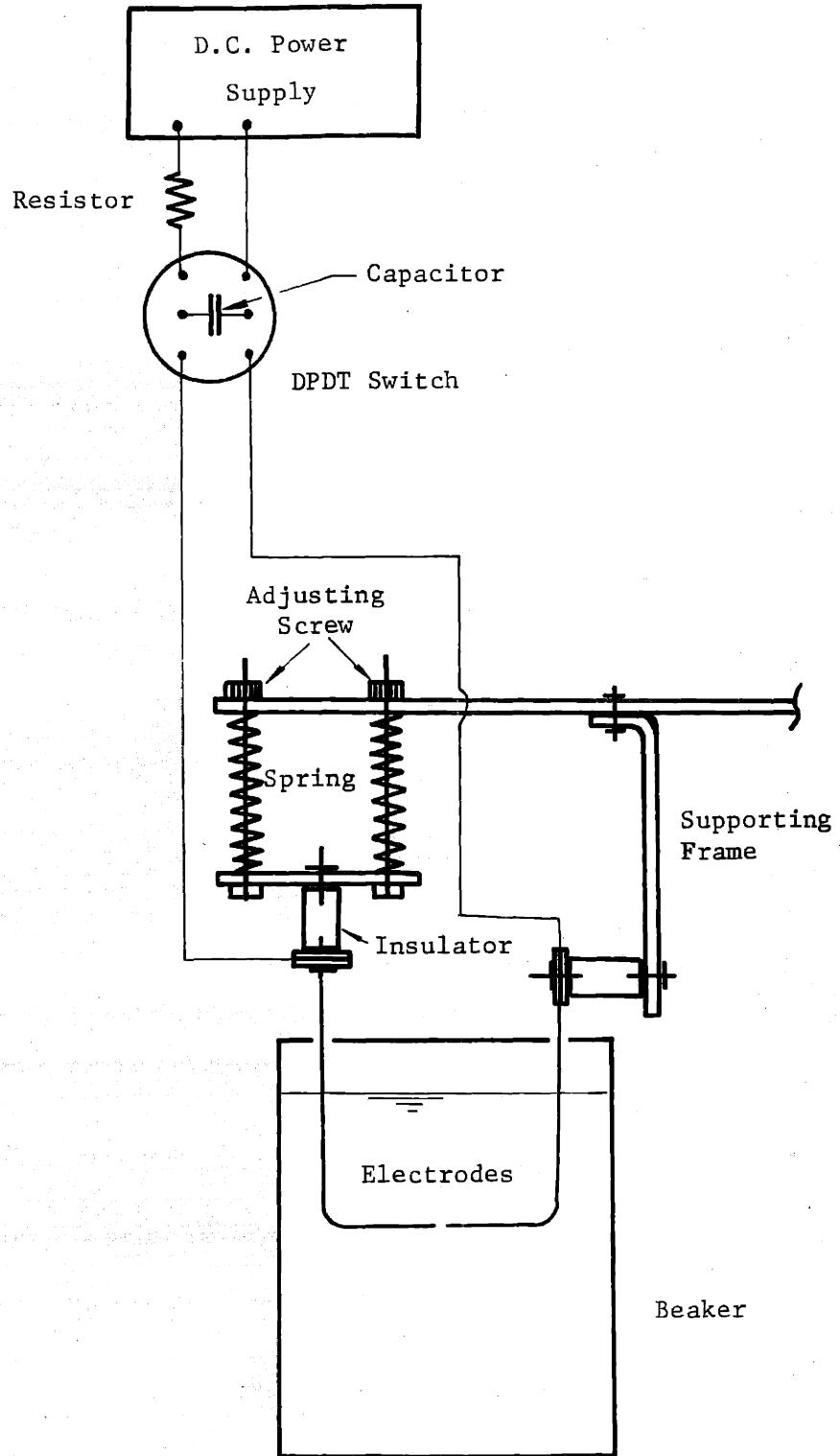


Figure 3 Sketch of the Bubble Triggering Device

Time interval between two frames is 0.0005 sec

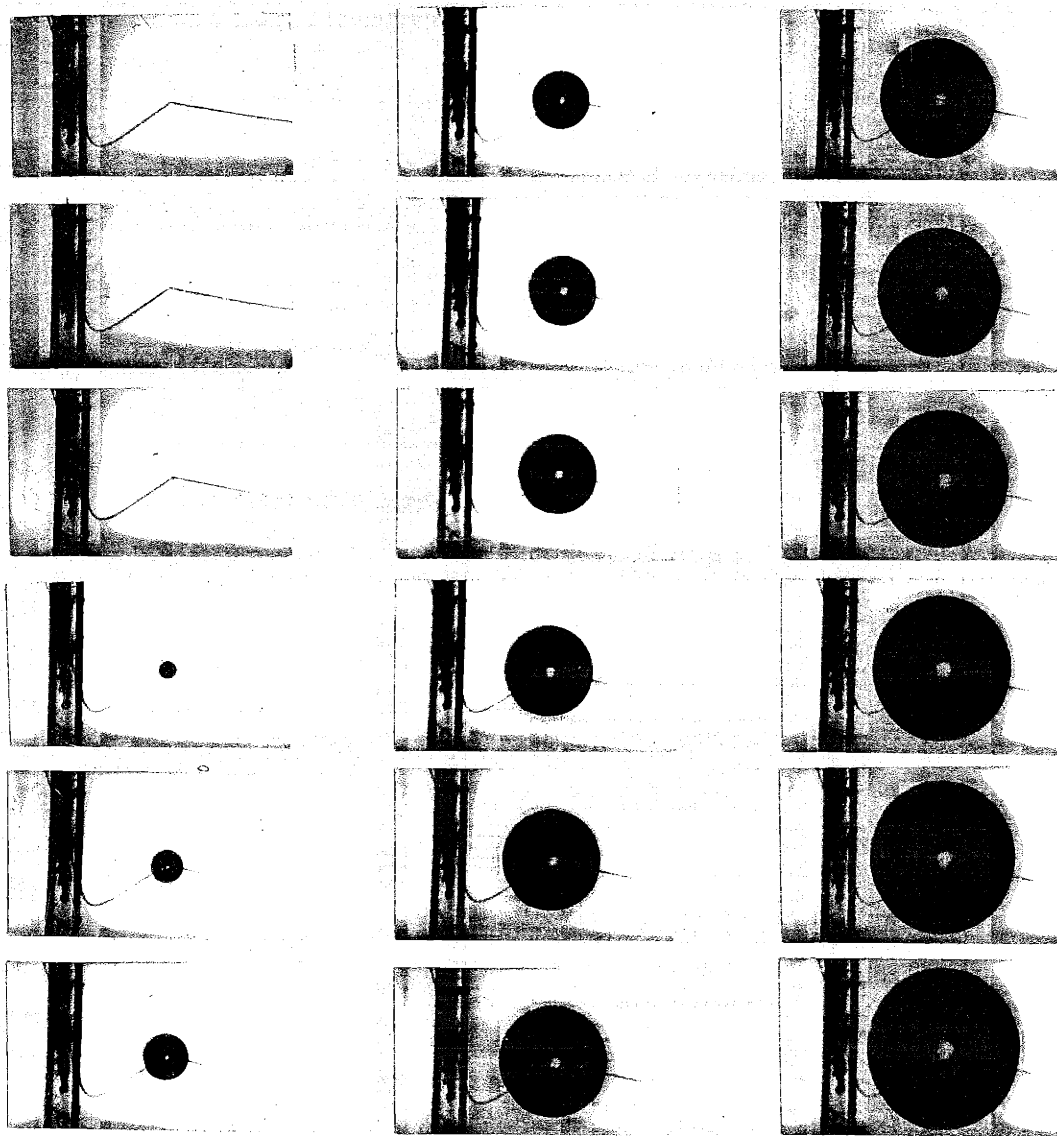


FIGURE 4 PHOTOGRAPHIC HISTORY OF BUBBLE B6

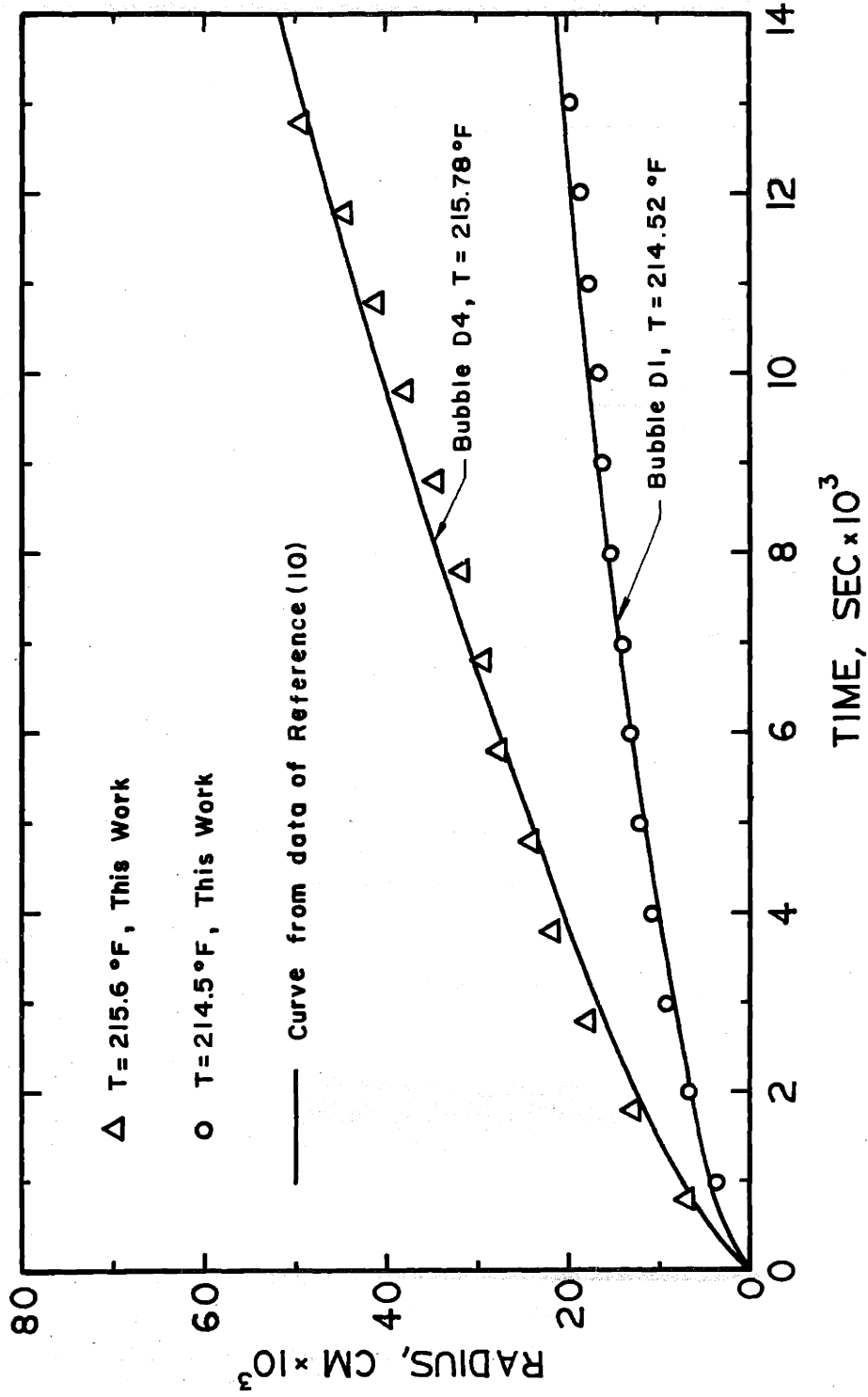


Figure 5 Comparison of Atmospheric Bubble Growth Data

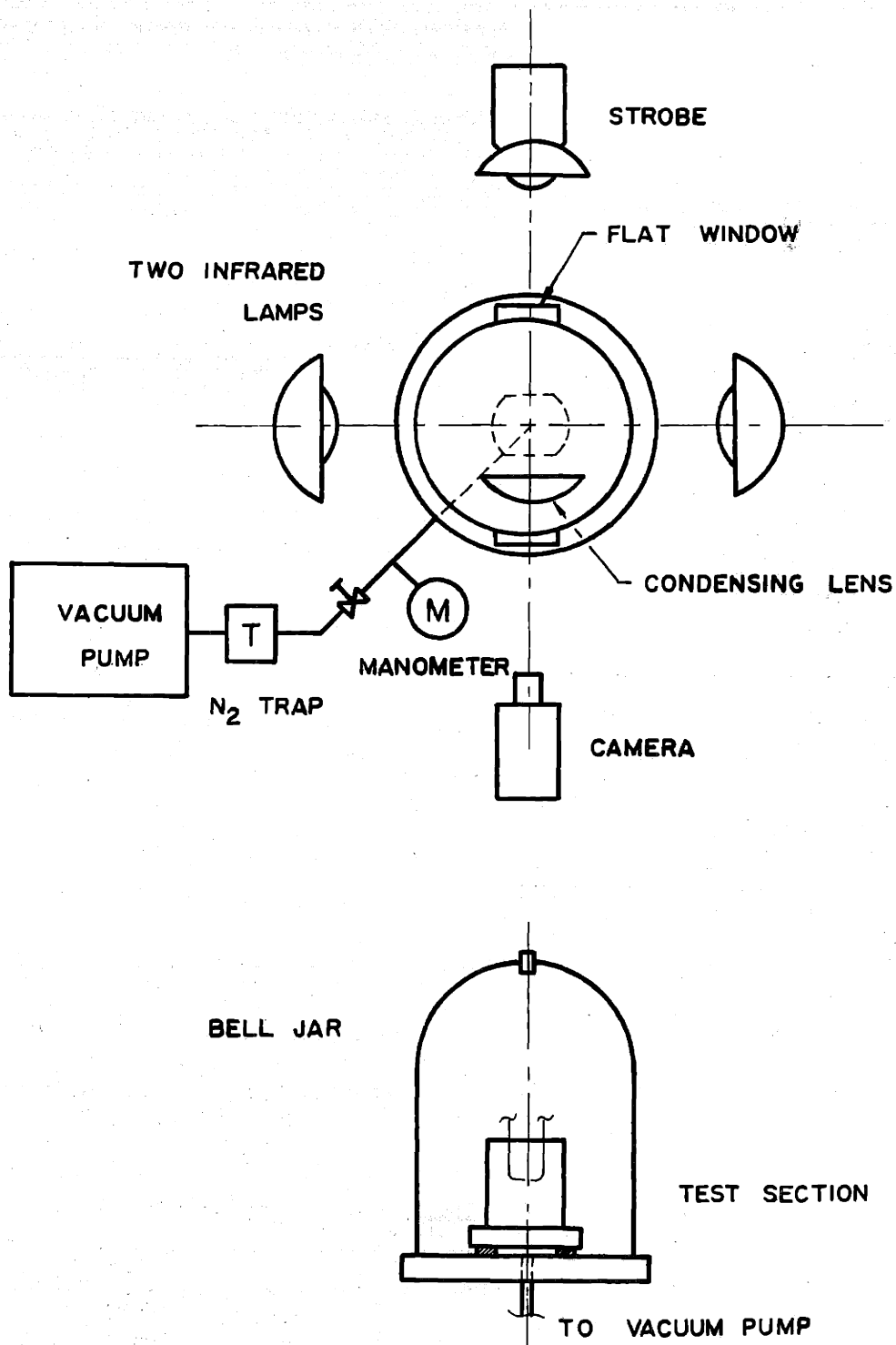


Figure 6 Schematic of Apparatus

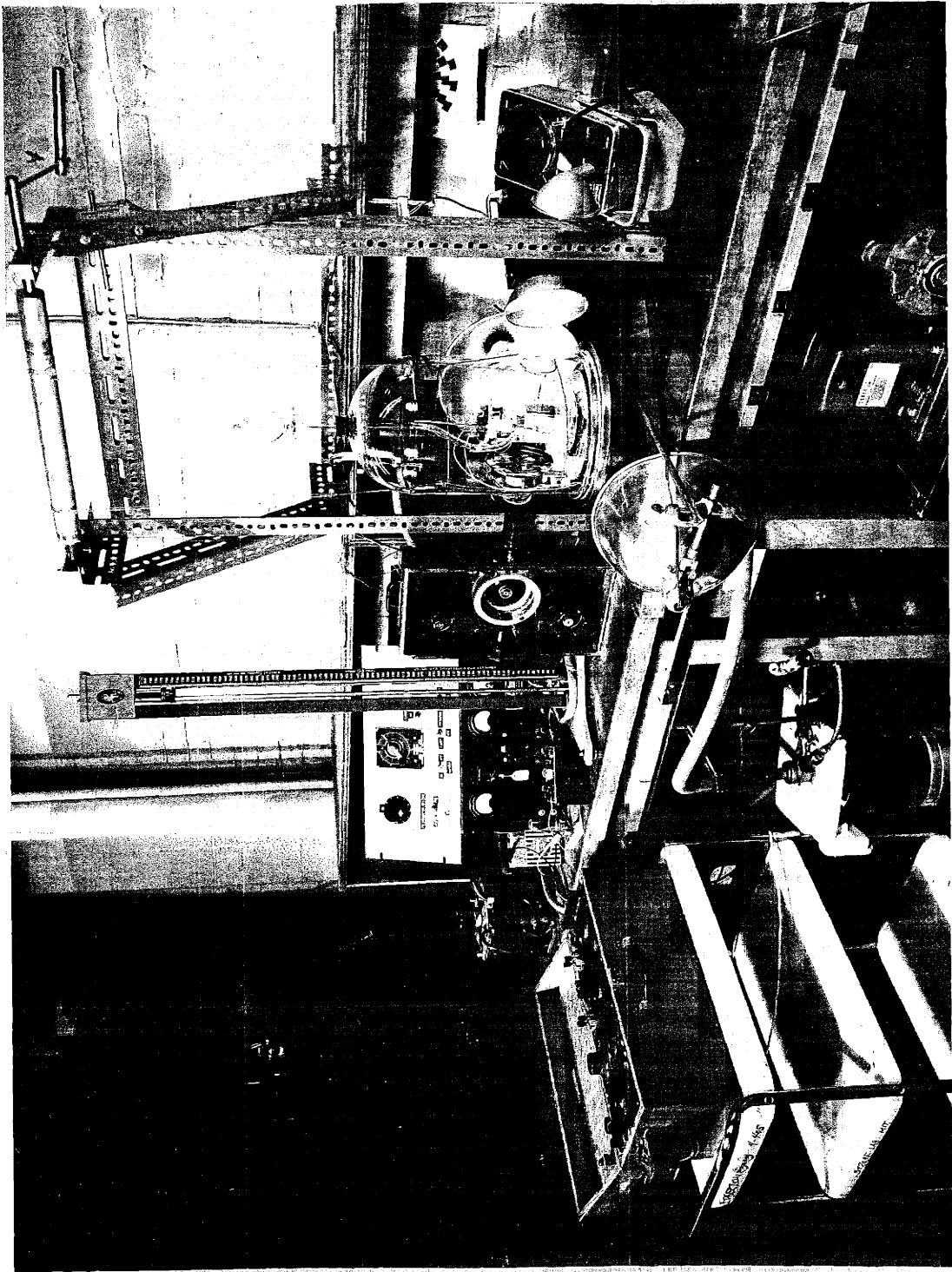


Figure 7 Photograph of Experimental Setup

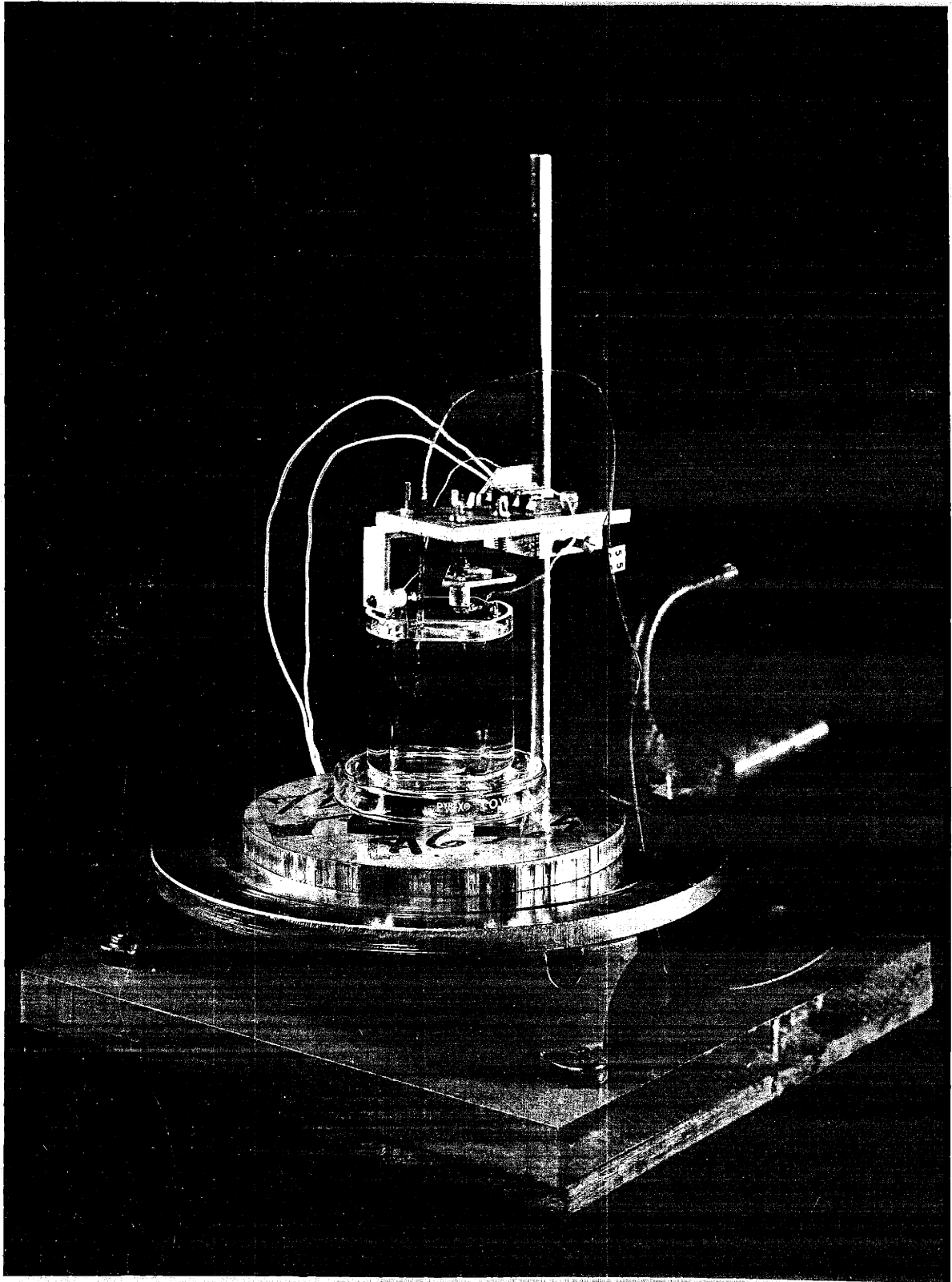


Figure 8 Close-up Picture of Test Section

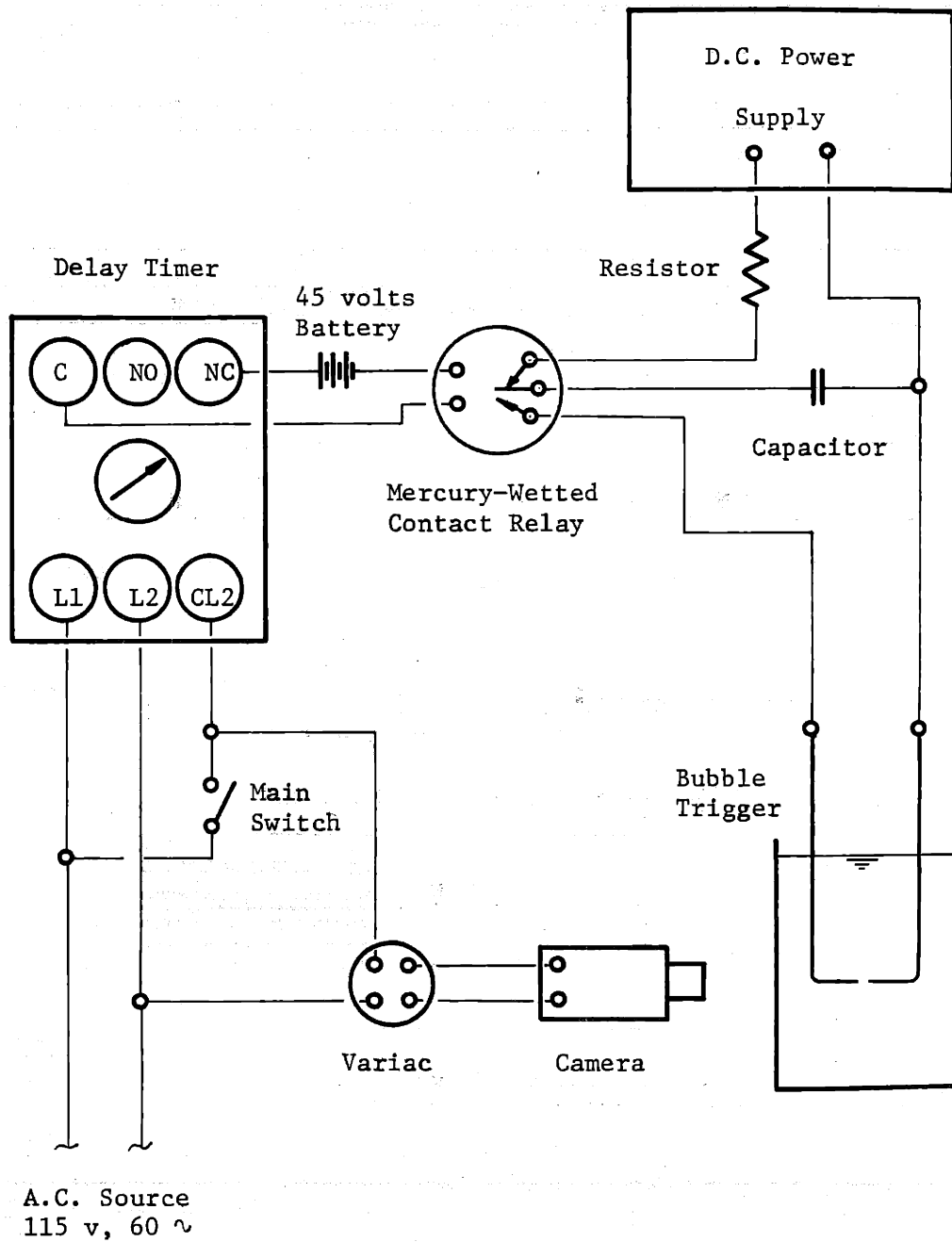


Figure 9 Wiring Diagram of Instrumentation

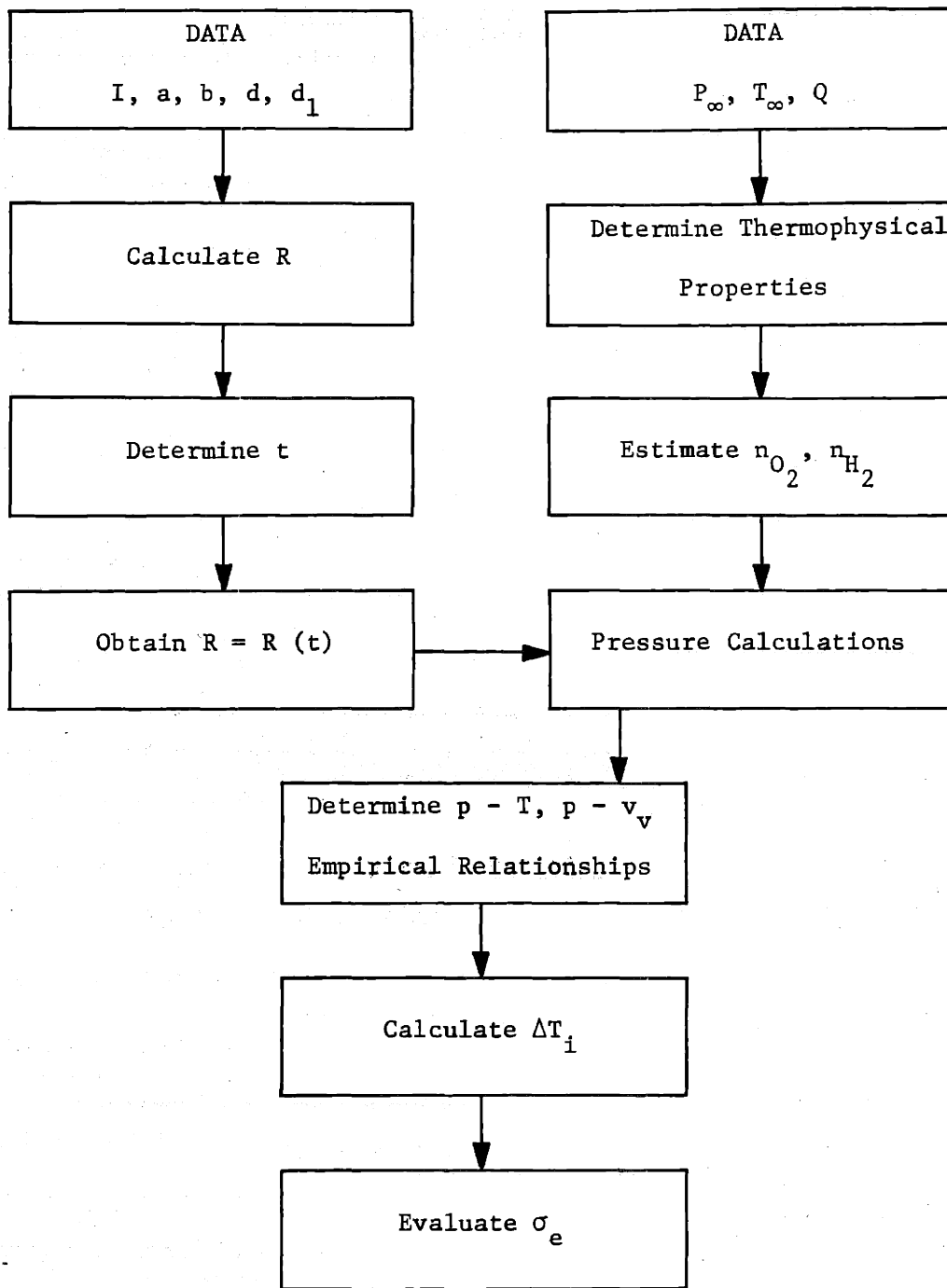


Figure 10 Flow Diagram of Data Reduction

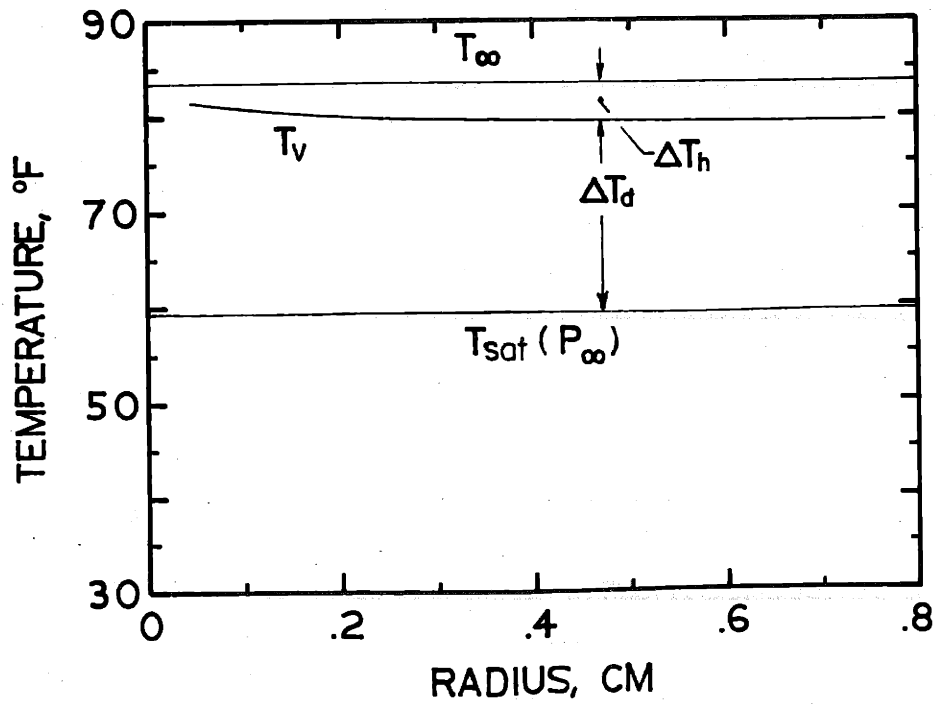
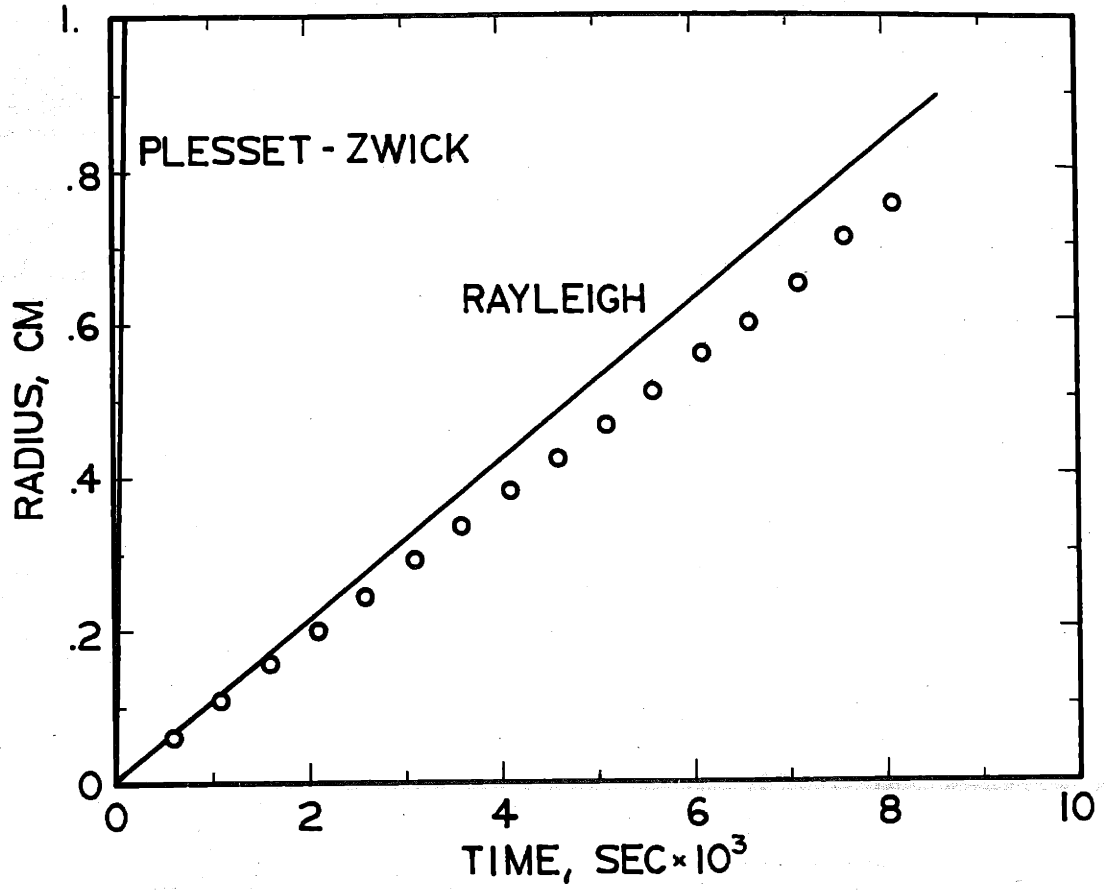


Figure 11 Radius vs Time and Temperature vs Radius Curves of Bubble B1

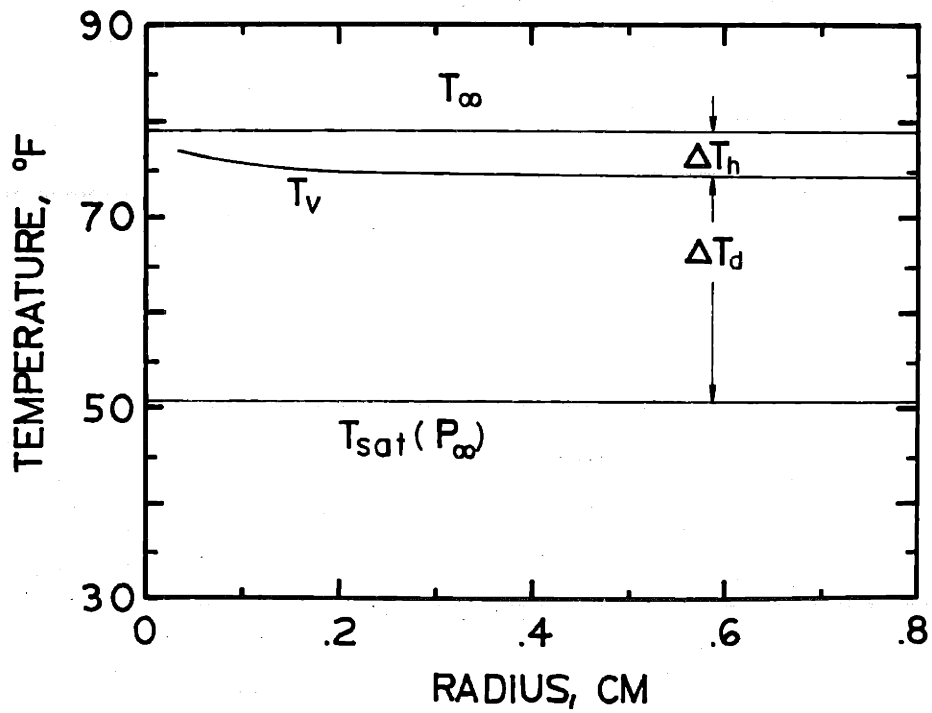
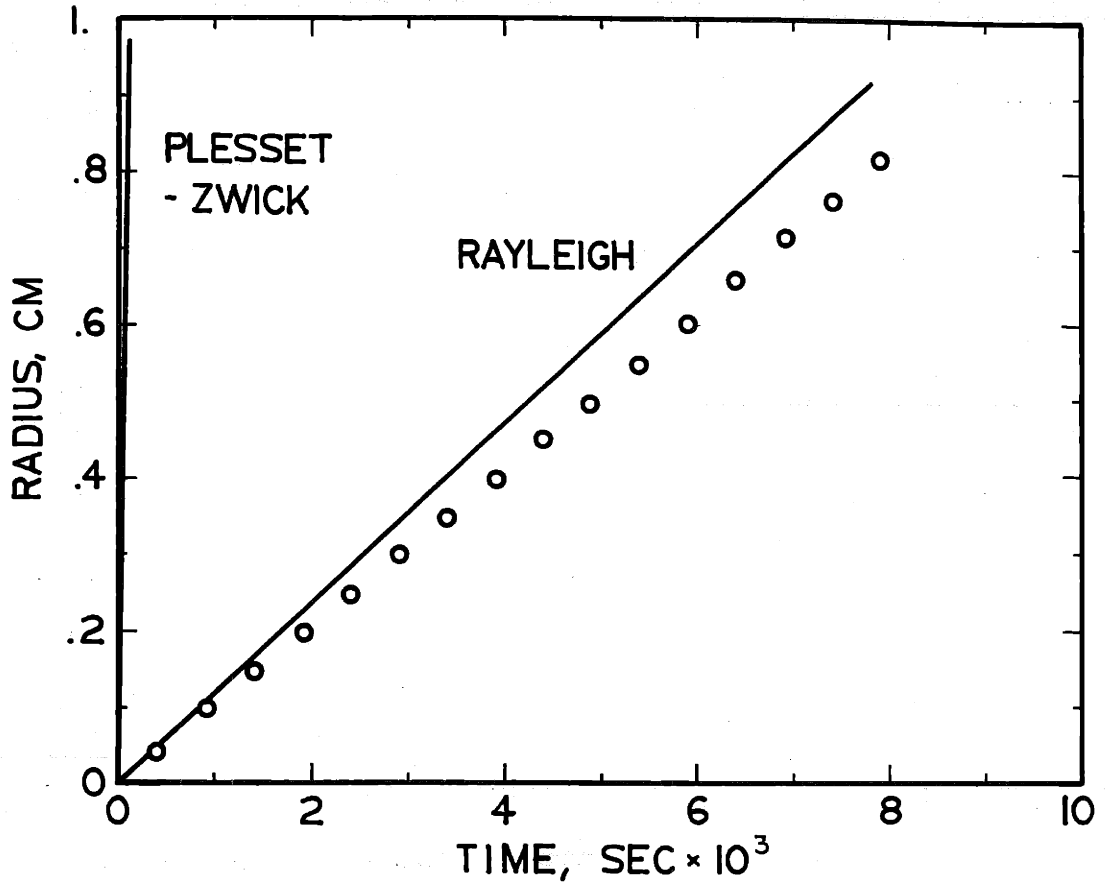


Figure 12 Radius vs Time and Temperature vs Radius Curves of Bubble B2

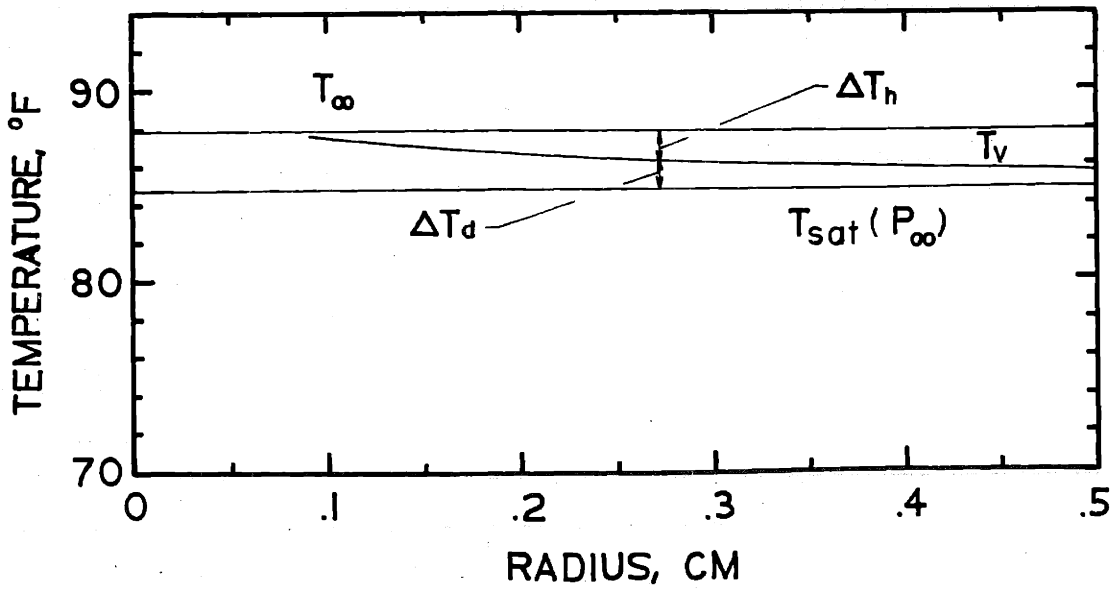
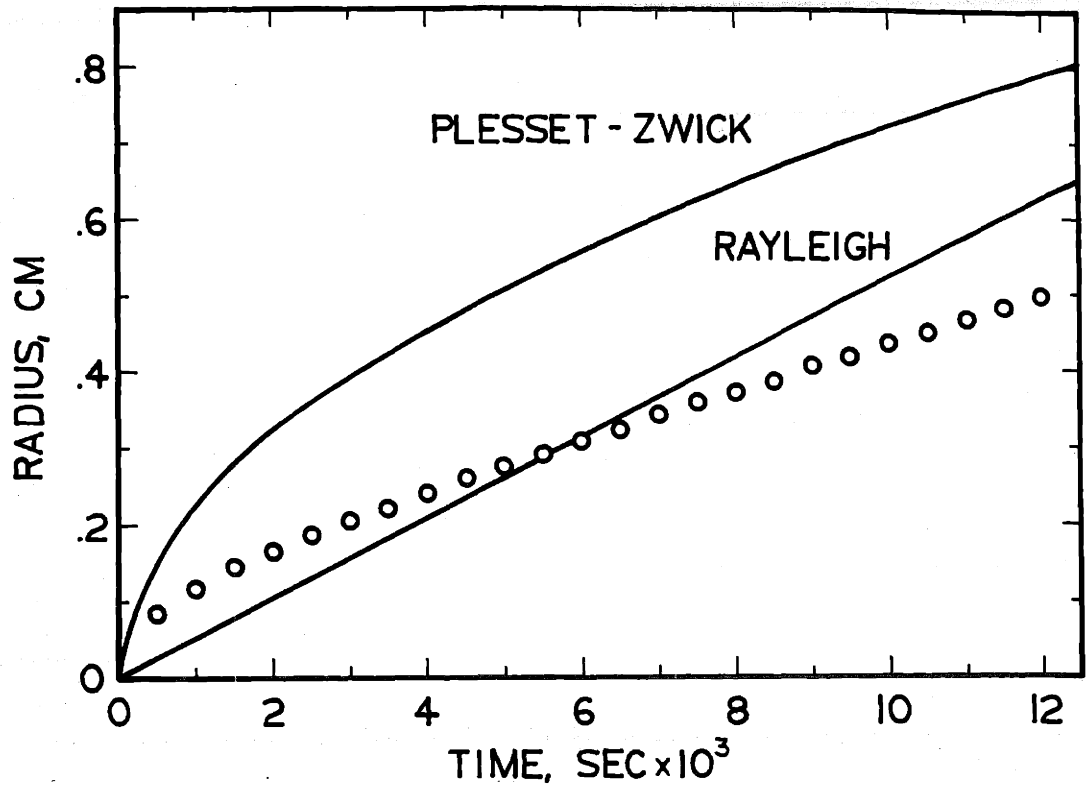


Figure 13 Radius vs Time and Temperature vs Radius Curves of Bubble B3

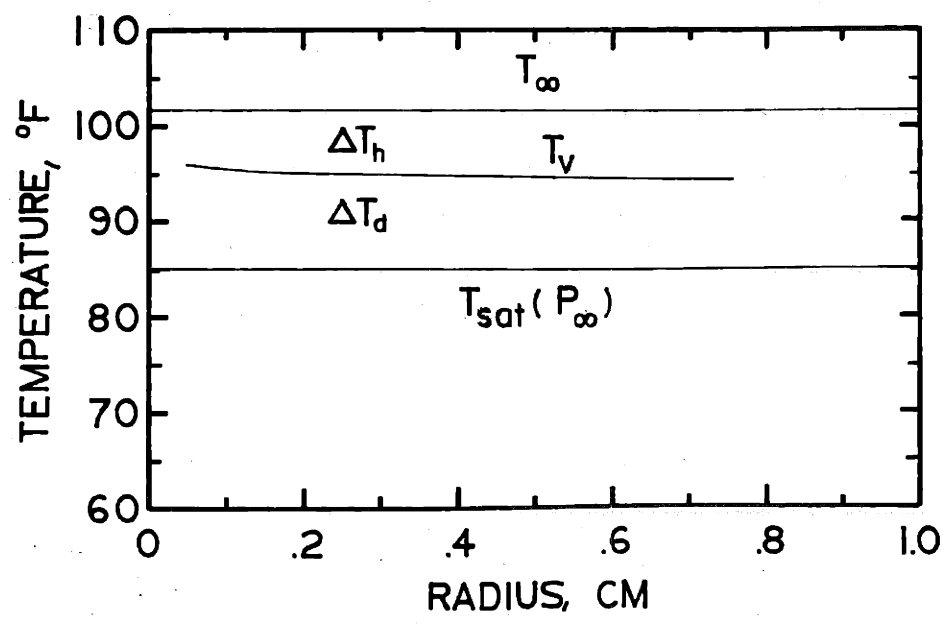
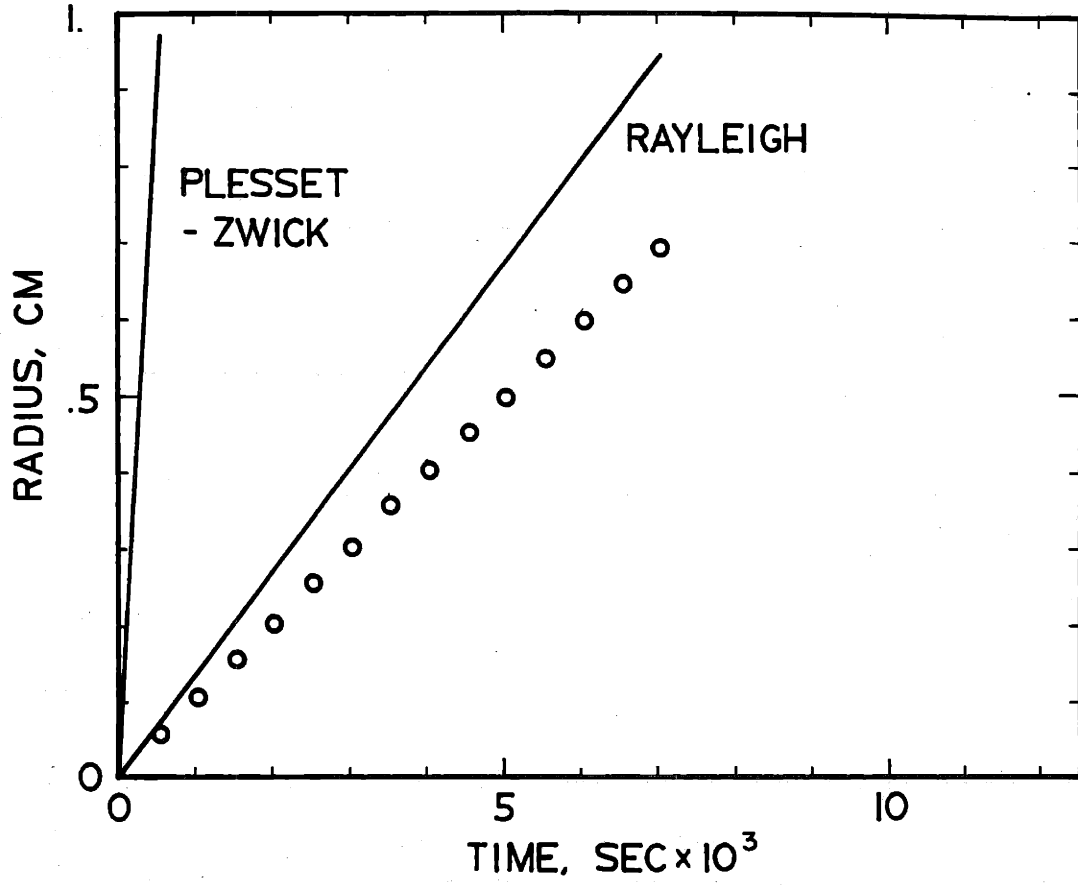


Figure 14 Radius vs Time and Temperature vs Radius Curves of Bubble B4

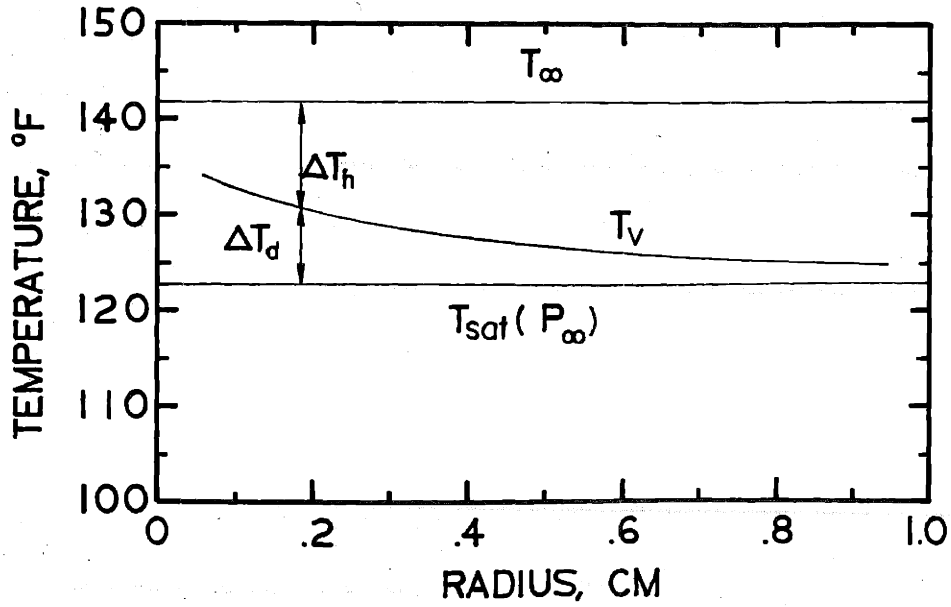
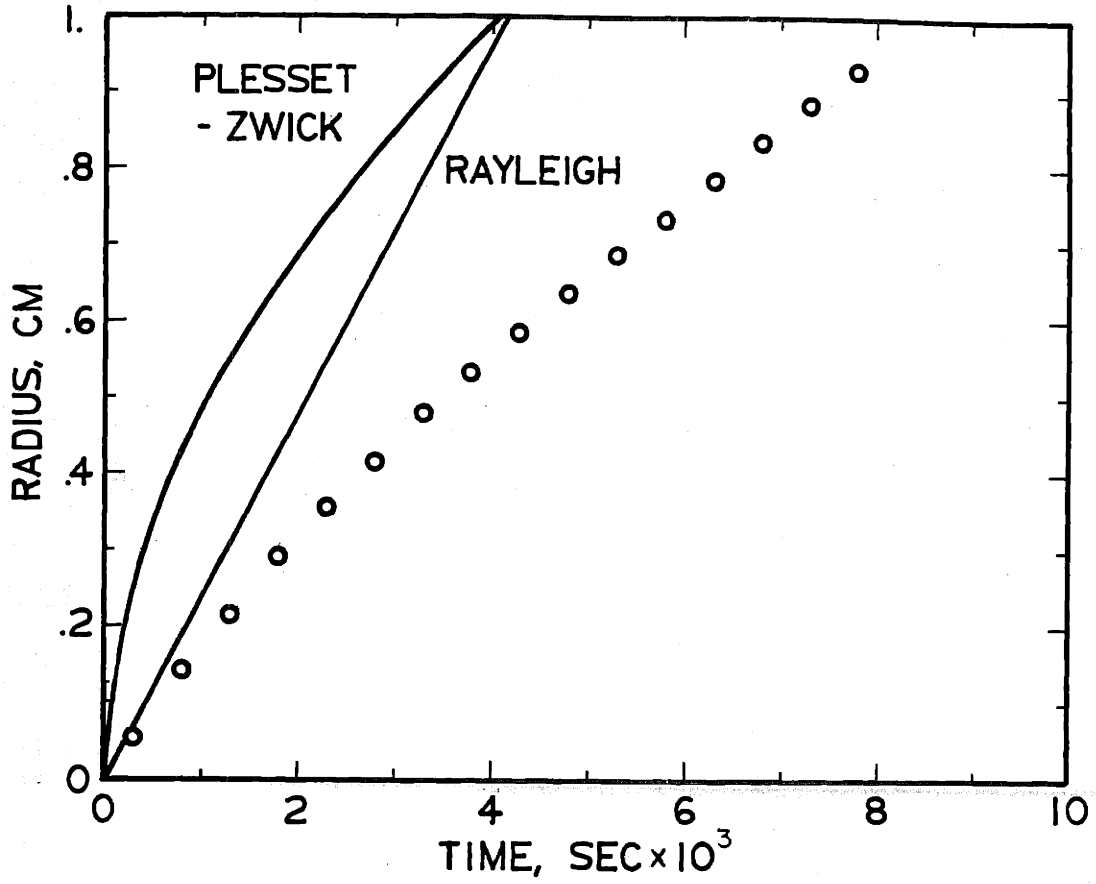


Figure 15 Radius vs Time and Temperature vs Radius Curves of Bubble B5

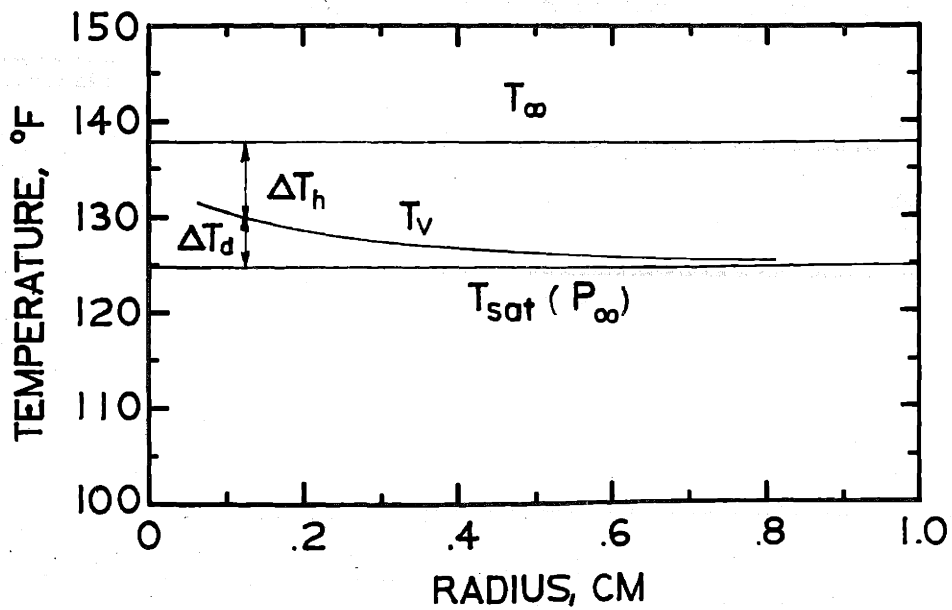
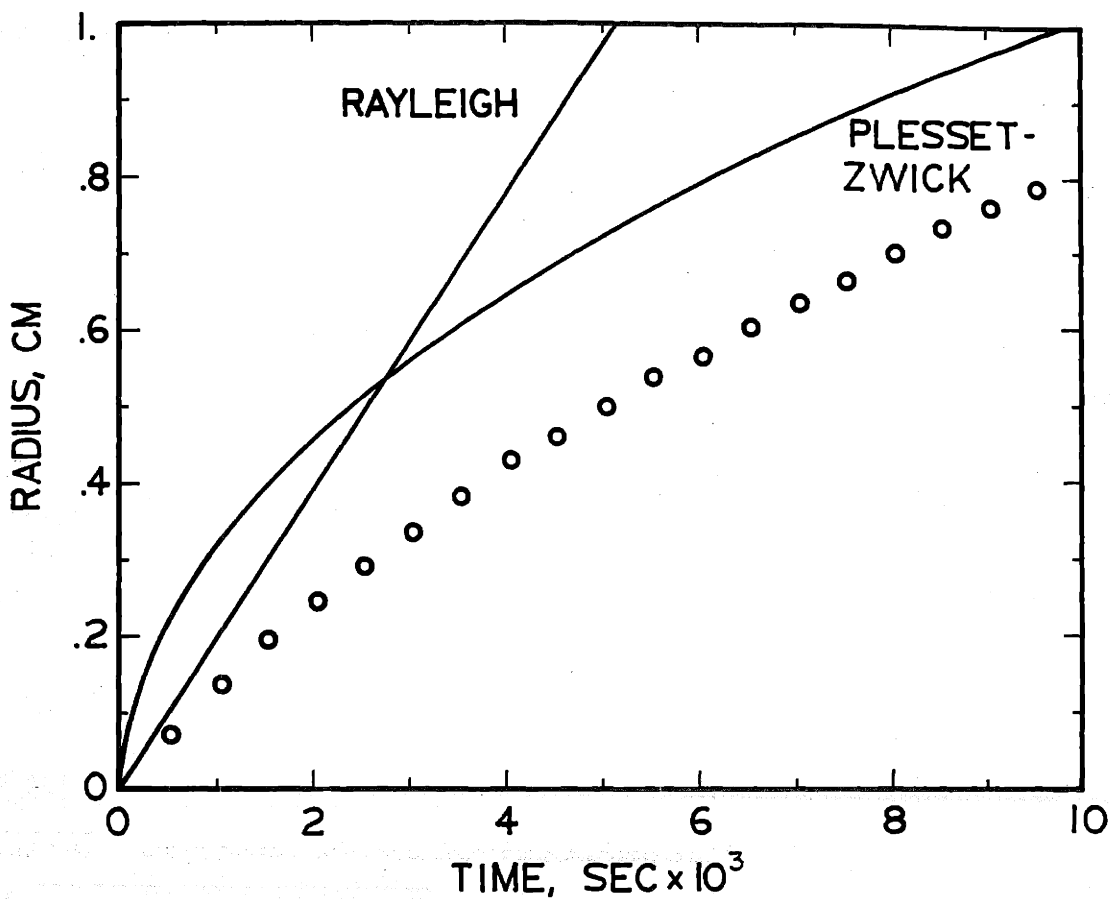


Figure 16 Radius vs Time and Temperature vs Radius Curves of Bubble B6

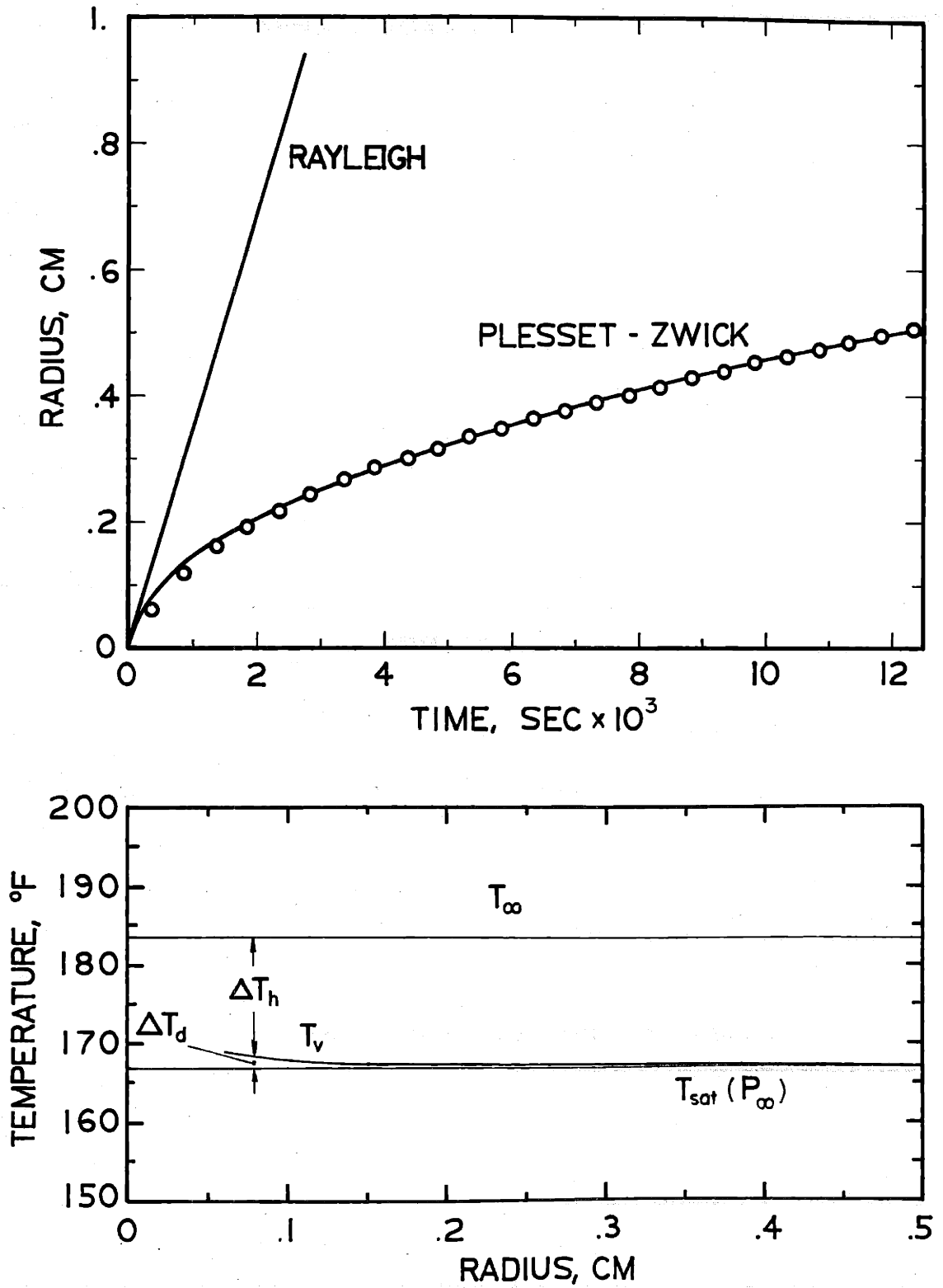


Figure 17 Radius vs Time and Temperature vs Radius Curves of Bubble B7

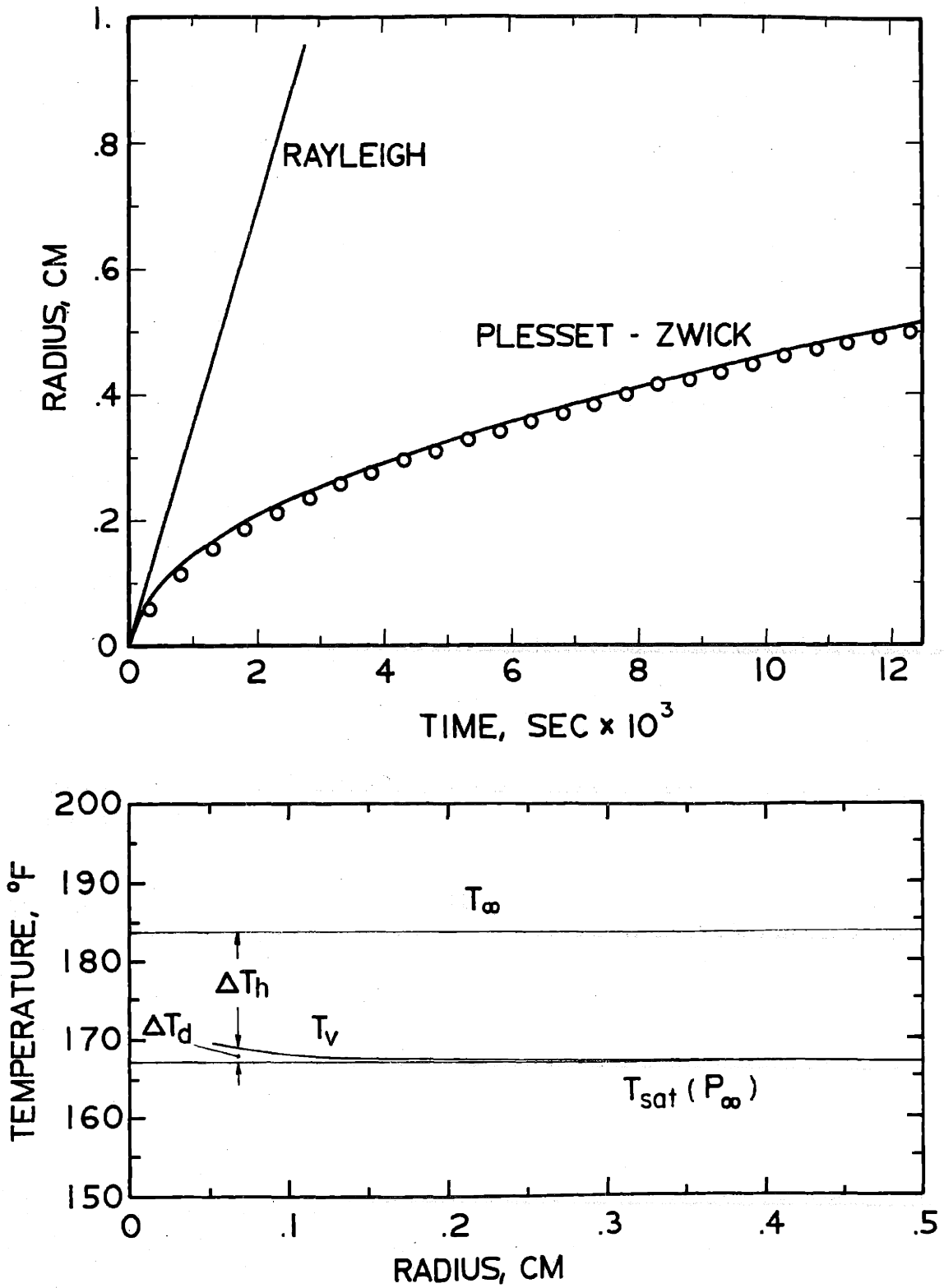


Figure 18 Radius vs Time and Temperature vs Radius Curves of Bubble B8

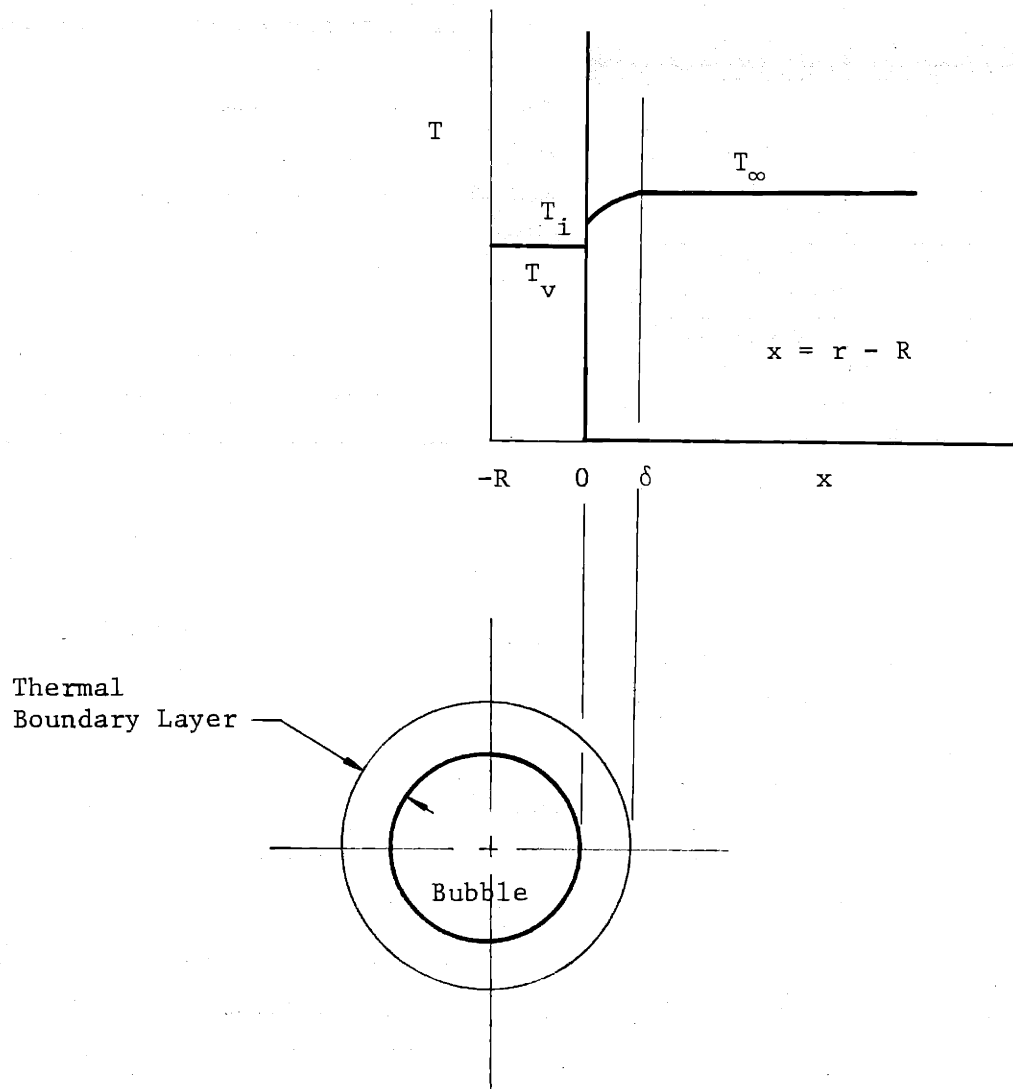


Figure 19 Coordinate System for Temperature Distribution Function

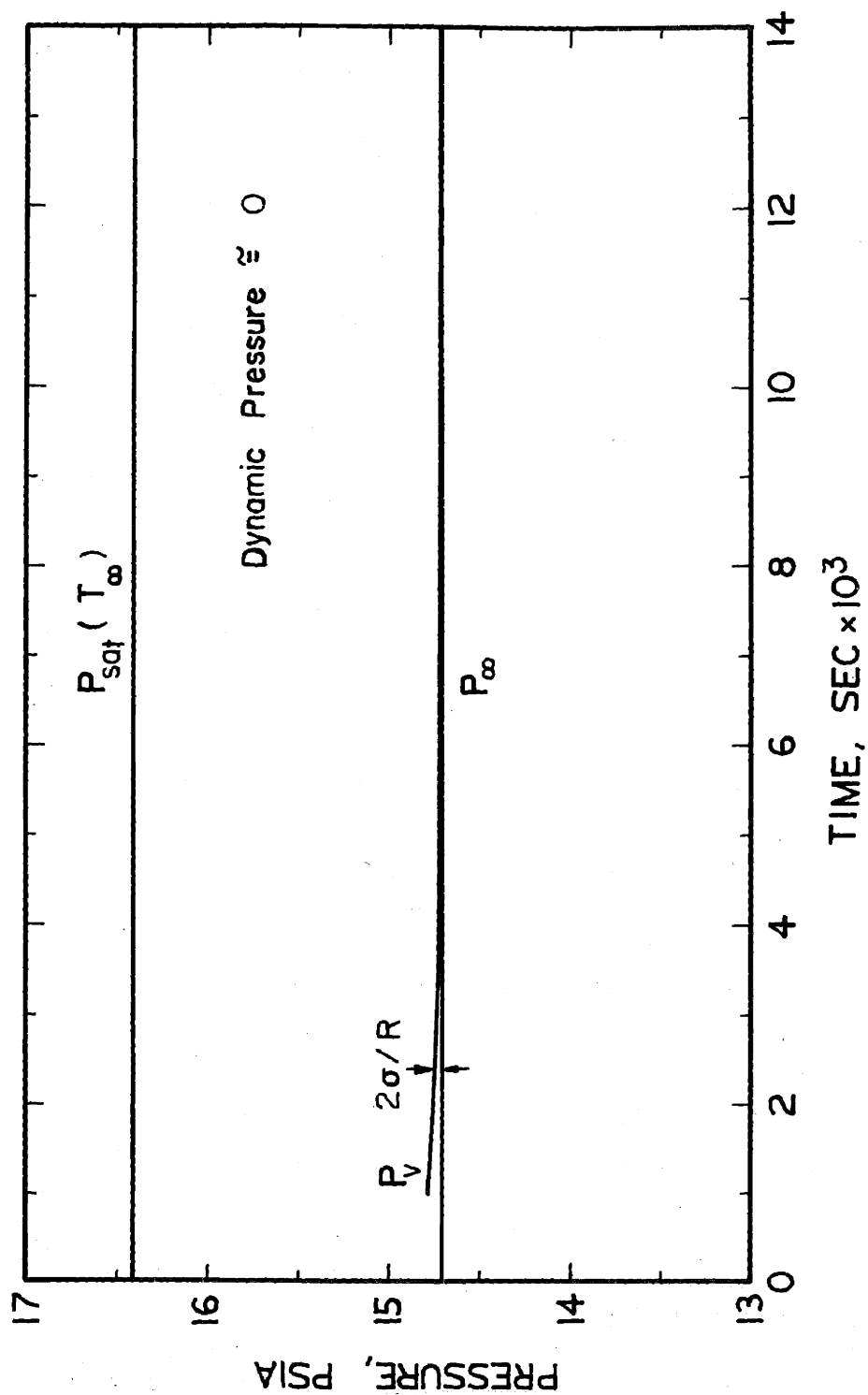


Figure 20 System Pressure Curves for Bubble D7

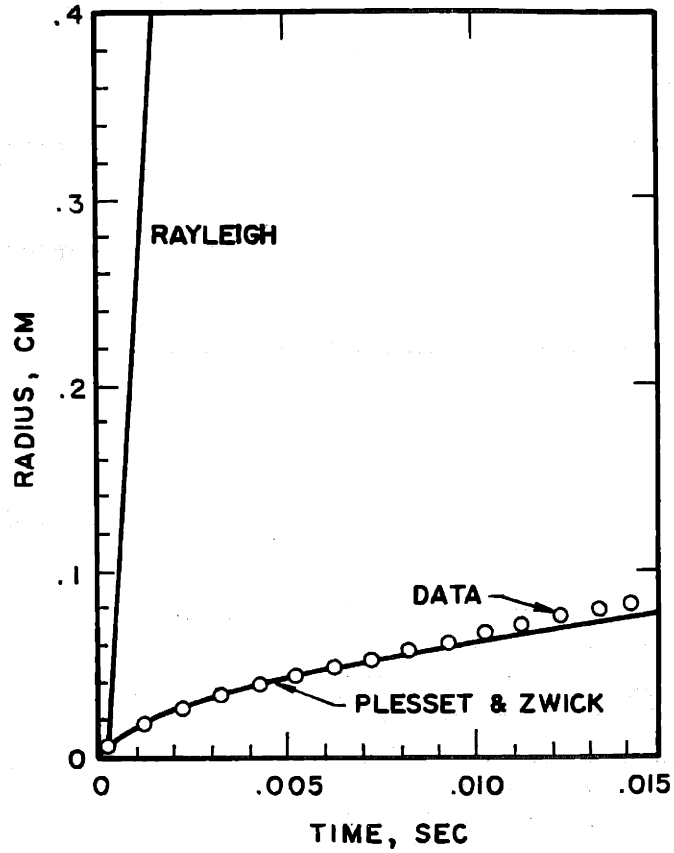


Figure 21 Bubble Growth Data of Water at Atmospheric Pressure and 103.1°C are compared to the analytical expressions of Rayleigh (Eq. II - 7) and Plesset and Zwick (Eq. II-15). From Dergarabedian (10).

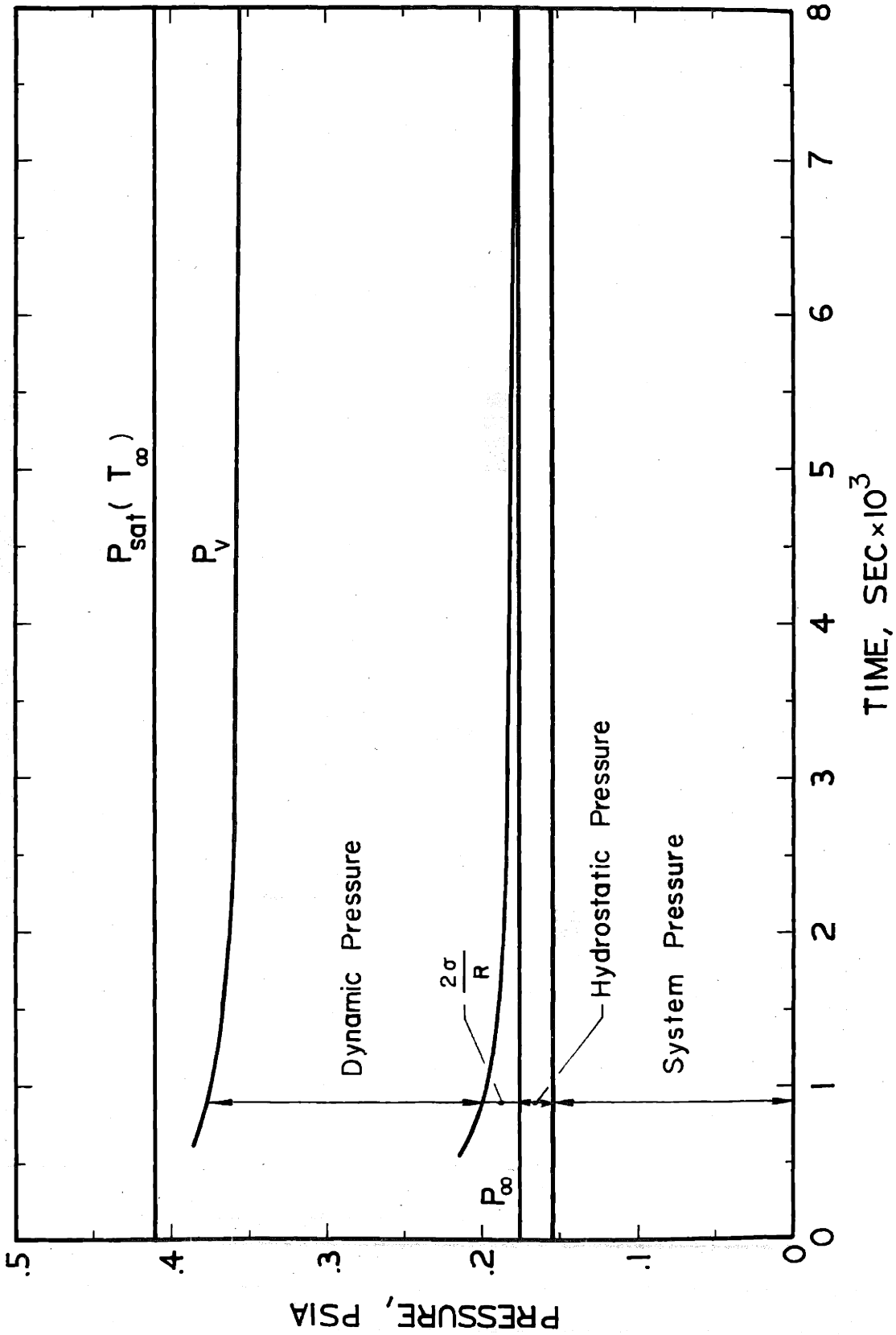


Figure 22 System Pressure Curves for Bubble B1

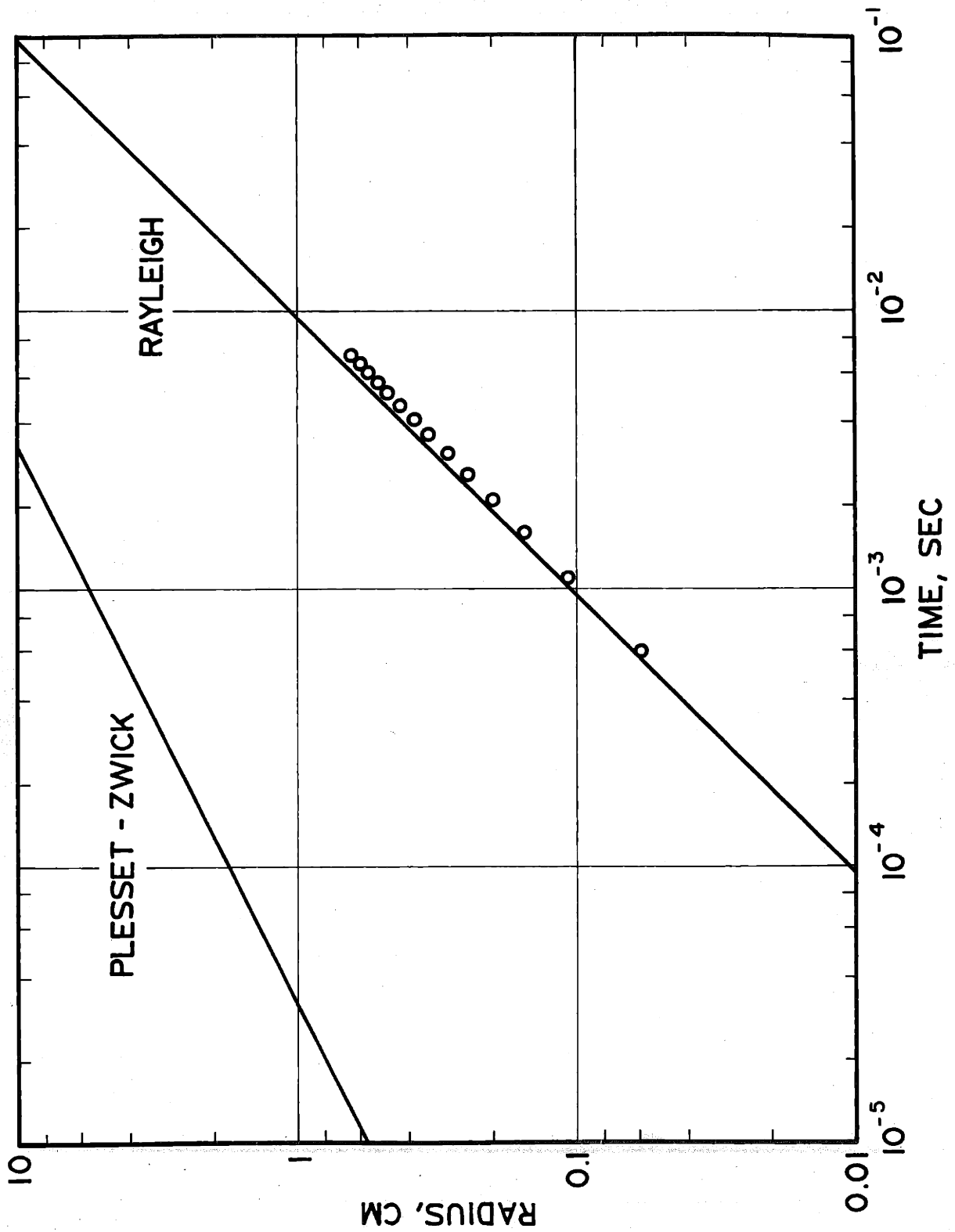


Figure 23 Log-Log Plots of Radius vs Time, Bubble B1

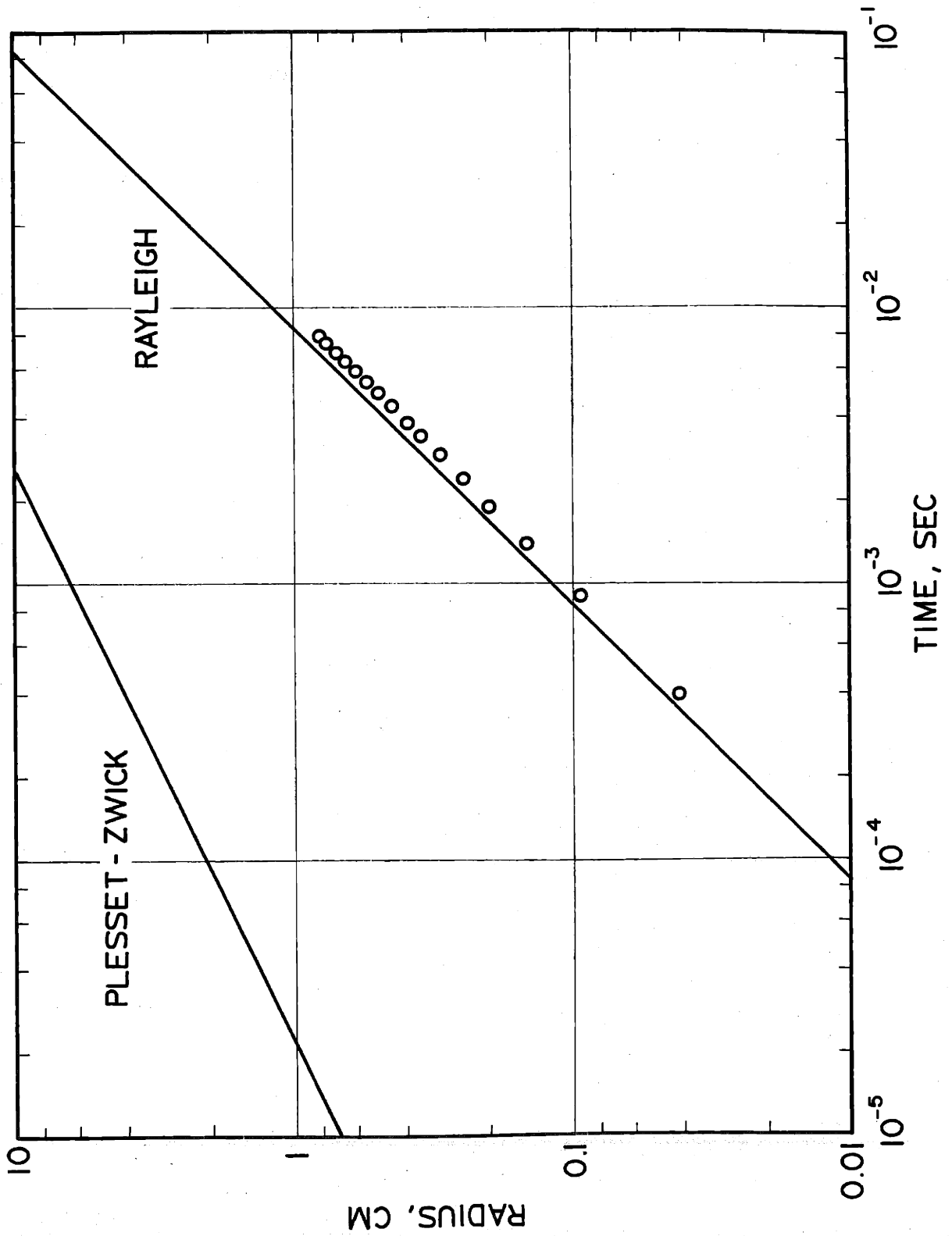


Figure 24 Log-Log Plots of Radius vs Time, Bubble B2

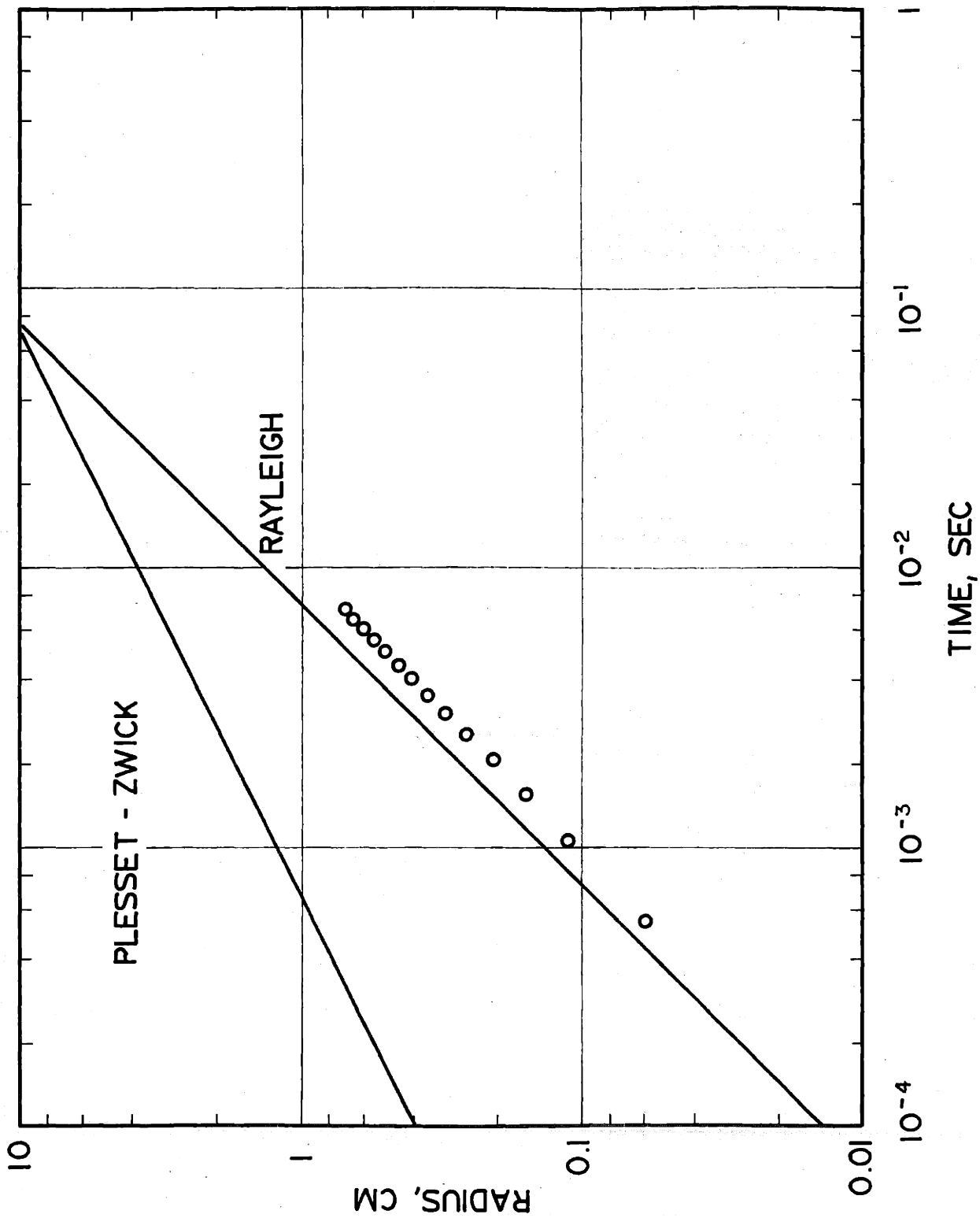


Figure 25 Log-Log Plots of Radius vs Time, Bubble B4

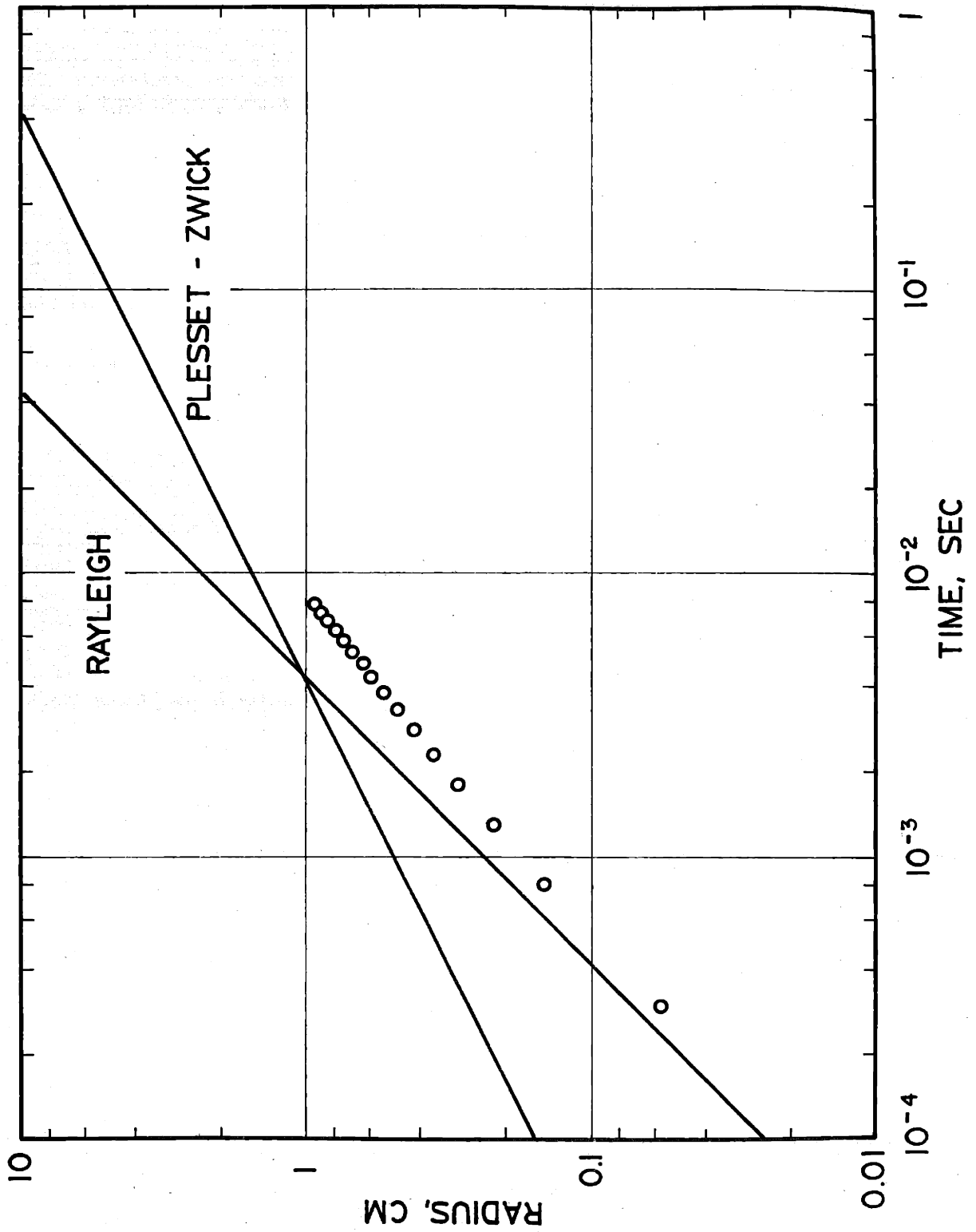


Figure 26 Log-Log Plots of Radius vs Time, Bubble B5

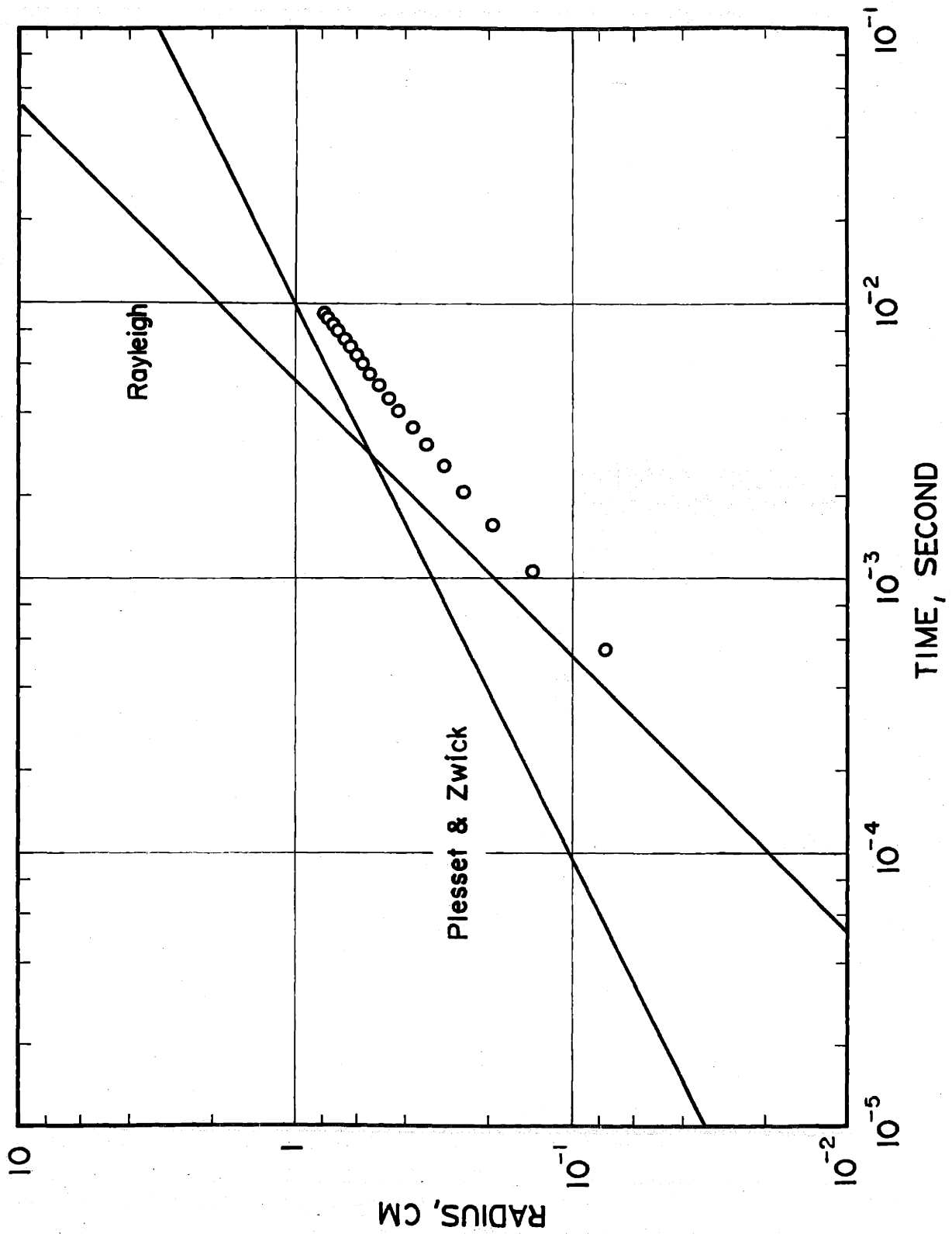


Figure 27 Log-Log Plots of Radius vs Time, Bubble B6

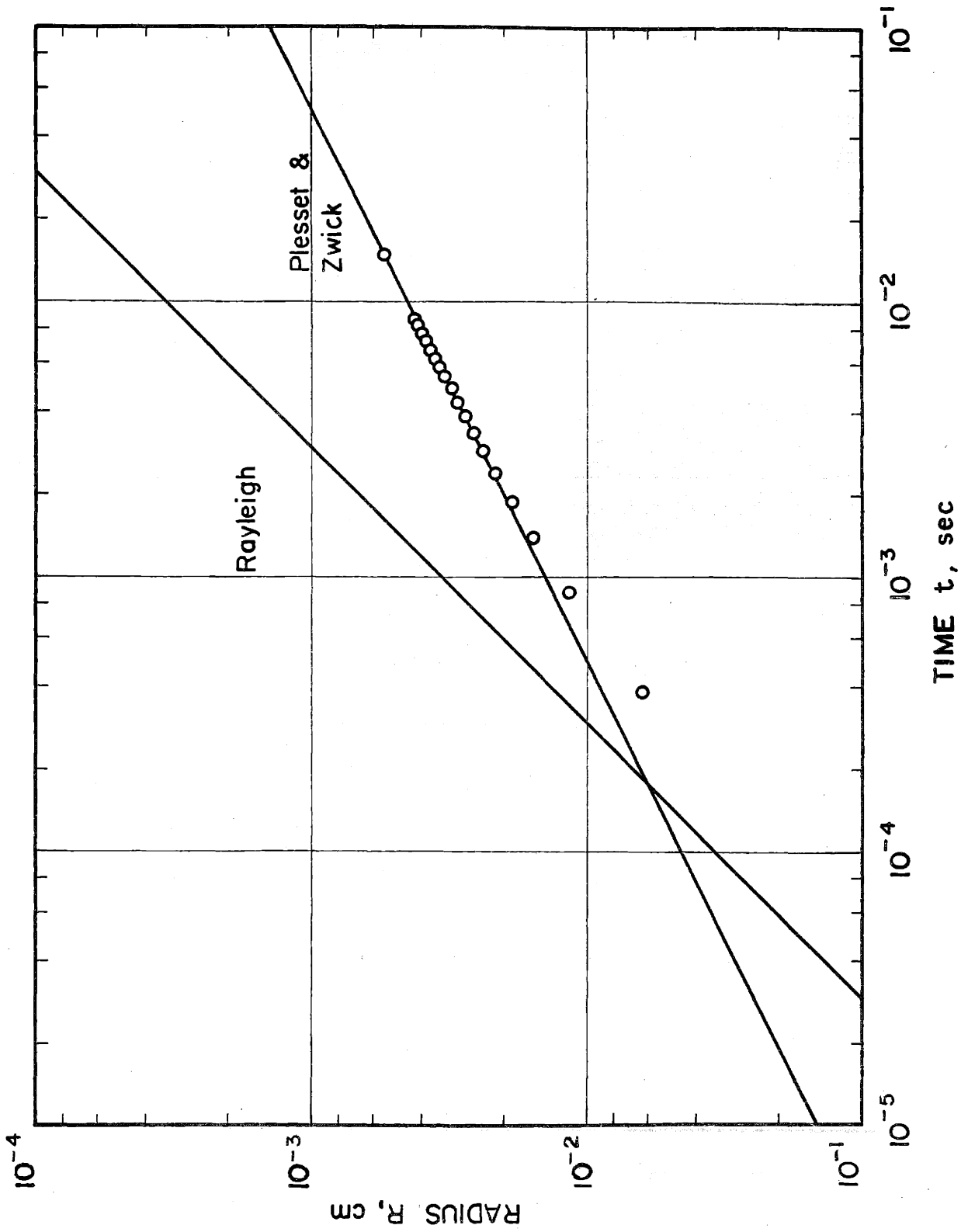
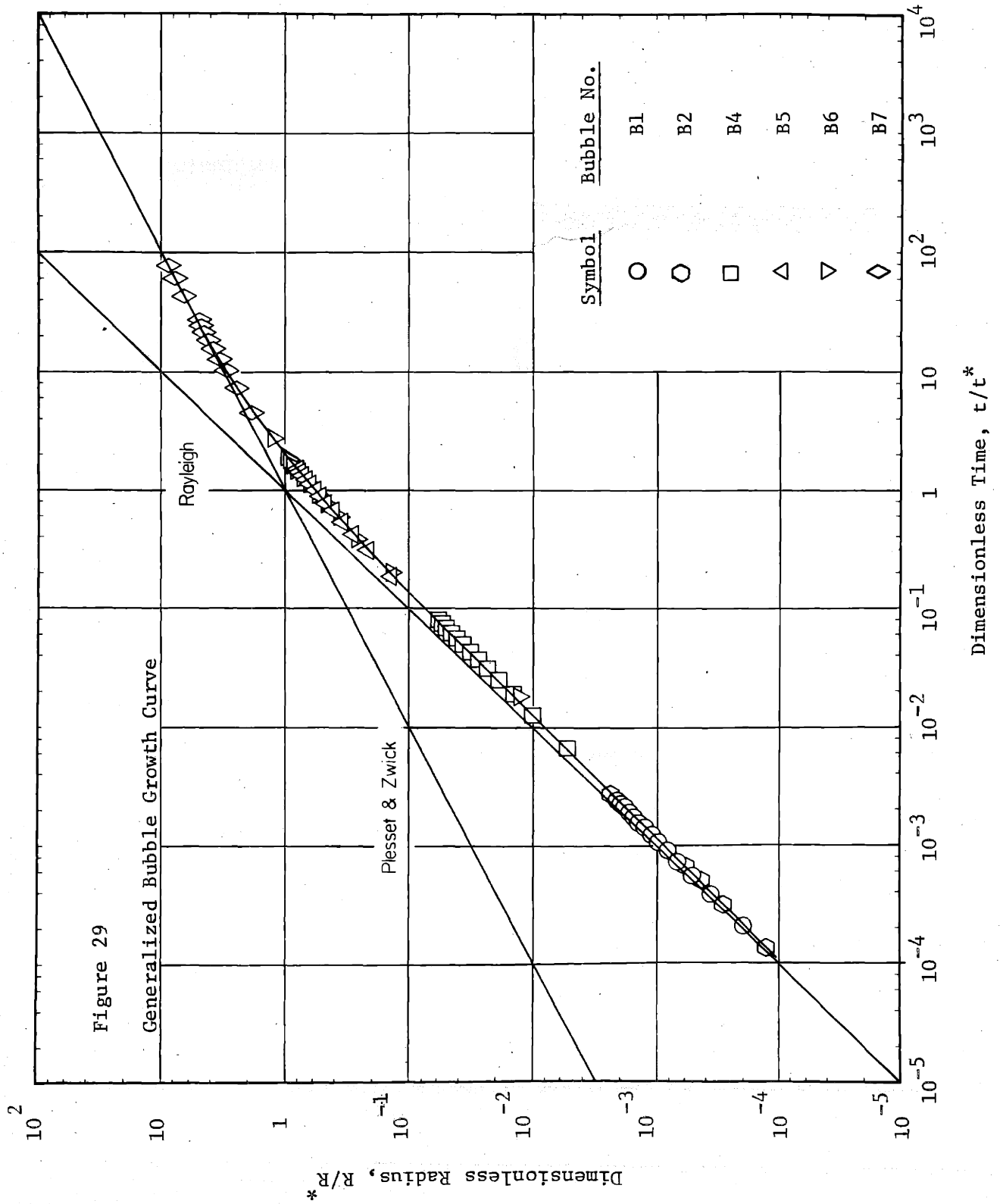


Figure 28 Log-Log Plots of Radius vs Time, Bubble B7



APPENDIX B - RAW DATA

TABLE B-1

EXPERIMENTAL DATA FOR BUBBLE B1

1. System Pressure, $p_{\infty} = 0.1759$ psia
2. Liquid Superheat, $\Delta T_s = 23.95$ °F
3. Jakob Number, $Ja = 2370.0$
4. Liquid Temperature, $T_{\infty} = 73.61$ °F
5. Capacitance, $C = 0.001$ μ fd; Voltage, $E = 300$ volts
6. Bubble Radius - Time Data:

<u>Frame No., I</u>	<u>Radius R, cm</u>	<u>Time t, sec</u>
1	0.0592	0.0006
2	0.1076	0.0011
3	0.1532	0.0016
4	0.1994	0.0021
5	0.2432	0.0026
6	0.2893	0.0031
7	0.3341	0.0036
8	0.3777	0.0041
9	0.4214	0.0046
10	0.4663	0.0051
11	0.5092	0.0056
12	0.5543	0.0061
13	0.5963	0.0066
14	0.6470	0.0071

TABLE B-2

EXPERIMENTAL DATA FOR BUBBLE B2

1. System Pressure, $p_{\infty} = 0.1831$ psia
2. Liquid Superheat, $\Delta T_s = 28.34$ °F
3. Jakob Number, $Ja = 2690.0$
4. Liquid Temperature, $T_{\infty} = 79.08$ °F
5. Capacitance, $C = 0.001$ μ fd; Voltage, $E = 300$ volts
6. Bubble Radius - Time Data:

<u>Frame No., I</u>	<u>Radius R, cm</u>	<u>Time t, sec</u>
1	0.0430	0.0004
2	0.0974	0.0009
3	0.1481	0.0014
4	0.1963	0.0019
5	0.2481	0.0024
6	0.2979	0.0029
7	0.3469	0.0034
8	0.3963	0.0039
9	0.4464	0.0044
10	0.4968	0.0049
11	0.5482	0.0054
12	0.5993	0.0059
13	0.6559	0.0064
14	0.7153	0.0069
15	0.7686	0.0074
16	0.8174	0.0079

TABLE B-3

EXPERIMENTAL DATA FOR BUBBLE B3

1. System Pressure, $p_{\infty} = 0.5922$ psia
2. Liquid Superheat, $\Delta T_s = 3.09$ °F
3. Jakob Number, $Ja = 95.6$
4. Liquid Temperature, $T_{\infty} = 87.89$ °F
5. Capacitance, $C = 0.003$ μ fd; Voltage, $E = 400$ volts
6. Bubble Radius - Time Data:

<u>Frame No., I</u>	<u>Radius R, cm</u>	<u>Time t, sec</u>
1	0.0848	0.0005
2	0.1195	0.0010
3	0.1429	0.0015
4	0.1651	0.0020
5	0.1850	0.0025
6	0.2033	0.0030
7	0.2213	0.0035
8	0.2397	0.0040
9	0.2571	0.0045
10	0.2743	0.0050
11	0.2898	0.0055
12	0.3073	0.0060
13	0.3237	0.0065
14	0.3410	0.0070
15	0.3552	0.0075
16	0.3713	0.0080
17	0.3862	0.0085
18	0.4023	0.0090
19	0.4181	0.0095
20	0.4322	0.0100
21	0.4490	0.0105
22	0.4655	0.0110

TABLE B-4

EXPERIMENTAL DATA FOR BUBBLE B4

1. System Pressure, $p_{\infty} = 0.5962$ psia
2. Liquid Superheat, $\Delta T_s = 16.56$ °F
3. Jakob Number, $Ja = 509.1$
4. Liquid Temperature, $T_{\infty} = 101.56$ °F
5. Capacitance, $C = 0.001$ μ fd; Voltage, $E = 300$ volts
6. Bubble Radius - Time Data:

<u>Frame No., I</u>	<u>Radius R, cm</u>	<u>Time t, sec</u>
1	0.0587	0.00055
2	0.1104	0.00105
3	0.1573	0.00155
4	0.2056	0.00205
5	0.2547	0.00255
6	0.3025	0.00305
7	0.3536	0.00355
8	0.4026	0.00405
9	0.4501	0.00455
10	0.4981	0.00505
11	0.5459	0.00555
12	0.5931	0.00605
13	0.6476	0.00655
14	0.6880	0.00705

TABLE B-5

EXPERIMENTAL DATA FOR BUBBLE B5

1. System Pressure, $p_{\infty} = 1.8259$ psia
2. Liquid Superheat, $\Delta T_s = 19.21$ °F
3. Jakob Number, $Ja = 201.1$
4. Liquid Temperature, $T_{\infty} = 141.96$ °F
5. Capacitance, $C = 0.001$ μ fd; Voltage, $E = 300$ volts
6. Bubble Radius - Time Data:

<u>Frame No., I</u>	<u>Radius R, cm</u>	<u>Time t, sec</u>
1	0.0578	0.0003
2	0.1446	0.0008
3	0.2190	0.0013
4	0.2904	0.0018
5	0.3542	0.0023
6	0.4155	0.0028
7	0.4761	0.0033
8	0.5317	0.0038
9	0.5868	0.0043
10	0.6370	0.0048
11	0.6872	0.0053
12	0.7326	0.0058
13	0.7803	0.0063
14	0.8366	0.0068
15	0.8819	0.0073
16	0.9257	0.0078

TABLE B-6

EXPERIMENTAL DATA FOR BUBBLE B6

1. System Pressure, $p_{\infty} = 1.9345$ psia
2. Liquid Superheat, $\Delta T_s = 13.21$ °F
3. Jakob Number, $Ja = 130.8$
4. Liquid Temperature, $T_{\infty} = 138.07$ °F
5. Capacitance, $C = 0.001$ μ fd; Voltage, $E = 300$ volts
6. Bubble Radius - Time Data:

<u>Frame No., I</u>	<u>Radius R, cm</u>	<u>Time t, sec</u>
1	0.0069	0.00005
2	0.0746	0.00055
3	0.1380	0.00105
4	0.1936	0.00155
5	0.2440	0.00205
6	0.2893	0.00255
7	0.3343	0.00305
8	0.3770	0.00355
9	0.4282	0.00405
10	0.4599	0.00455
11	0.4974	0.00505
12	0.5371	0.00555
13	0.5669	0.00605
14	0.6002	0.00655
15	0.6294	0.00705
16	0.6629	0.00755
17	0.6986	0.00805
18	0.7302	0.00855
19	0.7593	0.00905
20	0.7816	0.00955

TABLE B-7

EXPERIMENTAL DATA FOR BUBBLE B7

1. System Pressure, $p_{\infty} = 5.6072$ psia
2. Liquid Superheat, $\Delta T_s = 16.21$ °F
3. Jakob Number, $Ja = 57.5$
4. Liquid Temperature, $T_{\infty} = 183.34$ °F
5. Capacitance, $C = 0.001$ μ fd; Voltage, $E = 300$ volts
6. Bubble Radius - Time Data:

<u>Frame No., I</u>	<u>Radius R, cm</u>	<u>Time t, sec</u>
1	0.0626	0.00038
2	0.1192	0.00088
3	0.1572	0.00138
4	0.1880	0.00188
5	0.2142	0.00238
6	0.2371	0.00288
7	0.2569	0.00338
8	0.2760	0.00388
9	0.2943	0.00438
10	0.3103	0.00488
11	0.3271	0.00538
12	0.3406	0.00588
13	0.3561	0.00638
14	0.3699	0.00688
15	0.3862	0.00738
16	0.3987	0.00788
17	0.4119	0.00838
18	0.4257	0.00888
19	0.4345	0.00938
20	0.4462	0.00988
21	0.4586	0.01038
22	0.4701	0.01088
23	0.4795	0.01138
24	0.4895	0.01188
25	0.5002	0.01238
26	0.5103	0.01288
27	0.5200	0.01338
28	0.5325	0.01388
29	0.5384	0.01438
30	0.5491	0.01488

TABLE B-8

EXPERIMENTAL DATA FOR BUBBLE B8

1. System Pressure, $p_{\infty} = 5.6324$ psia
2. Liquid Superheat, $\Delta T_s = 16.42$ °F
3. Jakob Number, $Ja = 58.0$
4. Liquid Temperature, $T_{\infty} = 183.74$ °F
5. Capacitance, $C = 0.001$ μ fd; Voltage, $E = 300$ volts
6. Bubble Radius - Time Data:

<u>Frame No., I</u>	<u>Radius R, cm</u>	<u>Time t, sec</u>
1	0.0569	0.0003
2	0.1150	0.0008
3	0.1529	0.0013
4	0.1828	0.0018
5	0.2117	0.0023
6	0.2358	0.0028
7	0.2547	0.0033
8	0.2740	0.0038
9	0.2920	0.0043
10	0.3104	0.0048
11	0.3261	0.0053
12	0.3401	0.0058
13	0.3552	0.0063
14	0.3705	0.0068
15	0.3839	0.0073
16	0.3990	0.0078
17	0.4118	0.0083
18	0.4234	0.0088
19	0.4346	0.0093
20	0.4485	0.0098
21	0.4621	0.0103
22	0.4693	0.0108
23	0.4804	0.0113
24	0.4887	0.0118
25	0.5003	0.0123
26	0.5125	0.0128
27	0.5210	0.0133
28	0.5315	0.0138
29	0.5400	0.0143
30	0.5494	0.0148

APPENDIX C - REDUCED DATA

TABLE C-1

REDUCED DATA FOR BUBBLE BI

<u>R, cm</u>	<u>P_v, psia</u>	<u>T_v, °R</u>	<u>T_i, °R</u>	<u>ΔT_i, °F</u>	<u>σ_e</u>
0.1076	0.3720	530.67	532.42	1.75	0.190
0.1532	0.3660	530.20	532.21	2.01	0.165
0.1994	0.3627	529.94	532.02	2.08	0.158
0.2432	0.3607	529.78	531.87	2.09	0.158
0.2893	0.3593	529.67	531.72	2.05	0.159
0.3341	0.3583	529.59	531.58	1.99	0.163
0.3777	0.3575	529.53	531.46	1.93	0.168
0.4214	0.3569	529.48	531.34	1.86	0.173
0.4663	0.3564	529.45	531.22	1.77	0.180
0.5092	0.3560	529.41	531.12	1.71	0.187
0.5543	0.3557	529.39	531.01	1.62	0.194
0.5963	0.3554	529.36	530.92	1.56	0.203
0.6470	0.3551	529.34	530.81	1.47	0.213

TABLE C-2

REDUCED DATA FOR BUBBLE B2

<u>R, cm</u>	<u>P_v, psia</u>	<u>T_v, °R</u>	<u>T_i, °R</u>	<u>ΔT_i, °F</u>	<u>σ_e</u>
0.0945	0.4341	535.84	537.71	1.87	0.230
0.1460	0.4270	535.07	537.40	2.33	0.185
0.1975	0.4234	534.73	537.14	2.41	0.178
0.2490	0.4212	534.54	536.92	2.38	0.179
0.3005	0.4198	534.42	536.71	2.29	0.184
0.3520	0.4188	534.33	536.52	2.19	0.192
0.4035	0.4180	534.27	536.35	2.08	0.200
0.4550	0.4175	534.22	536.18	1.96	0.211
0.5065	0.4170	534.18	536.03	1.85	0.222
0.5580	0.4166	534.15	535.88	1.73	0.235
0.6095	0.4163	534.12	535.74	1.62	0.250
0.6610	0.4160	534.10	535.60	1.50	0.266
0.7125	0.4158	534.08	535.47	1.39	0.284
0.7640	0.4156	534.06	535.34	1.28	0.305
0.8155	0.4154	534.05	535.22	1.17	0.329

TABLE C-3

REDUCED DATA FOR BUBBLE B3

<u>R, cm</u>	<u>P_v, psia</u>	<u>T_v, °R</u>	<u>T_i, °R</u>	<u>ΔT_i, °F</u>	<u>σ_e</u>
0.1198	0.6418	547.30	546.35	-0.95	-0.117
0.1429	0.6360	547.03	546.30	-0.73	-0.140
0.1640	0.6317	546.82	546.24	-0.58	-0.168
0.1843	0.6285	546.66	546.19	-0.47	-0.200
0.2037	0.6259	546.53	546.15	-0.38	-0.235
0.2225	0.6238	546.43	546.10	-0.33	-0.273
0.2406	0.6221	546.34	546.06	-0.28	-0.314
0.2583	0.6206	546.27	546.02	-0.25	-0.357
0.2756	0.6193	546.20	545.99	-0.21	-0.400
0.2926	0.6182	546.15	545.95	-0.20	-0.444
0.3092	0.6172	546.10	545.92	-0.18	-0.485
0.3255	0.6163	546.05	545.89	-0.16	-0.521
0.3416	0.6155	546.01	545.86	-0.15	-0.553
0.3574	0.6148	545.97	545.83	-0.14	-0.576
0.3731	0.6142	545.94	545.80	-0.14	-0.593
0.3885	0.6136	545.91	545.77	-0.14	-0.602
0.4037	0.6130	545.88	545.75	-0.13	-0.603
0.4187	0.6125	545.86	545.72	-0.14	-0.596
0.4336	0.6120	545.83	545.70	-0.13	-0.585
0.4483	0.6116	545.81	545.67	-0.14	-0.571
0.4629	0.6112	545.79	545.65	-0.14	-0.552

TABLE C-4

REDUCED DATA FOR BUBBLE B4

<u>R, cm</u>	<u>P_v, psia</u>	<u>T_v, °R</u>	<u>T_i, °R</u>	<u>ΔT_i, °F</u>	<u>σ_e</u>
0.1104	0.8229	555.28	558.90	3.62	0.074
0.1573	0.8170	555.06	558.41	3.35	0.079
0.2056	0.8139	554.94	557.97	3.03	0.086
0.2547	0.8120	554.86	557.57	2.71	0.096
0.3025	0.8107	554.81	557.22	2.41	0.107
0.3536	0.8098	554.77	556.88	2.11	0.122
0.4026	0.8091	554.75	556.57	1.82	0.139
0.4501	0.8085	554.72	556.29	1.57	0.160
0.4981	0.8081	554.71	556.01	1.30	0.188
0.5459	0.8077	554.69	555.76	1.07	0.226
0.5931	0.8074	554.68	555.51	0.83	0.280
0.6476	0.8072	554.67	555.24	0.57	0.382
0.6880	0.8070	554.66	555.05	0.39	0.516

TABLE C-5

REDUCED DATA FOR BUBBLE B5

<u>R, cm</u>	<u>P_v, psia</u>	<u>T_v, °R</u>	<u>T_i, °R</u>	<u>ΔT_i, °F</u>	<u>σ_e</u>
0.1446	0.2307 x 10	591.39	591.87	0.48	0.622
0.2190	0.2221 x 10	589.97	590.40	0.43	0.623
0.2904	0.2159 x 10	588.91	589.42	0.51	0.518
0.3542	0.2115 x 10	588.14	588.74	0.60	0.428
0.4155	0.2080 x 10	587.52	588.21	0.69	0.363
0.4761	0.2051 x 10	587.00	587.77	0.77	0.315
0.5317	0.2028 x 10	586.60	587.42	0.82	0.283
0.5868	0.2009 x 10	586.25	587.12	0.87	0.259
0.6370	0.1994 x 10	585.96	586.87	0.91	0.241
0.6872	0.1980 x 10	585.71	586.64	0.93	0.227
0.7326	0.1969 x 10	585.51	586.46	0.95	0.217
0.7803	0.1959 x 10	585.32	586.27	0.95	0.208
0.8366	0.1948 x 10	585.11	586.07	0.96	0.200
0.8819	0.1940 x 10	584.96	585.93	0.97	0.194
0.9257	0.1933 x 10	584.83	585.79	0.96	0.190

TABLE C-6

REDUCED DATA FOR BUBBLE B6

<u>R, cm</u>	<u>P_v, psia</u>	<u>T_v, °R</u>	<u>T_i, °R</u>	<u>ΔT_i, °F</u>	<u>σ_e</u>
0.0746	2.2878	591.08	591.50	0.42	0.581
0.1380	2.1949	589.53	589.93	0.40	0.533
0.1936	2.1413	588.61	589.05	0.44	0.456
0.2440	2.1058	587.98	588.46	0.48	0.404
0.2893	2.0810	587.54	588.03	0.49	0.373
0.3343	2.0612	587.19	587.67	0.48	0.354
0.3770	2.0458	586.91	587.38	0.47	0.344
0.4282	2.0307	586.64	587.08	0.44	0.341
0.4599	2.0228	586.50	586.92	0.42	0.344
0.4974	2.0146	586.35	586.74	0.39	0.351
0.5371	2.0071	586.21	586.57	0.36	0.364
0.5669	2.0022	586.12	586.45	0.33	0.377
0.6002	1.9972	586.03	586.33	0.30	0.396
0.6294	1.9932	585.95	586.23	0.28	0.418
0.6629	1.9891	585.88	586.12	0.24	0.449
0.6986	1.9852	585.80	586.01	0.21	0.493
0.7302	1.9821	585.75	585.92	0.17	0.545
0.7593	1.9795	585.70	585.85	0.15	0.606
0.7816	1.9776	585.66	585.79	0.13	0.668

TABLE C-7

REDUCED DATA FOR BUBBLE B7

<u>R, cm</u>	<u>P_v, psia</u>	<u>T_v, °R</u>	<u>T_i, °R</u>	<u>ΔT_i, °F</u>	<u>σ_e</u>
0.1572	5.6492	627.45	627.53	0.08	0.980
0.1880	5.6381	627.36	627.53	0.17	0.569
0.2142	5.6321	627.32	627.52	0.20	0.433
0.2371	5.6282	627.29	627.52	0.23	0.364
0.2569	5.6256	627.27	627.52	0.25	0.321
0.2760	5.6236	627.25	627.52	0.27	0.290
0.2943	5.6220	627.24	627.51	0.27	0.266
0.3103	5.6208	627.23	627.51	0.28	0.249
0.3271	5.6197	627.22	627.51	0.29	0.233
0.3406	5.6190	627.22	627.51	0.29	0.222
0.3561	5.6182	627.21	627.51	0.30	0.210
0.3699	5.6175	627.21	627.51	0.30	0.202
0.3862	5.6169	627.20	627.50	0.30	0.192
0.3987	5.6164	627.20	627.50	0.30	0.185
0.4119	5.6160	627.19	627.50	0.31	0.179
0.4257	5.6156	627.19	627.50	0.31	0.172
0.4345	5.6153	627.19	627.50	0.31	0.168
0.4462	5.6150	627.19	627.50	0.31	0.164
0.4586	5.6147	627.18	627.49	0.31	0.159
0.4701	5.6144	627.18	627.49	0.31	0.155
0.4795	5.6142	627.18	627.49	0.31	0.152
0.4895	5.6140	627.18	627.49	0.31	0.149
0.5002	5.6138	627.18	627.49	0.31	0.145
0.5103	5.6136	627.18	627.49	0.31	0.142
0.5200	5.6134	627.17	627.49	0.32	0.140
0.5325	5.6132	627.17	627.49	0.32	0.136
0.5384	5.6131	627.17	627.49	0.32	0.135
0.5491	5.6129	627.17	627.49	0.32	0.132

TABLE C-8

REDUCED DATA FOR BUBBLE B8

$R, \text{ cm}$	$P_v, \text{ psia}$	$T_v, \text{ }^\circ\text{R}$	$T_i, \text{ }^\circ\text{R}$	$\frac{\Delta T_i, \text{ }^\circ\text{F}}{T_i}$	$\frac{\sigma}{\rho}$
0.1529	5.6770	627.66	627.80	0.14	0.722
0.1828	5.6652	627.57	627.80	0.23	0.453
0.2117	5.6580	627.52	627.80	0.28	0.344
0.2358	5.6538	627.48	627.79	0.31	0.291
0.2547	5.6513	627.46	627.79	0.33	0.261
0.2740	5.6492	627.45	627.79	0.34	0.236
0.2920	5.6475	627.44	627.78	0.34	0.218
0.3104	5.6461	627.42	627.78	0.36	0.202
0.3261	5.6451	627.42	627.78	0.36	0.191
0.3401	5.6443	627.41	627.78	0.37	0.182
0.3552	5.6435	627.40	627.77	0.37	0.173
0.3705	5.6428	627.40	627.77	0.37	0.165
0.3839	5.6423	627.39	627.77	0.38	0.158
0.3990	5.6417	627.39	627.77	0.38	0.152
0.4118	5.6413	627.39	627.77	0.38	0.147
0.4234	5.6409	627.38	627.76	0.38	0.143
0.4346	5.6406	627.38	627.76	0.38	0.139
0.4485	5.6402	627.38	627.76	0.38	0.134
0.4621	5.6398	627.38	627.76	0.38	0.130
0.4693	5.6397	627.38	627.76	0.38	0.128
0.4804	5.6394	627.37	627.76	0.39	0.125
0.4887	5.6393	627.37	627.76	0.39	0.123
0.5003	5.6390	627.37	627.76	0.39	0.120
0.5125	5.6388	627.37	627.76	0.39	0.117
0.5210	5.6386	627.37	627.76	0.39	0.115
0.5315	5.6385	627.37	627.76	0.39	0.113
0.5400	5.6383	627.36	627.76	0.40	0.111
0.5494	5.6382	627.36	627.76	0.40	0.109

APPENDIX D

JUSTIFICATION FOR THE NEGLECT OF THE AIR CONTENT OF BUBBLE

Although the water used in the present bubble growth experiment is not air free, the presence of entrained air does not affect appreciably the total pressure, and hence the water vapor pressure within a bubble. In the data reduction program, the effect of air is completely neglected. It is justified because the quantity of air is very minute, as can be seen from the following calculations.

The amounts of dissolved air are estimated from the degassing conditions. These conditions are listed below:

<u>Bubble Numbers</u>	<u>Pressure, psia</u>	<u>Temperature, °F</u>
B1	0.1721	56.7
B2	0.1064	50.3
B3	0.1934	66.0
B4	0.2127	64.3
B5	0.1547	57.0
B6	0.1160	57.0
B7	0.0967	55.7
B8	0.0967	55.7

Sample calculations will now be made for the worst case, which corresponds to bubble B4, since the solubility of air is proportional to pressure. For convenience, let state "1" be that state of an air-water system which is identified by the atmospheric pressure p_1 and

the degassing temperature T. Also, let state "2" represent the state corresponding to the degassing pressure p_2 and temperature T. For the present problem, $p_1 = 14.7$ psia, $p_2 = 0.2127$ psia, and $T = 64.3$ °F (~ 18 °C).

If $V_{air,1}$ is the volume of air dissolved in $V_{water,1}$ volume of water under the condition of state 1, then according to Reference (41), p. 1533,

$$\frac{V_{air,1}}{V_{water,1}} \approx 0.01938 \quad (D-1)$$

Perfect gas law gives

$$n_{air,1} = \frac{p_1 V_{air,1}}{R_u T} \quad (D-2)$$

Applying the Henry's Law, one finds for the state 2,

$$n_{air,2} = \frac{p_2 V_{air,1}}{R_u T} \quad (D-3)$$

The above equation is obtained with an assumption that $n_{H_2O,1} \approx n_{H_2O,2}$. This assumption is plausible since the liquid density does not change much. The ratio of the number of molecules of air to that of the water molecule is, therefore,

$$\frac{N_{air,2}}{N_{water,2}} = \frac{\frac{p_2 V_{air,1}}{R_u T}}{\rho_L \cdot V_{water,1}} \quad (D-4)$$

The ratio $N_{air,2}/N_{water,2}$ for the case of bubble B4 is found to be equal to 4.2×10^{-10} . Thus the amount of air that migrates into the bubble is indeed negligible.

APPENDIX E

EMPIRICAL EQUATIONS

Empirical equations relating the bubble radius to the growth time have been derived from observed data by the method of least squares. The following is a summary of the equations that fit the data satisfactorily.

<u>Bubble No.</u>	<u>Empirical Equation</u>
B1	$R = 90 t$
B2	$R = 103 t$
B3	$R = 14.242 t^{0.79} + 0.059$
B4	$R = 98 t$
B5	$t = 0.0055 R + 0.00325 R^2$
B6	$t = 0.00668 R + 0.00698 R^2$
B7	$t = 0.000374 R + 0.04825 R^2$
B8	$t = 0.000383 R + 0.047845 R^2$

In these equations R is in centimeters, and t in seconds. This set of equations has been used in the data reduction program to calculate R and R.

APPENDIX F

ERROR ANALYSIS

An error analysis has been performed to estimate the probable errors in the results presented in Appendices B and C. The analysis follows the procedures suggested by Kline and McClintock (52). Uncertainty level in each result was computed for the bubbles B1 and B8, which represent the lowest and the highest pressures covered in the present investigation. For each bubble, calculations were made for two different bubble sizes. Based on the results of these sample calculations, it is found that the error in bubble growth-rate data is within 5 percent. On the other hand, the uncertainty level in the calculated value of ΔT_1 is so large that the probable error in ΔT_1 is greater than 50 percent. Consequently, the evaporation coefficient of water cannot be inferred from the calculated ΔT_1 .

The uncertainty in a quantity X is denoted as U_x . If G is a function of n independent variables y_1 , each of which is normally distributed, then

$$U_G = \left[\left(\frac{\partial G}{\partial y_1} U_{y_1} \right)^2 + \left(\frac{\partial G}{\partial y_2} U_{y_2} \right)^2 + \dots + \left(\frac{\partial G}{\partial y_n} U_{y_n} \right)^2 \right]^{1/2} . \quad (F-1)$$

The following analysis is based on this equation, which is referred to as the "second-power equation." The uncertainties in the measured variables are estimated to be

<u>Measured Variables</u>	<u>Uncertainty</u>
T_{∞}	$U_{T_{\infty}} = 0.5 \text{ } ^{\circ}\text{F}$
P_{∞}	$U_{P_{\infty}} = 0.2 \text{ mm Hg}$
R	$U_R = 0.005 \text{ cm}$
t	$U_t = .01t$

The derived variables can be expressed in terms of the measured variables, either directly or indirectly, as

$$\begin{aligned} \dot{R} &= \dot{R}(R, t) \\ \ddot{R} &= \ddot{R}(R, t) \\ P_v &= P_v(P_{\infty}, R, \dot{R}, \ddot{R}) \\ T_v &= T_v(P_v) \\ V_v &= V_v(P_v) \\ T_i &= T_i(T_{\infty}, R, \dot{R}, V_v) \\ \Delta T_i &= \Delta T_i(T_i, T_v) \\ \Delta T_s &= \Delta T_s [T_{\infty}, T_{\text{sat}}(P_{\infty})] \\ \Delta T_d &= \Delta T_d [T_v, T_{\text{sat}}(P_{\infty})] \\ \Delta T_h &= \Delta T_h (T_{\infty}, T_v) \end{aligned}$$

The exact functional relationships between these variables have been established in other parts of this thesis. It can be shown that by applying Equation (F-1) to those exact relationships, one obtains easily the following expressions describing the uncertainties in the quantities of interest:

$$\frac{U_{\dot{R}}}{R} = \left[\left(\frac{U_R}{R} \right)^2 + \left(\frac{U_t}{t} \right)^2 \right]^{1/2}$$

$$\frac{U_{\cdot}^{\cdot}}{R} = \left[\left(\frac{U_R}{R} \right)^2 + \left(2 \frac{U_t}{t} \right)^2 \right]^{1/2}$$

$$\frac{U_{P_v}}{P_v} = \frac{1}{P_v} \left[U_{P_{\infty}}^2 + \left(\rho_l R - \frac{2\sigma_s}{R^2} \right) U_R^2 + \left(3R\rho_l U_R \right)^2 + \left(\rho_l R U_R \right)^2 \right]^{1/2}$$

$$\frac{U_{T_v}}{T_v} = f_1 \left(\frac{U_{P_v}}{P_v} \right)$$

$$\frac{U_{V_v}}{V_v} = f_2 \left(\frac{U_{P_v}}{P_v} \right)$$

$$\frac{U_{T_i}}{T_i} = \frac{1}{T_i} \left[U_{T_{\infty}}^2 + \left(\frac{1}{2} \frac{U_R}{R} \right)^2 + \left(\frac{1}{2} \frac{U_{\cdot}^{\cdot}}{R} \right)^2 + \left(\frac{U_{V_v}}{V_v} \right)^2 \right]^{1/2}$$

$$\frac{U_{\Delta T_i}}{\Delta T_i} = \frac{1}{\Delta T_i} \left[U_{T_i}^2 + U_{T_v}^2 \right]^{1/2}$$

$$\frac{U_{\Delta T_s}}{\Delta T_s} = \frac{1}{\Delta T_s} \left[U_{T_{\infty}}^2 + U_{T_{sat}}^2 (P_{\infty}) \right]^{1/2}$$

$$\frac{U_{\Delta T_d}}{\Delta T_d} = \frac{1}{\Delta T_d} \left[U_{T_v}^2 + U_{T_{sat}}^2 (P_{\infty}) \right]^{1/2}$$

$$\frac{U_{\Delta T_h}}{\Delta T_h} = \frac{1}{\Delta T_h} \left[U_{T_{\infty}}^2 + U_{T_v}^2 \right]^{1/2}$$

Results of representative uncertainty calculations are shown in Table F-1. The quantities U_{T_v}/T_v and U_{V_v}/V_v are estimated from Steam Tables on the basis of U_{P_v}/P_v .

TABLE F-1

Results of Representative Uncertainty Calculations

	<u>Bubble B1</u>		<u>Bubble B8</u>	
<u>Radius R, cm</u>	0.1076	0.4663	0.1529	0.3990
U_R/R	0.0465	0.0107	0.0327	0.0125
U'_R/R	0.0475	0.0146	0.0342	0.016
U_{P_v} , psi	0.0171	0.0064	0.0039	0.0039
U_{P_v}/P_v	0.046	0.018	~ 0	~ 0
U_{T_v} , °F	1.34	0.58	0.03	0.03
U_{T_v}/T_v	0.0025	0.0011	~ 0	~ 0
U_{V_v} , ft ³ /lb	36.4	18.1	0.0422	0.0422
U_{V_v}/V_v	0.0429	0.0205	~ 0	~ 0
U_{T_i} , °F	0.504	0.503	0.625	0.527
$U_{\Delta T_i}$, °F	1.43	0.77	0.625	0.528
ΔT_i , °F	1.7497	1.7794	0.143	0.379
$U_{\Delta T_i}/\Delta T_i$, %	81.7	43.2	437.0	139.0
<hr/>				
$U_{T_{sat}(P_\infty)}$, °F	0.59	0.59	0.03	0.03
$U_{\Delta T_s}$, °F	0.773	0.773	0.501	0.501
$U_{\Delta T_s}/\Delta T_s$	0.0323	0.0323	0.0305	0.0305
$U_{\Delta T_d}$, °F	1.46	0.827	0.0424	0.0424
$U_{\Delta T_d}/\Delta T_d$	0.0695	0.0418	0.1246	0.605
$U_{\Delta T_h}$, °F	1.43	0.765	0.501	0.501
$U_{\Delta T_h}/\Delta T_h$	0.486	0.184	0.0312	0.0306

A few comments are made concerning the above results:

1. At reduced pressure, the pressure-temperature curve of water is very steep. Thus in the case of bubble B1 with $R = 0.1076$ cm, an uncertainty in pressure P_v of 0.0171 psi corresponds to an uncertainty of 1.34 °F with regard to the vapor temperature T_v . Although 1.34 °F is negligibly small compared to the absolute value of T_v , it is the major contribution to the uncertainty $U_{\Delta T_i}$, which is 1.43 °F. Since ΔT_i is the difference between two large quantities, T_i and T_v , the error in ΔT_i is bound to be large, as is shown in Table F-1. In this case, an error of 4.6 percent in P_v results in 81.7 percent error in the value of ΔT_i . For the same bubble with $R = 0.4663$ cm, the error of P_v is only 1.8 percent, but the corresponding value of ΔT_i is in error by 43.2 percent. It shows that under reduced pressure condition, the reliability of the calculated value of ΔT_i , and hence the evaporation coefficient σ_e , is very poor even with improved measurement techniques.
2. Concerning the data of bubble B8, it is seen that the uncertainty in ΔT_i is mostly due to error in the measured liquid temperature T_∞ . Judged from the facts that the calculated values of ΔT_i , which are listed in Table C-8 of Appendix C, are well within the estimated uncertainty level, and that the data agree with the heat diffusion limited theory which neglects the interfacial effect, it appears that the integral technique used in the data reduction program is probably acceptable.

BIOGRAPHICAL NOTE

Yeong-Cheng Lien was born in Kien-Yang, Fu Kien, China, on May 30, 1943. In 1948, he moved with his family to Taiwan, China. In 1962, he was graduated from Taipei Institute of Technology, majoring in Mechanical Engineering. He spent the following year in the Chinese Air Force as a Second Lieutenant. Upon honorary discharge from the military services, he came to the United States in September 1963.

During the 1963-1965 academic years, he was a teaching assistant in the Department of Mechanical Engineering of the Pratt Institute, Brooklyn, New York. He received the Master of Mechanical Engineering degree from Pratt in June 1965.

He has been at the Massachusetts Institute of Technology since September 1966, pursuing graduate studies toward the Doctor of Science degree. He is a research assistant in the Heat Transfer Laboratory since February 1967.

As a mechanical engineer, he worked with Crawford and Russell, Inc., and later with Ebasco Services, Inc., between June 1965 and September, 1966. In the summer of 1968, he worked for the General Electric Company in the Atomic Power Equipment Department. He is an associate member of the American Nuclear Society and a student member of the American Society of Mechanical Engineers.